EXPERIMENTAL INVESTIGATION OF THE INFLUENCE OF HUB TAPER ANGLE ON THE PERFORMANCE OF PUSH AND PULL CONFIGURATION PODDED PROPELLERS

ROCKY SCOTT TAYLOR

EXPERIMENTAL INVESTIGATION OF THE INFLUENCE OF HUB TAPER ANGLE ON THE PERFORMANCE OF PUSH AND PULL CONFIGURATION PODDED PROPELLERS

by

©ROCKY SCOTT TAYLOR

A thesis submitted to the School of Graduate Studies

in partial fulfillment of the requirements for the

degree of Master of Engineering

Faculty of Engineering and Applied Science

Memorial University of Newfoundland

May 2006

St. John's Newfoundland Canada

Your file Votre référence
ISBN: 978-0-494-19404-1
Our file Notre référence
ISBN: 978-0-494-19404-1

Abstract

The influence of propeller hub taper angle and mode of operation on open water baseline and podded propeller performance have been experimentally evaluated for push and pull mode propellers with 15^{o} and 20^{o} hub taper angles. Results from two series of experiments considering performance with and without the presence of the pod and strut geometry are presented.

Discussions of the testing methods used for 'propeller only' tests and 'podded propeller unit' tests have been provided. Limitations of these methods are included and test procedures to evaluate the influence of fairing adapters on 'propeller only' results are suggested.

The effect of hub taper angle on both 'propeller only' and 'podded propeller unit' performance are provided along with suggestions of how these findings may be used to better adapt propeller designs to the operational profile of the vessel.

Variation in performance as a function of mode of operation is described, along with discussion of potential causes of observed differences. Recommendations are provided to guide future research in this area.

Experimental uncertainty analysis methods and results are detailed for both 'propeller only' tests and for 'podded propeller unit' tests. Approaches to reduce uncertainty levels in future experiments are suggested.

Acknowledgments

I would like to extend my sincere gratitude to Dr. Brian Veitch for his enthusiastic support and guidance throughout the course of my studies. His personal dedication and commitment to excelling in his field of research were crucial elements in helping me decide to pursue higher education. I would also like to thank Dr. Neil Bose for his expert feedback throughout my program, as well as Dr. Bruce Colbourne for helping me put the finishing touches on my thesis.

For their financial support, I would like to thank NSERC, the Associate Dean's Office and the School of Graduate Studies. Thanks to SNAME for their support, in addition to the many opportunities I have had to expand my professional development through involvement with their organization.

Special thanks to Moya Crocker and the staff in the S.J Carew building for the years of help on my journey through the program.

I would also like to thank the other graduate students who I have had the privilege of working with on this project, particularly Andrew MacNeill. His expert knowledge of design, manufacturing and practical engineering principles have been pivotal to the technical viability and success of this project. His commitment to quality and innovation has had a profound impact on my own perspective of problem solving and design engineering. It was a privilege to study and learn from him the many things that can never be learned from books or courses. For this I am truly grateful.

I would also like to thank the staff at IOT and OERC, particularly Jim Gosse, for helping me throughout the course of my testing program. Thanks to the crew at MUN Technical Services for their practical insights and quality craftsmanship.

Finally, I would like to express my gratitude for those who motivate and support me in all that I do in life: Alexander, Skye and my parents, Lloyd and Kay. Your love is the foundation upon which I build my life.

Table of Contents

Abstract ii

Acknowledgments iii

List of Tables vi

List of Figures ix

List of Appendices xii

Chapter 1 - Introduction 1

1 .1 Aim 1

1.2 Scope 1

1.3 Background 2

1.4 Overview of Podded Propellers 4

1.5 Why Pods Have Become So Popular 6

1.6 Current Problems within the Research Community 7

1.7 Addressing These Problems 10

1.8 Data Reduction Equations 12

Chapter 2 – Literature Survey 18

2.1 Scope 18

2.2 Hydrodynamic Considerations 18

2.3 Related Experimental Work 25

2.4 Commercial Applications 28

2.5 Military Applications 31

Chapter 3 – Experimental Apparatus 34

3.1 Scope 34

3.2 Model Propeller Geometry 34

3.3 Model Pod Shell and Strut Geometry 37

3.4 Instrumentation for Baseline Propeller Experiments 39

3.5 Instrumentation for Podded Propeller Experiments 43

Chapter 4 - Methodology 46

4.1 Scope 46

4.2 Instrumentation Calibration 46

4.3 Testing Procedures 51

Chapter 5 - Results 56

5.1 Scope 56

5.2 Assessment of the Influence of Reynolds Number 56

5.3 Baseline Propeller Open Water Test Results 60

5.4 Podded Propeller Open Water Test Results 66

5.5 Influence of Propeller Hub Taper Angle 71

5.6 Comparison of Push and Pull Configurations 77

Chapter 6 - Uncertainty Analysis 85

6.1 Scope 85

6.2 Uncertainty Analysis Methodology 85

6.3 Uncertainty Estimates for Baseline Tests 88

6.4 Uncertainty Estimates for Podded Propeller Tests 91

6.5 Discussion 94

Chapter 7 - Conclusions and Recommendations 100

7.1 Scope 100

7.2 Baseline Propeller Tests 100

7.3 Podded Propeller Tests 101

7.4 Comparison of Testing Approaches 102

7.5 Influence of Hub Taper Angle 103

7.6 Comparison of Push and Pull Configuration 104

7.7 Uncertainty Analysis 106

7.8 Design Considerations 107

Bibliography 109

List of Tables

Table 1.1: Standard Non-dimensionalized Coefficients for Coventional Screw Propellers 13

Table 1.2: Final Forms of Data Reduction Equations 14

Table 1.3: Definition of Data Reduction Terms 15

Table 2.1: Summary of Publications Examining Commercial Vessel Types Other than Cruise Ships 31

Table 3.1: Propeller Configurations Studied 35

Table 3.2: Geometric Particulars of Model Propellers 36

Table 3.3: Geometric Particulars of Model Pods 39

Table 4.1: Experimental Test Program 53

Table 5.1: Overall Error in Thrust, Torque and Advance Coefficient for Baseline Results 58

Table 5.2: Overall Error in Propeller Thrust, Unit Thrust, Torque and Advance Coefficient for Podded Propeller Results 59

Table 5.3: Bollard Condition Results for Baseline Propeller Tests 63

Table 5.4: Baseline Propeller Open Water Efficiencies at J = 0.7 65

Table 5.5: Bollard Condition Results for Podded Propeller Tests 70

Table 5.6: Percent Difference in 20° Pull Propeller Results Compared to 15° Pull Propeller Results 72

Table 5.7: Percent Difference in 20° Push Propeller Results Compared to 15° Push Propeller Results 74

Table 5.8: Percent Difference in 20° Pull Podded Propeller Compared to 15° Pull Podded Propeller Results 75

Table 5.9: Percent Difference in 20° Push Podded Propeller and 15° Push Podded Propeller Results 77

Table 5.10: Comparison of Data for 15° Pull Propeller (Baseline) and 15° Push Propeller (Baseline) 79

Table 5.11: Comparison of Data for 20° Pull Propeller (Baseline) and 20° Push Propeller (Baseline) 80

Table 5.12: Comparison of Data for 15° Pull Propeller (Podded) and 15° Push Propeller (Podded) 81

Table 5.13: Comparison of Data for 20° Pull Propeller (Podded) and 20° Push Propeller (Podded) 83

Table 6.1: Data Reduction Equations 86

Table 6.2: Baseline Propeller Test Bias and Precision Limits 89

Table 6.3: Overall Uncertainty Estimates for Baseline Propeller Variables 90

Table 6.4: Overall Error in Thrust, Torque and Advance Coefficients 90

Table 6.5: Podded Propeller Test Bias and Precision Limits 92

Table 6.6: Overall Uncertainty Estimates for Podded Propeller Variables 93

Table 6.7: Overall Uncertainty in Propeller Thrust, Unit Thrust, Torque and Advance Speed 93

Table 6.8: Major Factors Influencing Uncertainty 95

List of Figures

Figure 1.1: Podded Propulsion Concept vs. Conventional Screw Propulsion..... 4

Figure 1.2: Pull Mode Configuration vs. Push Mode Configuration 5

Figure 1.3: Concial Hub Propeller for Podded Drives vs. Conventional Propeller 9

Figure 1.4: Overview of Project – Systematic Investigation of Azimuthing Podded Propeller Performance 11

Figure 3.1: Identification of Hub Taper Angle in Push and Pull Mode Podded Propellers 35

Figure 3.2: Finished Model Propellers 37

Figure 3.3: Geometric Parameters Used to Define Model Pod Geometry 38

Figure 3.4: Kempf & Remmers Dynamometer Used for Baseline Propeller Tests 40

Figure 3.5: Baseline Propeller and Adapters 41

Figure 3.6: Nose and Tail Cone Adapters for Baseline Propeller Tests 42

Figure 3.7: Instrumentation Mounted on Towing Carriage Rails 43

Figure 3.8: Podded Propeller Instrumentation Package 44

Figure 3.9: Lift System Feature of Podded Propeller Instrumentation 45

Figure 4.1: Pod Unit Mounted for Unit Thrust Calibration 48

Figure 4.2: Pod Unit Mounted in Calibration Fixture 49

Figure 4.3: Arrangement for Calibration of Propeller Torque 51

Figure 5.1: Comparison of Baseline Propeller Data at 9 rps, 12 rps and 15 rps 58

Figure 5.2: Consideration of Uncertainty in Baseline Propeller Data for 9 rps, 12 rps and 15 rps 59

Figure 5.3: Graphical Indicators for Baseline Propeller Configurations 60

Figure 5.4: Performance Curve for Baseline 15° Pull Propeller 61

Figure 5.5: Performance Curve for Baseline 15° Push Propeller 61

Figure 5.6: Performance Curve for Baseline 20° Pull Propeller 62

Figure 5.7: Performance Curve for Baseline 20° Push Propeller 63

Figure 5.8: Graphical Indicators for Podded Propeller Configurations 66

Figure 5.9: Performance Curve for 15° Push Podded Propeller 67

Figure 5.10: Performance Curve for 15° Pull Podded Propeller 68

Figure 5.11: Performance Curve for 20° Push Podded Propeller 69

Figure 5.12: Performance Curve for 20° Pull Podded Propeller 70

Figure 5.13: Performance Plot - 15° and 20° Pull Propellers 72

Figure 5.14: Performance Plot - 15° and 20° Push Propellers 73

Figure 5.15: Performance Plot - 15° and 20° Pull Podded Propellers 75

Figure 5.16: Performance Plot - 15° and 20° Push Podded Propellers 76

Figure 5.17: Comparison of Push and Pull Mode - 15° Baseline Propellers 78

Figure 5.18: Comparison of Push and Pull Mode - 20° Baseline Propellers 79

Figure 5.19: Comparison of Push and Pull Mode - 15° Podded Propellers..... 81

Figure 5.20: Comparison of Push and Pull Mode - 20° Podded Propellers..... 82

Figure 6.1: Uncertainty Analysis Results for Baseline Propeller Tests 91

Figure 6.2: Uncertainty Analysis Results for Podded Propeller Tests 94

List of Appendices

Appendix A – Dimensional Analysis of Podded Propeller Peformance

Appendix B – Laboratory Procedures

Appendix C – Tabular Data for Baseline Propeller Tests

Appendix D – Tabular Data for Podded Propeller Tests

Appendix E – Uncertainty Analysis For Baseline Propeller Tests

Appendix F – Uncertainty Analysis For Podded Propeller Tests

Chapter 1 - Introduction

1 .1 Aim

The focus of this thesis is the experimental characterization of the performance of model scale, single screw, push mode and pull mode podded propellers operating at zero pitch, roll and yaw angles in steady, open water conditions. The aim is to fill in knowledge gaps within the research community regarding experimental procedures for testing podded propellers and to extend the boundaries of scientific knowledge surrounding the present understanding of the performance of podded propulsors and the conical hub propellers they utilize. To this end, a series of experiments have been conducted to investigate the baseline, open-water performance of a set of four conical hub propellers used with podded propulsors, without the presence of the pod and strut geometry. In addition, a series of tests which considered the performance of the same set of propellers operating as integral components of podded propeller units have been included. The results of these experiments serve to provide a guide for future work in the characterization of podded propeller performance for both push-mode and pull-mode podded propellers.

1.2 Scope

The primary objective of this chapter is to provide background information on podded propeller technology, to identify some of the common variations of the technology and to draw focus on the need for the research work considered in this study. Furthermore, this chapter discusses many issues considered during the planning phase of this project and as such provides the rationale for the specific test program that was implemented. Consideration of the development

and selection of appropriate data reduction equations has been given, in addition to a brief summary of current literature on experimental studies of podded propulsor hydrodynamics.

1.3 Background

As with many advanced technological developments, the concept of podded propellers has military roots. Research in this field began in the mid 1970s when the US Navy conducted intermittent project specific investigations of the hydrodynamics of podded propulsion. As described by Karafiath (1998), initial work in this area focused primarily on applications with destroyer type surface combatants.

It was Rains et al. (1979) who published the first paper describing podded propellers as a general propulsion concept for applications on U.S. naval destroyers. Two years later, the first published results of an experimental investigation of podded propulsor hydrodynamics were published by Rains et al. (1981). This series of tests examined the performance of a set of first generation conceptual podded drives. The geometry of these conceptual designs was based on the use of compact, high power-density superconducting electric motors mounted in watertight shells fixed to the hull of the vessel. The lack of sufficiently developed superconducting motor technology or viable alternatives posed problems for early pod developments, as it was not possible to build full scale versions of the model propulsors being tested. In addition, the initial variations of podded drives lacked many of the modern design features which make this propulsion alternative so attractive. For these reasons, pod research was limited for several years.

Nearly a decade after the publication of the first description of podded propellers, the concept of podded propeller technology resurfaced. This time, however, podded propulsors were considered in a commercial context as a

propulsion alternative for icebreaking vessels. Interestingly, advances in the development of alternating current (AC) electric motors during the 1980s played a crucial role in making podded propellers technically feasible. While these newer motor designs were not as compact as the proposed superconducting motors, they offered sufficient power-to-weight ratios to serve as a viable alternative. The development of the first electric-drive podded propeller was also assisted by advances in control system electronics during the same time period.

The first commercial azimuthing electric-drive podded propeller, the Azipod®, was the product of a joint project between Kvaerner Masa-Yards Inc. and Asea-Brown-Boveri (ABB) Industry Oy of Finland in 1988. According to Niini (1997), the original focus of this project was the development of a new, efficient propulsion system for ice transiting ships and icebreakers. As was quickly discovered, other types of vessels, particularly large cruise ships, could take advantage of the benefits offered by this concept.

Once the ABB pods had successfully broken into the conventional propulsion market, other vendors recognized the potential of this technology and began working on their own podded drives. Presently there are three major vendors supplying podded propulsion technology: ABB, Rolls-Royce and Seimens-Schottel. Much of the commercial research work supporting these products is proprietary and as such, very little has been published.

Since the late 1990s it has been recognized that additional information about podded propeller performance and about the performance of ships with podded drives is needed to allow for the proliferation of this technology. Through the assistance of technical organizations such as the International Towing Tank Conference (ITTC) and others, researchers and engineers have collaborated with industry partners to study podded propulsion in an effort to increase the availability of such technical information. Through these efforts, it is hoped that a greater understanding of this technology may be attained.

1.4 Overview of Podded Propellers

As with any commercial technology, there are different variations of the basic podded propeller design. When trying to systematically study specific elements of any type of system, it is necessary to establish a benchmark for comparison. This benchmark should consist of a generic form, without any additional features. Taking such an approach allows for rapid assessment of the influence of any design modifications against the established benchmark. Examining the wide variety of commercial podded propellers presently available, one can quickly determine that the factors which may influence the hydrodynamic performance of the pod unit vary significantly from those of a traditional screw propeller and rudder configuration. For this reason, it was necessary to assess current podded propeller technology and identify the most common features.

As illustrated in Figure 1.1, the concept of podded propulsion represents a significant departure from conventional screw propulsion configurations. By using electric motors, podded propellers offer flexibility in machinery arrangement and many of the other benefits afforded by electric propulsion. The absence of the rudder, shafting and supporting appendages in the podded propeller arrangement helps reduce hull drag, which in turn helps to increase the overall efficiency of the vessel. Furthermore, pods may be arranged such that they allow greater flexibility in hull form design than is presently possible with a traditional screw propeller system.

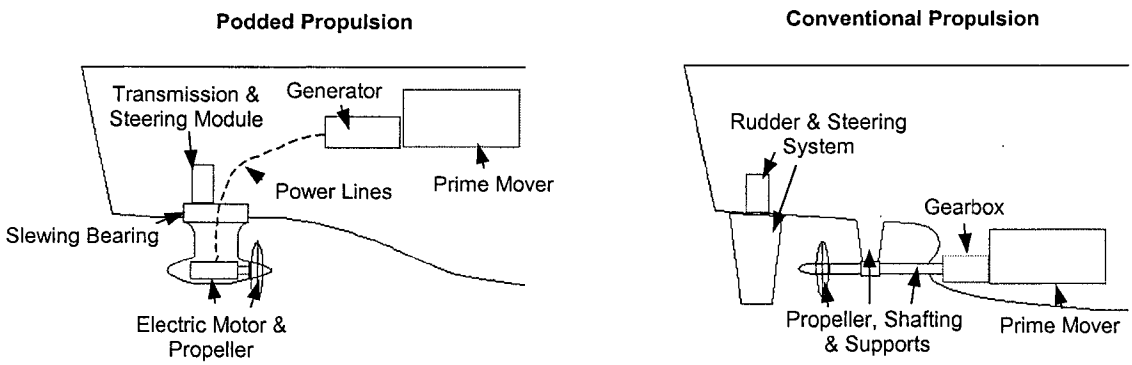

Figure 1.1: Podded Propulsion Concept vs. Conventional Screw Propulsion

The most common form of podded propulsion has been identified as having a single, fixed-pitch propeller directly coupled to the shaft of an electric propulsion motor, much like the one in the above diagram. The electric motor is encapsulated in a streamlined pod that is strut-mounted to a slewing bearing module. These slewing bearings transfer the propulsion loads to the hull structure, while allowing the unit to rotate about its vertical axis. Slip-rings permit the pod unit to azimuth, or rotate 360° about its vertical axis, without twisting and stressing the electrical connections, and are housed in a transmission and steering module. This module also contains the hydraulic actuators, which provide directional control of the podded propeller unit.

Podded propellers also offer an additional level of operational flexibility in that they may be designed to operate such that the propeller is located in front of the pod body and strut (pull mode) or with the propeller located aft of the pod body and strut (push mode), as illustrated in Figure 1.2 below.

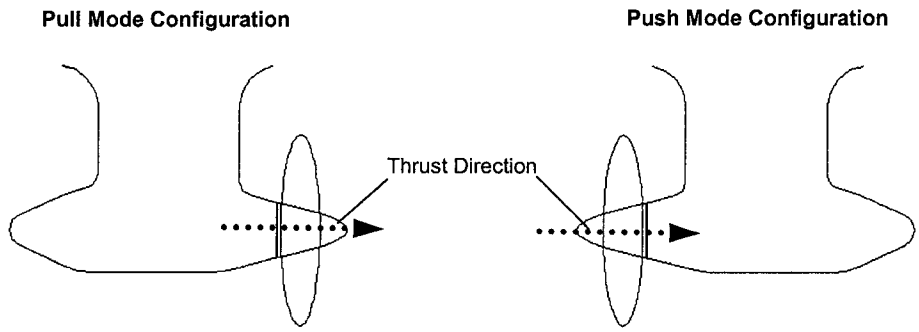

Figure 1.2: Pull Mode Configuration vs. Push Mode Configuration

For the purpose of this study, the generic terms 'podded propulsion', 'podded propellers', 'podded drives', 'pod units', 'pods' or any other adaptation of these terms are used to refer strictly to single screw, fixed pitch propeller, azimuthing, electric-drive propulsion units as described above unless otherwise specified.

1.5 Why Pods Have Become So Popular

For any propulsion technology to gain the widespread application and implementation that podded propellers have seen in recent years, it must clearly exhibit technical and economic advantages over other propulsion alternatives. The advantages of podded propellers are widely known and published. Ninni (1997), Trouwborst (1998), Brown (2003), and Tinsley (2004), amongst others, have examined the pros and cons of this propulsion concept in a variety of applications. Podded propellers combine the benefits of a conventional diesel-electric system with a number of hydrodynamic advantages specific to a podded configuration. The most common advantages cited by the above authors include:

- enhanced maneuverability characteristics
- increased hydrodynamic efficiency and fuel efficiency
- reduced cavitation, noise and vibration
- improved flexibility locating machinery/prime mover within vessel
- wider selection of prime movers possible due to location flexibility
- electric motors provide simple, reliable reversing capability
- high power density and small component sizes
- electric motors operate efficiently over entire RPM range
- well suited to ships with highly variable loads
- can use fixed pitch propellers instead of controllable pitch propellers
- can place propulsor in optimal position relative to ship wake
- well suited to ships with a large number of electrical auxiliaries
- propulsion arrangement offers more flexibility in hull form design
- propulsion unit can be built at a separate facility
- pod unit can be delivered later in the ship building schedule
- well suited to modular ship building; saves fabrication time and costs

Despite the many advantages offered by this technology, the development of podded propellers has had to face some significant technical challenges. Kontes and Kontes (2004) discuss a number of the mechanical and electrical failures encountered during the operation of Festival cruise liners fitted with pods, in addition to the methods used to resolve these problems.

Many of these problems have been of a mechanical nature. Due to the high magnitude and variability of the hydrodynamic loads acting on the pod units, according to Kontes and Kontes (2004), the most commonly reported problem areas are failed seals and bearings. In some instances failure of the lubricating oil system was found to be responsible for insufficient cooling of radial and thrust bearings. Additional problems with electrical components, such as electromagnetic interference, failed slip-rings and transformers, as well as some control issues have also been reported by Kontes and Kontes (2004).

Such problems are generally regarded as design specific issues and are typically addressed by the pod vendors and ship owners, rather than the naval architects and researchers designing the ships which use podded propulsion. One of the major challenges for these vendors is characterizing the hydrodynamic loading on the pod unit. Despite improvements, significant knowledge gaps still exist within the research community regarding pod-related hydrodynamics issues.

1.6 Current Problems within the Research Community

The majority of the current problems within the research community stem from the lack of scientific understanding about the behavior of podded propellers. They are innately more complex than conventional screw propellers because of fluid-structure interactions that occur between the propeller and the body of the pod unit. The overall propulsion efficiency of the pod unit must not only account

for the efficiency of the propeller, but should also factor in the influence of the pod body and strut on the propeller flow field, as well as the parasitic drag on the pod.

The development of appropriate methods to deal with these additional factors has presented challenges for members of the research community, and there is still some debate about what is the best approach to use. Unlike conventional screw propulsion, which has well established standards for instrumentation, testing procedures, and numerical modeling tools, only provisional standards exist for evaluating the performance of podded propellers.

It is not feasible for committees such as the ITTC to develop standard methods for every novel propulsor type and due to the low number of units in service in the early days of podded propellers, from a model-testing point of view, they were initially treated as unconventional propulsors. It was not until pods had gained more widespread application that it became necessary to develop testing standards specifically for podded propulsion. In an attempt to develop a standard approach, a provisional procedure, ITTC 7.5-02-03-01.3 (2002) has been published. These guidelines combine the testing methods developed for conventional screw propulsion with the advice of leading researchers in this field.

This knowledge gap has been identified by other researchers as well. The review of issues relevant to the design and application of podded propellers by Terwisga et al. (2001) concluded that while the concept of podded propellers and its design attributes are well known, there are "a number of pitfalls for the designer" as "relatively little empirical knowledge has yet been accumulated". Terwisga et al. (2001) continue by suggesting that this knowledge may be accumulated through comprehensive model testing, supplemented with CFD computations and full-scale measurement campaigns. Some of the specific hydrodynamic issues that require further investigation include questions regarding the effects of hub taper angle, pod-strut interactions, and pod-strut geometry on podded propeller performance, as well as several other instrumentation and testing related questions.

As illustrated in Figure 1.3, the geometry of the body and strut of a podded propulsor necessitates that the propeller have a conically tapered hub to allow for a smooth transition between subsequent sections of the propulsor. Since conventional screw propellers typically do not have tapered hubs, the influence of the taper angle on the performance of the conical hub propellers used with podded drives, in both push and pull configuration, have not been studied in great detail.

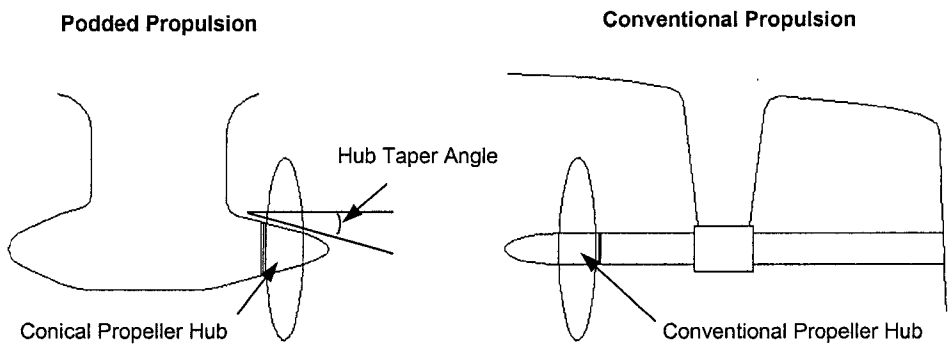

Figure 1.3: Conical Hub Propeller for Podded Drives vs. Conventional Propeller

In addition, there is presently some debate about the value of considering the open water efficiency of the propeller operating without the presence of the pod body and strut, much in the same manner as is presently done with a conventional screw propeller. While testing the propeller by itself is much simpler than testing as a podded propeller unit, this approach does not correctly model the true arrangement. The rationale provided by ITTC 7.5-02-03-01.3 (2002) for the 'propeller only' tests is that these tests allow one to determine the open water characteristics that may be used in propulsion tests and predictions.

In addition, it is indicated that these tests provide data that is useful for propeller design and as an estimation of the characteristics of the final design of the propellers. It may be argued that such results do not reflect the true

performance of the propellers in operation and so it is not valid to make such predictions. Without supporting evidence, however, it is difficult to justify such an argument. As such, additional research is necessary to assess the validity of such rationale and to address the knowledge gaps.

1.7 Addressing These Problems

To address some of the present questions arising within the podded propeller research community, a project has been undertaken at Memorial University of Newfoundland to systematically investigate many aspects of podded propeller performance. The importance of this project to the scientific and engineering community has been recognized through funding support from the Natural Sciences and Engineering Research Council (NSERC) and the National Research Council (NRC), along with industry partners Oceanic Consulting Corporation and Thordon Bearings.

As illustrated in Figure 1.4, this project consists of two parallel streams of research: experimental and numerical. The rationale behind the parallel development of both streams was to allow for the comparison and validation of results. As identified in the figure below, the focus of the research work considered in this study falls under the experimental branch of the project. One of the major challenges for the experimental team was the development of the specialized equipment necessary to study all of the desired elements of performance. The foundation of the entire experimental research program has been built on a custom-made instrumentation platform more commonly known as a propeller boat. This piece of equipment was required to evaluate the performance of podded drives and consists of a series of sensors and force transducers designed to measure the loads acting on the model-scale propulsor.

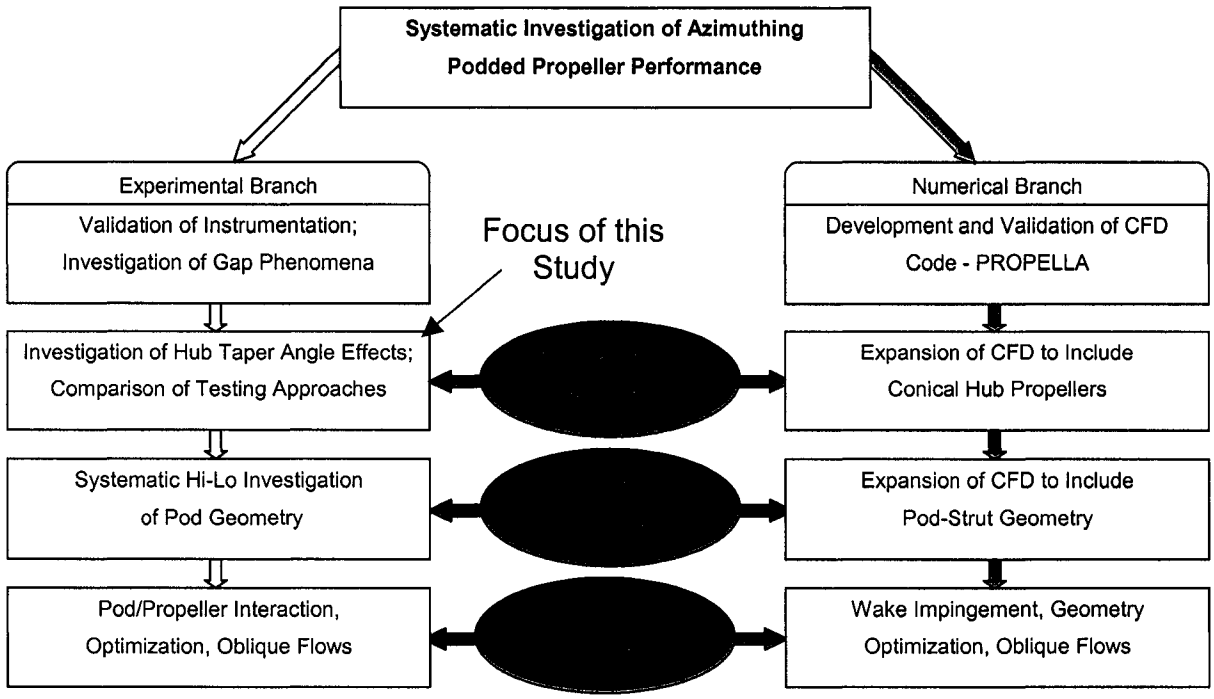

Figure 1.4: Overview of Project – Systematic Investigation of Azimuthing Podded Propeller Performance

In addition to investigating of the performance of model podded propellers, it was further decided that testing should be conducted in a manner that provides a basis for comparing the two testing approaches described in the provisional testing procedures recommended by the ITTC. For this reason, two series of experiments were conducted to allow for comparison of the results. The first series of tests consisted of a set of 'baseline' propeller tests, which considered the performance of the conical hub propellers using the same techniques utilized for conventional screw propellers without the pod body and strut present. The second group of experiments utilized the custom-made instrumentation to measure the forces and moments acting on the propellers with the pod and strut present, as well as the overall loads present on the entire podded propeller unit.

For the remainder of this thesis, the term 'baseline' has been used to describe this first series of experiments since the propellers were operating in the open water condition without the presence of the pod and strut. This condition

has been used as a 'baseline' for comparison with the results of the second series of tests.

When conducting commercial research, the main reason for measuring the forces and moments on the model-scale podded propeller units is that the results obtained simulate the loads that would be transferred from a full-scale podded propeller to the hull of the ship as it is propelled through the water. The magnitudes of the measured forces and torques on the model-scale propulsion unit are only a fraction of the full-scale loads. While the extrapolation of the data from model-scale to full-scale is beyond the scope of this study, the implications of non-dimensionalizing the results are still very relevant. Non-dimensionalization of the measured loads is vital in allowing for direct comparison of the results of each set of data. Therefore, further discussion of dimensional analysis and appropriate methods for data reduction are warranted to ensure the results obtained are presented in a relevant manner.

1.8 Data Reduction Equations

Prior to the development of a test plan it was decided that general consideration of the desired performance outcomes should be examined in further detail. The standard form of the data reduction equations identified in ITTC 7.5-02-03-02.1 (2002) for propeller open water tests for conventional screw propellers are outlined below in Table 1.1. These non-dimensional coefficients are typically plotted in the form of K_T, $10K_Q$, η_o vs. J charts, which is the most frequently used method of displaying propeller performance curves.

Performance Chararcteristic	Data Reduction Equation
K_T (Thrust Coefficient)	$T/(\rho n^2 D^4)$
K_Q (Torque Coefficient)	$(Q-Q_o)/(\rho n^2 D^5)$
J (Advance Coefficient)	$V/(nD)$
η_o (Open Water Efficiency)	$(K_T J)/(2\pi K_Q)$
Where:	
T = thrust	n = shaft speed
Q = torque	D = propeller diameter
Q_o = frictional torque	V = advance speed
ρ = density	

Table 1.1: Standard Non-dimensionalized Coefficients for Conventional Screw Propellers

Given the additional level of complexity of the podded propeller experiments, it was decided that a complete dimensional analysis of a generalized podded propeller should be conducted. The details of this generalized dimensional analysis are given in Appendix A. The forms of the equations used in this analysis were purposely generalized to allow for investigation of non-dimensional forms other than the standard set of coefficients. This was useful in confirming that the forms of the non-dimensional expressions shown in Table 1.1 are in fact the most appropriate alternatives available for the required performance results.

Using this analysis as a guide, it was then possible to adapt the generalized equations to the forms required for each of the measured parameters for both series of experiments as shown in Table 1.2.

Baseline Propeller Open Water Tests	
Performance Chararcteristic	Data Reduction Equation
K_T - Thrust Coefficient	$T/(\rho n^2 D^4)$
K_Q - Torque Coefficient	$(Q-Q_o)/(\rho n^2 D^5)$
J - Advance Coefficient	$V/(nD)$
η_o - Baseline Efficiency	$(K_T J)/(2\pi K_Q)$
Where:	
T = thrust	n = shaft speed
Q = torque	D = propeller diameter
Q_o = frictional torque	V = advance speed
ρ = density	

Podded Propeller Open Water Tests	
Performance Chararcteristic	Data Reduction Equation
K_{Tprop} - Propeller Thrust Coefficient	$T_{PROP}/(\rho n^2 D^4)$
K_{Tunit} - Unit Thrust Coefficient	$T_{UNIT}/(\rho n^2 D^4)$
K_Q - Torque Coefficient	$Q/(\rho n^2 D^5)$
J - Advance Coefficient	$V/(nD)$
η_{PROP} - Propeller Efficiency (on Pod)	$(K_{Tprop} J)/(2\pi K_Q)$
η_{UNIT} - Unit Efficiency (on Pod)	$(K_{Tunit} J)/(2\pi K_Q)$
Where:	
T_{PROP} = propeller thrust	n = shaft speed
T_{UNIT} = unit thrust	D = propeller diameter
Q = torque	V = advance speed
ρ = density	

Table 1.2: Final Forms of Data Reduction Equations

As shown above, the measurement variables of interest for the baseline experiments were identified as thrust, torque and advance speed. All remaining experimental parameters were held constant for these tests. For the podded propeller experiments the variables of interest were the propeller thrust, torque, advance speed and the overall thrust of the pod unit (unit thrust). For clarification, the definitions of all non-dimensional coefficients and terms shown above are explained in further detail in Table 1.3.

Baseline Test Definitions
K_T **(Thrust Coefficient):** Non-dimensional form of the baseline propeller thrust
K_Q **(Torque Coefficient):** Non-dimensional form of the baseline propeller torque
J (Advance Coefficient): Non-dimensional ratio of the advance speed to the shaft speed
η_o **(Baseline Efficiency):** Open water efficiency of the propeller without pod and strut present
T (Thrust) : The axial component of force generated by the rotating propeller blades
Q (Torque): The axial moment required to rotate the propeller at the desired shaft speed
Q_o **(Frictional Torque):** The additional torque component due to friction in bearings and seals
Podded Propeller Test Definitions
K_{Tprop} **(Propeller Thrust Coefficient):** Non-dimensional form of the thrust of the propeller installed on the pod
K_{Tunit} **(Unit Thrust Coefficient):** Non-dimensional form of the unit thrust of the podded propeller
K_Q **(Torque Coefficient):** Non-dimensional form of the torque on the propeller shaft
J (Advance Coefficient): Non-dimensional ratio of the advance speed to the shaft speed
η_{PROP} **(Propeller Efficiency):** Open water efficiency of the propeller operating on the pod unit
η_{UNIT} **(Unit Efficiency):** Overall efficiency of the entire pod unit, which factors in the drag of the pod and strut
T_{PROP} **(Propeller Thrust):** Axial component of force generated by the propeller when installed on the pod unit
T_{UNIT} **(Unit Thrust):** Net axial thrust generated by the pod unit; Includes the drag of the pod and its influence on the prop
Q (Torque): The axial moment required to rotate the propeller at the desired shaft speed
General Definitions
ρ **(Density):** The calculated density of fresh water at the test temperature
n (Shaft Speed): The rotational speed of the propeller shaft
D (Propeller Diameter): The diameter of a circle which circumscribes the tips of the propeller blades
V (Advance Speed): The speed at which the tow carriage advances the propeller down the tank

Table 1.3: Definition of Data Reduction Terms

The final selected forms of the equations also had to factor in some of the practical considerations of the equipment and procedures used. As explained in Chapter 6, differences in the data collection and analysis procedures for each series of experiments had implications for the uncertainty analysis. Based on this knowledge, further discussion of the reasoning behind the forms of the equations is warranted here.

As observed in Table 1.2, the torque coefficient for the podded propeller tests was modified such that it does not require the subtraction of a frictional torque term. This data set was not influenced by friction, as this custom built instrumentation was designed such that there were no bearings or seals located between the propeller and the strain gauges. Correspondingly, no friction term is

included in the data reduction equation for torque for the results of the podded propeller tests.

The propeller shaft of the instrumentation used in the baseline series of tests has bearings and seals between the strain gauges and the propeller, and as such the frictional influence of these components must be subtracted from the measured torque value. Because this is a post-processing subtraction and not merely part of the data collection process, the frictional toque must be treated as a separate variable.

As can be seen, all of the thrust coefficient equations are of the same basic form as the generalized equation shown in Table 1.1. For this measurement, additional consideration of the data collection and analysis is also beneficial to clarify the difference in treatment between tare thrust and frictional torque. As discussed in Chapter 3, a piece of instrumentation is typically calibrated and zeroed, so that it outputs zero voltage when there is no load applied. Sealed thrust measurement equipment offers a slight variation to this concept since a non-zero voltage reading may be present even after calibrating and zeroing the equipment. This observation may be explained by static friction in the seals and bearings, which causes these components to retain small amounts of residual loading that prevents the propeller shaft from completely moving back into its rest position.

To eliminate the influence static friction on the shaft has on the thrust reading, the zero thrust value is taken by measuring tare thrust while the propeller turns at a very slow shaft speed, as is described in more detail in Chapter 3. The main premise behind this approach is that at such a slow speed the propeller is not generating any thrust, but the rotation serves to break the static friction between the shaft and its bearings and seals. This releases any residual axial loading that may have been in these components and in doing so, ensures that the load cell is in the true no-load condition.

The tare thrust is measured at the beginning of each individual test run and is contained within the same data file as the actual thrust reading for that particular run. This is much different than frictional torque, which is determined from a separate set of tests specifically designed to characterize the dynamic frictional behavior of the instrumentation. The tare thrust is, in effect, the zero-thrust point within a particular data file and this subtraction is an internal part of the data analysis process. This is not a post-processing calculation using a separate data stream, as is this case with the torque reading. For this reason, the data reduction equations do not include a separate term for the tare thrust values.

Chapter 2 – Literature Survey

2.1 Scope

The primary focus of this section is to provide a snapshot of the current state of experimental research in the field of podded propulsion through a review of the published literature. Given the relatively small time lag between the development of podded propellers and their commercialization, there is little non-proprietary performance research available on this topic. Much of the information that is available in this area is general and qualitative in nature. Furthermore, many of the available publications are written by representatives of commercial pod vendors and have inherent biases in the information they present. Given the focus of this thesis, the literature review has been written to provide both a technical review and contextual overview of podded propeller research. The first two sections of this chapter summarize the technical aspects of hydrodynamics and related experimental publications, while the latter two sections attempt to present a summary of research in the context of both commercial and military applications.

2.2 Hydrodynamic Considerations

In the early days of podded propeller research, experiments were sporadic and topics covered by researchers varied widely, as initial interests were focused on acquiring a broad understanding of the propulsion system and assessing if pods were a viable propulsion alternative.

Rains et al. (1979) published the first description of the podded propeller concept for naval applications. The first published results of model tests conducted specifically to investigate podded propulsor hydrodynamics were

published by Rains et al. (1981). The results of Rains et al. (1981) examined the total drag of the pod unit and discussed powering predictions for vessels fitted with pods. This study only considered non-azimuthing pods (fixed to the hull) and used hull forms that were not modified to take advantage of the flexibility offered by podded drives. The main conclusion of this initial study was that without removing appendages or modifying the hull form to take advantage of this flexibility, the podded propulsors studied did not show hydrodynamic advantages over a conventional propulsion arrangement.

Hydrodynamic investigations focused specifically on the performance of podded propulsors did not come into the mainstream research community until the 1990s, when the use of commercial podded propulsion began to gain momentum. Kurimo et al. (1997) presented the results of a comprehensive series of model tests conducted during the development of the ABB Azipod®. It was concluded that pull type podded propellers offered clear hydrodynamic advantages over push type pods. Furthermore, for the same hull it was concluded that podded propellers could provide a 3-4% savings in the measured delivered power when compared to a conventional twin screw arrangement.

Holtrop (2001) presented a discussion of methods used for extrapolating model scale results to full scale for powering predictions. This work identified the need for enhanced knowledge of the drag present on the pod housing and strut. Furthermore it provided a discussion of blade thrust and shaft thrust in podded propeller instrumentation and the differences between these measurements. It was noted that the size and shape of the hub, along with other pod particulars caused the blade thrust to depart from the shaft thrust by several percent. Holtrop (2001) defined experimentally the drag of the pod housing and strut as the difference between the propeller thrust and the unit thrust.

Mewis (2001) has presented the results of a series of open water tests for a number of test configurations. Included is a discussion of the influence of the width of the gap between the back face of the propeller hub and the front face of

the pod body on the measurement of the thrust generated by the propeller. The pressure in this gap was investigated as a function of the gap width. Based on these results, it was concluded that the unit thrust is not influenced by the width of this gap, but the propeller thrust is highly dependant on gap spacing. Recommendations were made to use only the unit thrust for comparison of propulsion efficiency. This work also included a discussion of instrumentation and testing issues, and examined the influence of Reynolds number on thrust readings.

In addition, Mewis (2001) provided a comparison of the efficiency of a podded propulsion system with that of a conventional propeller and rudder configuration. For these tests, the conventional propeller and rudder were observed to have an efficiency 5% higher than the pod unit at the design advance ratio.

Szantyr (2001) presented measurements of lift forces, drag forces and moments for a variety of propulsor configurations tested at different yaw angles and advance coefficients. Included in these are a pod/strut model without a propeller, a push mode pod unit (with propeller) and a pull mode unit (with propeller). He concluded that the axial force is higher for small non-zero angles, than for a zero yaw angle.

Others have considered the effects of the geometry of pod body and strut on the performance of the propulsion unit. Halstensen and Leivdal (1990) concluded that the choice of the strut profile is one of the most important design aspects of pull mode pod units designed for high speed applications. Included in this discussion was a description of the impact of strut cavitation on the resistance of the pod and the overall efficiency of the unit. By using an appropriate strut profile which allowed for the recovery of some of the rotational energy in the propeller slipstream, Halstensen and Leivdal (1990) indicated that it was possible to reduce the overall resistance of the strut and pod.

The paper by Heinke and Heinke (2003), as well as Karafiath and Lyons (1999) provide a discussion of the influence of various geometric particulars, such as the length and diameter of the pod body and the propeller arrangement, on the open water performance of podded propellers. In these papers, the authors distinguish between the unit thrust and the propeller thrust.

Bertaglia et al. (2004) examined a variety of aspects of design and optimization of hull forms for podded propellers with four, five and six blades. This paper considered the systematic investigation of the influence of the number of blades on the performance of the propeller from a powering and cavitation point of view.

Goubault and Perree (2004) discussed parametric investigations of pod geometry aimed at focusing pod technology developments, based on optimizing various characteristic ratios, including the ratio of propeller diameter to pod diameter.

Heinke (2004) presented results of model tests carried out with four and five bladed model podded propellers in both push and pull mode. This study included an investigation of the interaction between the propeller and the pod body, as well as the influence of the propeller hub geometry. Only two propeller hub arrangements were considered, the pull hub and the push hub, for both four and five bladed propeller models. These two hubs had nearly the same hub ratios, and the influence of the taper angle was not varied or considered. The effect of steering angle on the forces and moments acting on push and pull mode podded propellers has also been presented.

This study showed that the 'propeller only' performance was the same for the four and five bladed propellers. For the podded drives, the five bladed versions had higher total efficiencies than the four bladed podded drives. Furthermore, Heinke (2004) concluded that cavitation only has a small influence on the moments and forces for propellers with a low number of revolutions and for blocked propellers.

In addition to focusing on the hydrodynamics of the pod units themselves, a number of researchers have presented results of studies focused on the overall performance of model-scale vessels fitted with pods. Cheng et al. (1989) present an evaluation of various hull forms with podded propellers using computational methods for use in conjunction with experimental methods to design pods for naval vessels. Lavini (2000) discussed twin screw ships with podded drives and provided a description of design considerations for exisiting hull forms, slightly modified hull forms and completely redesigned stern geometry for new vessels. In addition, Lavini (2000) proposed a new blade design approach for designing propellers for pods. Lepeix (2001) also considered hydrodynamic issues related to hull form design, with a particular focus on large cruise ships with pods. Topics discussed in this paper include an overview of changes in the hull lines due to the flexibility offered by pods, in addition to the effect this has on the ship's wake, the resistance of the hull and the building process. Nakatake et al. (2004) considered the propulsive performance of a small bulk-carrier model fitted with twin podded propellers, while Ball (2004) examined hull motion responses, together with propeller shaft and pod strut loads during calm water, free maneuvering experiments.

A number of researchers haves focused specifically on cavitation, noise and vibration aspects of podded propeller hydrodynamics. Chen and Tseng (1995) published a paper on pull mode pods in applications with high-speed vessels, in which they discussed the cavitation performance of the propulsor, as well as some powering issues. Heinke (2001) presents model test results for pull mode pods fitted to a corvette and examines power requirements, wake field, cavitation and maneuverability behavior. Based on the effects of the cavitation, he concludes that the strut should be asymmetrical.

Pustoshny and Kaprantsev (2001) described observations of full-scale cavitation behavior made during maneuvering and speed trials, while Friesh (2001) has presented the results of cavitation observations and wake field

measurements combined with noise and pressure fluctuation measurements for different model-scale pod arrangements. Friesh (2001) showed that for twin screw vessels, pull mode pod drives display advantages in terms of cavitation and noise behavior when compared to conventional propulsion. Further work in this area, by Friesh (2004), considered cavitation, noise and vibration aspects of both stationary and moving podded drives in several different configurations.

Others have examined more specialized cavitation conditions, such as those presented by Atlar et al. (2003), which described the specialized test set up and preliminary results for cavitation observations on ice-class propellers during ice milling operations. Hämäläinen and Heerd (2003) provided a discussion of the influence of a wave damping after body on improving hull efficiency, as well as the wake field and the implications this has on the cavitation pattern and propeller induced pressure pulses.

As one of the main advantages of podded propulsion, maneuverability aspects of vessel performance have also received considerable attention. Toxopeus and Leoff (2002) considered maneuverability aspects of fast ship applications for conventional and podded propulsion systems, highlighting many of the benefits of pods.

Kurimo et al. (2003) present the results of full-scale maneuvering trials for the cruise ship, Costa Atlantica. These full-scale results are correlated with model-scale results and a discussion of scale effects in mathematical maneuvering simulations for both model and full scale is provided.

Kobylinski (2004) presented the results of a series of maneuverability tests for model-scale vessels fitted with podded propulsors. These tests included a variety of standard and non-standard tests aimed at characterizing the ease of handling of the ship under different operational conditions.

Ayaz et al. (2004) provided a description of a variety of maneuvering aspects of pod driven ships and compare maneuvering with podded propulsion to that of a conventional propeller-rudder configuration. Investigations of directional

stability and the effect of the large pod-induced heel angles on the turning capabilities are considered.

Others have focused on the steering system itself. Thomsen (1999) discussed the features of the analog steering system used to control the ABB Azipod®. Stettler et al. (2004) provided a discussion of the maneuvering dynamics of podded propulsors from a control and simulation point of view and included preliminary results of model-scale towing tank tests and particle image velocimetry (PIV) tests.

Terwisga et al. (2001) provide a review of issues relevant to the design and application of podded propellers, with a particular focus on the design of the Seimens-Shottel SSP podded propulsor. The authors describe a number of different hydrodynamic issues, such as thrust effectiveness, thrust density and maneuverability. This paper describes many practical aspects of the performance of the full scale podded propellers and identifies the need for further hydrodynamics research to assist designers.

Lepeix (2001) also provided a discussion of the influence of changes in hull form to the maneuverability of the ship, as well as the levels of pressure pulse induced hull vibrations. Ruponen and Matusiak (2004) presented a description of a calculation method for estimating the steering forces of a podded propulsor operating in a hybrid contra-rotating arrangement. This method has been validated through comparison with data obtained from an extensive model test program.

Turan et al. (2004) have examined the effect of podded propulsors on the roll behavior of passenger vessels. Sarioz et al. (2004) examined operability aspects of high-speed podded ships in rough sea conditions.

Other researchers, such as Boushkovsky et al. (2003) and Woodward et al. (2004) have focused on aspects of modeling ship behavior under very specific operational procedures, such as during various types of emergency crash stop maneuvers.

2.3 Related Experimental Work

Most publications in the podded propulsion field focus primarily on the results of the experiments rather than on the design of the complex instrumentation required to test them. As such, very little technical information has been published on this topic and most authors give only brief, if any, descriptions of the equipment used. Most authors describe the capabilities of their instrumentation, but not the specifics of the design.

Mewis (2001) provided a valuable overview of the basic requirements of the equipment necessary to conduct open water tests on podded propulsion. This paper provides a good set of guidelines for the conceptual design phase of an instrumentation package.

The paper by Akinturk et al. (2003) which discusses performance tests for podded propellers operating in ice, also includes a description of the model podded propeller unit and the instrumentation design. Similarly, Ukon et al. (2004) provided a general description of the capabilities of custom instrumentation designed and manufactured to test concentric shaft, contra rotating podded propulsor models.

The paper published by MacNeill et al. (2004) offered a detailed description of both the capabilities of the podded propeller instrumentation, in addition to many of the details of its design. This paper offers a great deal of insight into the workings of the instrumentation used for conducting podded propeller open water experiments. The instrumentation package described in this paper has been used to collect all experimental data for the model podded propellers studied in this thesis.

DiFelice et al. (2004) presented a description of Laser Doppler Velocimetry (LDV) and Particle Image Velocimetry (PIV) equipment and techniques used in applications for experimentally investigating flow fields around a variety of

propulsion systems, including podded propulsors. The authors determined that these techniques are very valuable for enhancing the understanding of flow around complex propulsors and for use in the development and validation of numerical tools.

Wang et al. (2004) provided a similar description of the Laser Doppler Anemometry (LDA) equipment and procedures used to characterize flow fields around a podded propeller unit. Based on the results presented by Wang et al. (2004) it may be concluded that the pod has a noticeable effect on the magnitude and distribution of the wake and that LDA is a useful technique for measuring the velocity distributions needed to characterize the wash velocity of the podded propeller.

Several specialized applications of podded propulsors have also gained considerable attention within the research community. The two most widely covered of these are the contra rotating propeller (CRP) concept with a podded drive and ice applications for podded propulsion.

The benefits of contra-rotating propellers are widely known, as described by Friesh (2004). This contra-rotating capability has taken a new form with podded propulsors, whereby the sterns of existing single screw vessels may be modified to accommodate a podded propeller with opposite propeller rotation direction installed directly behind the conventional screw propeller. The pros and cons of this type of propulsion arrangement are presented by Backlund and Kuuskoski (2000).

A number of authors have explored various other aspects of this contra-rotating podded propulsion concept. Kim et al. (2002) presented model test results for the CRP podded propulsor arrangement, along with a variety of propulsion alternatives for use with ultra large containerships. Hämäläinen and Heerd (2003) also considered a contra-rotating propulsor concept, using a combination of conventional and podded propulsion with a wave damping aftbody hull design. This paper included a description of the analytical and experimental

results obtained from tests conducted to evaluate this propulsion arrangement. Boushkovsky et al. (2004) presented results of a series of model tests on a CRP podded propeller system which examined the cavitation behavior, as well as periodic forces and crash stop loads.

Ruponen and Matusiak (2004) examined steering forces of a podded propulsor operating in a CRP podded propulsor configuration, while Seokcheon et al. (2004) presented model testing procedures and performance predictions for this type of propulsion arrangement. Based on the results presented, Seokcheon et al. (2004) suggest a method for conduction powering performance evaluations for ships fitted with CRP podded propeller configurations.

Chen and Tseng (1995) and Ukon et al. (2004) have considered a different type of CRP pod concept. These authors have presented results of studies considering single podded propeller units with two contra-rotating propellers mounted on concentric shafts (similar to conventional contra-rotating screw propellers). Ukon et al. (2004) examined a variety of aspects of the performance of the individual propellers, the total performance of the propellers operating together, as well as the overall unit performance of the podded propeller unit. This propulsor is considered in both open water and self-propulsion type tests.

A number of researchers have focused their efforts on ice applications for podded propellers. Veitch (1995) conducted a study on propeller-ice interactions related to pod development. Akinturk et al. (2003) published a description of equipment used to measure blade loads, propeller shaft and bearing loads, as well as the global loads acting on podded propellers in ice, with the intent of filling in knowledge gaps required to update arctic shipping regulations for vessels fitted with podded drives. The preliminary results of this research were presented by Akinturk et al. (2004) and demonstrated the functionality of the equipment used in this test program. Atlar et al. (2003) investigated the influence of blockage and milling on the performance of ice class propellers during ice-milling operations.

Another description of ice applications for podded propulsion has been published by Sasaki et al. (2004) for double acting tankers, which are tankers designed with a bulbous bow for efficient open water operations and an ice breaking stern, which allows the vessel to operate in ice-infested waters. This paper provides a discussion of extensive experience obtained from tests conducted at both model-scale and full-scale. Trägärdh et al. (2004) provided a description of experience obtained through model testing and full-scale trials with double-acting tankers, with a particular focus on the hydrodynamic characteristics of the propulsion system designed for use in both open water and ice applications.

2.4 Commercial Applications

Several papers have been published by commercial vendors describing the experience gained during the development of their podded propulsion systems. For instance, a number of papers were published discussing the ABB Azipod® used in cruise ship applications. This includes a paper discussing hydrodynamic and operational issues published by Laukia (1996), along with a paper by Niini (1997), which looks at some application-specific issues regarding maneuverability, efficiency and various other hydrodynamic concerns relevant to large cruise ships. Niini (1997) also provided a thorough discussion of possible hull design improvements offered for vessels using podded propulsors from the point of view of machinery location as well as cargo capacity.

A paper by Kurimo et al. (1997) presented the results of the Azipod® research and development program and described the findings of the different approaches taken to optimize the performance of the Azipod®. This discussion included aspects of pod drag, interactions between propeller and pod body, steering forces and moments, as well as flow conditions over the unit. These

measurements included model-scale towing tank and wind tunnel experiments. In another paper by Kurimo (1998), a description of the sea-trial results for the first passenger cruise ship fitted with podded propellers is provided. In this paper various hydrodynamic and operational issues of the full-scale ship are considered. This includes a discussion of cavitation observations, pressure pulses measured on the hull, in addition to a description of the performance of the vessel during speed and maneuverability trials.

A paper by Kron and Holmstrom (1999) described the results of the experimental and numerical hydrodynamics work required to bring the Mermaid® podded propulsor to market. This publication includes a description of the model test results and their use in validating numerical predictions. The authors discuss a variety of hydrodynamics issues including maneuverability, propulsion efficiency, cavitation and pressure pulse measurements. A discussion of practical considerations is presented and includes topics such as compromises between hydrodynamic performance and strength considerations, and the influence of the hydrodynamic loadings during maneuvering and crash stops on the strength requirements of the propulsion unit.

Many of the operational factors are tracked by trade news, regulatory bodies or are published by ship owners and operators to highlight where improvements may be achieved. In his paper on podded propulsors, Carlton (2002) provided a practical discussion of operational and design issues with pods based on in-service experience. This description included some common failure mechanisms in full-scale podded propulsors and potential solutions. Jones (2000) provided a discussion of the failure of the radial bearings in ABB Azipod® units, which led to the dry-docking of two vessels belonging to Carnival Cruise Lines.

Woodyard (2001) presented a discussion of ongoing developments in podded propeller technology, while Jones (2002a) published another discussion of bearing and seal failures, along with some of the underlying causes. As reported by Jones (2003), cruise operators began using stress wave analysis sensors and software to plot incidence of damage to a propulsor, thereby allowing for better monitoring of the condition of the bearings and other propulsion components. This in turn helped minimize the risk of future failures.

Kontes and Kontes (2004) presented an insightful description of the operational experience gained by Festival cruise lines from the operation of their cruise ships fitted with podded propulsors. This paper describes advantages and disadvantages of podded propulsion, along with a description of the mechanical and electrical failures. In addition, the methods used to resolve these problems are presented and evaluated.

Podded propulsion is well suited to many commercial vessel types, but it is difficult to make generalized statements of benefits without considering each vessel type and its operational profile. While the majority of commercial podded propellers presently in service are installed on cruise ships, a number of other vessel types have been either fitted with pods or considered for use with podded drives. While it is beyond the scope of this literature review to consider every possible vessel type fitted with podded propellers, a summary of publications considering application specific details has been included in Table 2.1 below.

Application	Authors
Offshore Vessels	Raynor (2000); White (2000)
Rigs/Small Vessels	Perttu and Matti (2001); Kaul (2004);
Semi-Submersibles	Jones (2002b)
Ropax Vessels	Sarioz et al. (2004)
Fast Ferries	Kanerva (1999); Mullins (2003)
Bulk-Carriers	Nakatake et al. (2004)
Cargo Vessels	Müller (1999)
LNG Tankers	Ikeda and Ikeda (2002)
Double-Acting Tankers	Sasaki et al. (2004); Trägärdh et al. (2004)
Ultra-Large Container Ships	Tozer and Penfold (2001); Kim et al. (2002); Holtrop and Valkhof (2003); Seokcheon et al. (2004)

Table 2.1: Summary of Publications Examining Commercial Vessel Types Other than Cruise Ships

2.5 Military Applications

As mentioned in previous sections, podded propeller research has military roots, as described by Karafiath (1998). Despite the fact that it was not until the late 1970s that pod-specific projects were undertaken, several earlier research programs undertaken by the U.S. Navy provided information relevant to podded propulsion research. One such example noted by the above authors included an investigation for escort ships using large non-azimuthing pods fixed to the hull of the vessel. In the configurations studied in these experiments, the propeller was mounted on the aft side of the 'hull pods' and a rudder was used for maneuvering. Several conceptual 'pod' designs were considered in this study, with the main objective being to examine the powering and cavitation performance.

Other early pod-related work described by Karafiath and Lyons (1999) included testing on hydrofoil propulsion systems. In these vessels, mechanically driven pod-strut propulsion was used for its ability to allow the propulsion unit and

the hydrofoil to be retracted out of the water. The knowledge gained from these tests was used as an early guide for podded propulsion research.

The first set of published experimental results focused specifically on podded propulsor hydrodynamics was provided by Rains et al. (1981). This paper provided a detailed look at several aspects of pod hydrodynamics, including consideration of the total drag of the pod and strut, as well as full-scale powering predictions for vessels with podded drives. The pods considered in this study did not have azimuthing capabilities, but rather were fixed to the hull of the vessel and as such the maneuverability advantages were not recognized. In addition, the hull forms used were not modified to take advantage of improved inflow to the propellers and appendages were not removed. As such, this initial study concluded that without removing appendages and improving hull form, the podded propulsors studied did not appear to offer significant advantages over conventional propeller and rudder configurations.

The application of podded propellers for surface combatants in the U.S. Navy was again considered by Facinelli and Muggeridge (1998) in a paper published on integrated system analysis and design. The analysis approach presented in this paper focused on the optimization of the cost and performance of the podded propeller system by using an integrated model which considered the cost and performance of all the major components of the propulsion system.

In addition to providing a synopsis of some of the research that has historical relevance to the development of podded propellers, Karafiath and Lyons (1999) discussed various hydrodynamics issues related to podded propulsion and presented a summary of the experimental research conducted by the U.S. Navy in this field. Karafiath and Lyons (1999) also provided a description of experimental results focused on investigating the hydrodynamic issues relevant to high speed vessels for the U.S. Navy.

While the U.S. Navy has published more experimental results of technical research on podded propellers than other navies, it is not the only country to

have considered this propulsion alternative for its naval fleet. Batsford (2002) provided a discussion of the viability of using podded propellers in future Canadian warships, while Jones and Dyck (2002) provided a description of the first UK Royal Navy vessel converted to use integrated electric propulsion and podded propellers. Sigrist et al. (2004) presented a description of potential approaches to take to militarize podded propulsor designs, including descriptions of methods and results of investigations aimed at characterizing the acoustic signatures, radiated noise levels and underwater shock resistance of pod designs.

Military propulsion systems have very strict specifications. At present, this technology has not advanced sufficiently to secure the same widespread acceptance amongst the world's navies as it has in many other industry sectors. As the understanding of podded propeller technology advances and vendors gain more operational experience, the likelihood of this propulsion alternative being able to meet these demands will increase.

Chapter 3 – Experimental Apparatus

3.1 Scope

The main purpose of this chapter is to describe in detail the equipment used to conduct the experiments in this investigation. Details of the propeller geometry, as well as the pod and strut geometry are presented. In addition, the experimental set-ups for the baseline propeller experiments and the podded propeller tests have been included. The first series of tests, the baseline propeller experiments, were conducted at the Institute for Ocean Technology (IOT) branch of the National Research Council of Canada (NRC). The second series of experiments, the podded propeller tests, were conducted at the Ocean Engineering Research Center (OERC) towing tank facilities at Memorial University of Newfoundland (MUN). Brief descriptions of these test facilities have been provided.

3.2 Model Propeller Geometry

One aspect of propellers designed for use with podded propulsors that distinguishes them from a conventional screw propeller design is that of the propeller hub geometry and the associated interface between the blade root and the hub. To provide a smooth transition between the geometry of the propeller and the geometry of the larger diameter pod body, it is necessary for the propeller to have a conical hub profile as illustrated in Figure 3.1 below. Depending on the overall length and the diameter of the fore and aft faces of the hub, the propeller hub will have a different taper angle. As described in the

previous chapter, the influence of this taper angle on the performance of propellers and podded propulsion units has not been characterized.

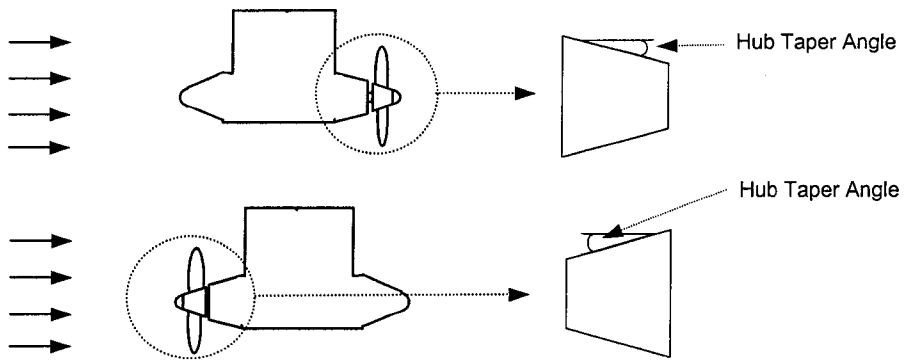

Figure 3.1: Identification of Hub Taper Angle in Push and Pull Mode Podded Propellers

To assess the influence of this taper angle on the performance, a series of four model propellers were designed by Dr. Pengfei Liu. This series consisted of propellers with 15° and 20° hub taper angles in both push and pull modes, as summarized in Table 3.1.

Hub Taper Angle	Mode of Operation
15°	Push
20°	Push
15°	Pull
20°	Pull

Table 3.1: Propeller Configurations Studied

All remaining geometric particulars of these propellers, except the taper angle and the mode of operation, were held constant. The geometry for these propellers was generated using a customized code as described by Islam (2004). This numerical code was originally developed for conventional cylindrical hub

screw propellers and was modified to include tapered hubs. The particulars of the propeller designs are outlined in Table 3.2 below.

Diameter (m)	0.270
Number of Blades	4
Rotation (viewing at downstream)	Right Hand
Design Advance Ratio, J	0.8
Hub-Diameter Ratio, H/D	0.26 (based on cylindrical hub)
Angular Speed (RPM)	2222
Section Thickness Form	NACA 66 (DTMB[1] Modified)
Section Meanline	NACA = 0.8
Expanded Area Ratio, EAR	0.6
Pitch Distribution	Constant, P/D=1.0
Skew Distribution	Zero
Rake Distribution	Zero
Blade Planform Shape	Based on DTMB[1] Model P4119

[1] DTMB - David Taylor Model Basin

Table 3.2: Geometric Particulars of Model Propellers

Additional details of the sectional geometry of these propellers have been published in a report by Kavanagh (2004) and as such further discussion of the normalized cross-sectional geometry has not been included here.

Figure 3.2: Finished Model Propellers

The propeller geometry generated with the above input parameters was used to produce a CAD model of each of the individual propellers. These CAD files were then used to generate the CNC code required to manufacture the model propellers. The machining of the model propeller was completed at the Technical Services division of Memorial University of Newfoundland using a computer numerically controlled milling machine. The final processing step for the model propellers shown in Figure 3.2 above was to hand polish the bronze blades to attain the desired surface finish.

3.3 Model Pod Shell and Strut Geometry

Prior to developing a model pod, it was first necessary to define the geometry of the pod shell and strut in terms of a general set of geometric parameters. Due to the large number of parameters required to completely define the pod geometry, certain simplifications were necessary. The resulting dimensions identified as being most important to the definition of the pod geometry are identified in Figure 3.3.

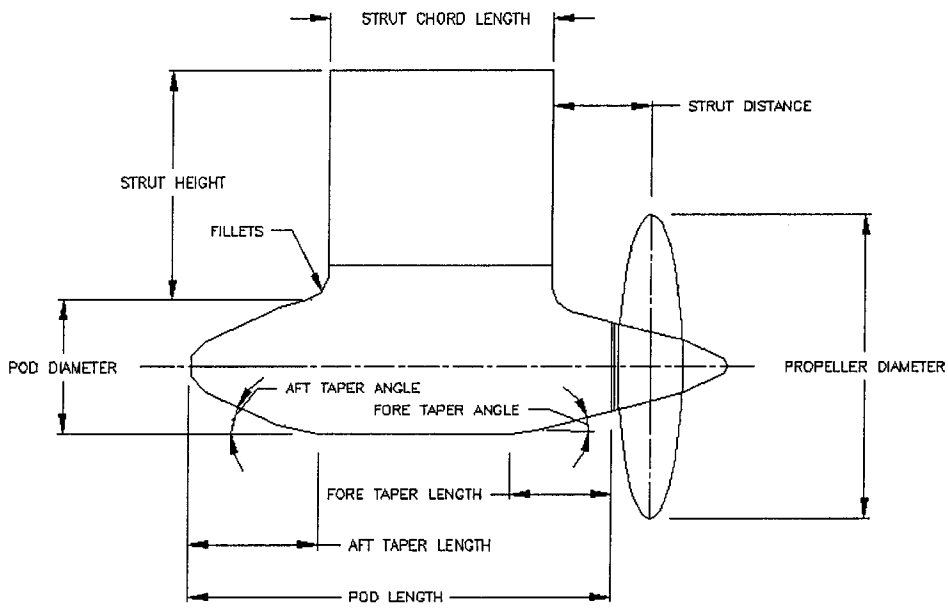

Figure 3.3: Geometric Parameters Used to Define Model Pod Geometry – after Molloy et al. (2004)

Once these parameters had been identified, the corresponding model pod geometry files were constructed using the parametric values indicated in Table 3.3 as explained in further detail by Molloy et al. (2004). Since the push and pull mode podded propellers used the same external pod geometries, only two different pod bodies were required. As indicated in the table below, the only difference between these two geometries was the fore taper angle of the pod. This parameter corresponded to the hub taper angle of the propeller to ensure smooth transition between the propeller and pod body.

Parameter	Pod No. 1	Pod No. 2
Pod Diameter	139 mm	139 mm
Pod Length	410 mm	410 mm
Strut Height	300 mm	300 mm
Strut Chord Length	225 mm	225 mm
Strut Distance	44 mm	44 mm
Strut Width	60 mm	60mm
Fore Taper Length	85 mm	85 mm
Fore Taper Angle	15°	20°
Aft Taper Length	125 mm	125 mm
Aft Taper Angle	25°	25°
Fillets	50 mm	50 mm

Table 3.3: Geometric Particulars of Model Pods

Using the above dimensions, the CAD files for the model pod bodies and struts were generated. These CAD files were then used to generate the CNC code required to machine the scale models. The actual models were machined out of Renshape^{TM} at MUN Technical Services. The desired surface finish was obtained by sanding and painting the models.

3.4 Instrumentation for Baseline Propeller Experiments

The main objective of these experiments was to provide a baseline evaluation of propellers designed for pod units operating in the open water condition without the presence of the pods. These experiments were conducted in the towing tank facility at the Institute for Ocean Technology (IOT). This facility is 200m in length, 12m in width and 7m in depth. The model propellers were towed through still water by a carriage spanning the width of the tank. The carriage speed capabilities range from a minimum of 0.001 m/s to a maximum of

10.0 m/s. The propeller instrumentation was aligned on the rails of this tow carriage and securely clamped in place.

The instrumentation used for these experiments was the Kempf & Remmers dynamometer depicted in Figure 3.4 below. This particular instrumentation package was selected based on its established reputation of producing very high quality data. This particular dynamometer allowed for the measurement of propeller thrust and torque data over the selected range of advance coefficients required to characterize the performance of the propellers of interest.

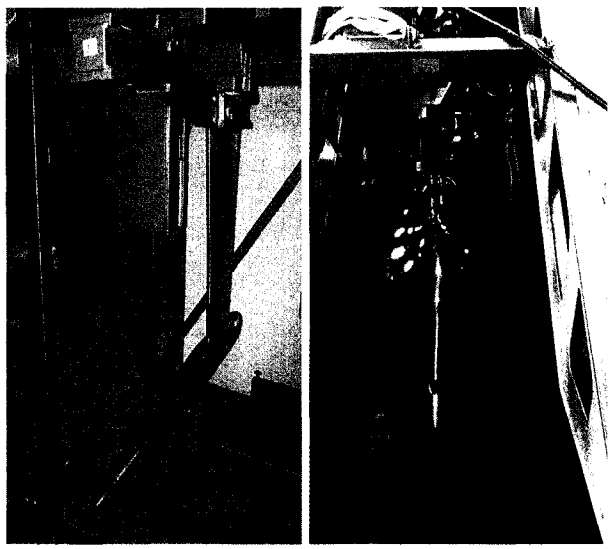

Figure 3.4: Kempf & Remmers Dynamometer Used for Baseline Propeller Tests

Due to the taper of the propeller hub, special nose and tail cone adapters were required to ensure smooth flow through the propeller. The designs of the adapters in Figure 3.5 below were based on the recommendations outlined in ITTC 7.5-02-03-02.1 (2002) and ITTC 7.5-02-03-01.3 (2002).

3.5 Instrumentation for Podded Propeller Experiments

The purpose of the podded propeller unit tests was to provide data about the performance of the model scale podded propeller configurations described in preceding sections. These experiments were conducted in the Ocean Engineering Research Center (OERC) towing tank at Memorial University of Newfoundland (MUN). This tank is approximately 58m in length, 4.5m in width and 2.2m in depth. The maximum speed capability of the towing carriage in this tank is 4.0 m/s. This carriage has two precision rails aligned with the towing direction, which are used to provide a secure mounting surface for the instrumentation as depicted in Figure 3.7.

Figure 3.7: Instrumentation Mounted on Towing Carriage Rails

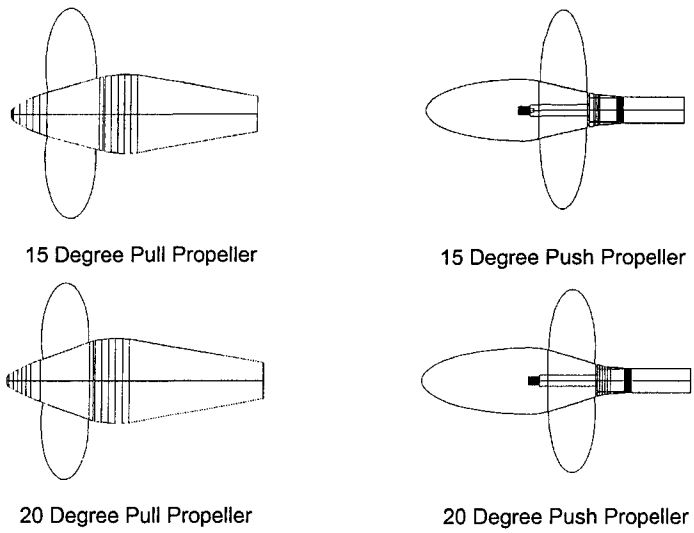

Figure 3.6: Nose and Tail Cone Adapters for Baseline Propeller Tests

For this instrumentation it was necessary to conduct a separate set of friction tests to characterize the frictional torque behavior of the bearings and seals as a function of shaft speed. This test procedure requires a solid cylindrical body, equal in mass to the propellers, which is known as a dummy hub. This dummy hub is submerged and rotated at a variety of shaft speeds to provide the necessary data. The premise behind this approach is that since there are no blades, no thrust is generated by the dummy hub and therefore the torque readings obtained provide a fair representation of the frictional torque over the selected range of shaft speeds.

For these tests the data acquisition system consisted of a VMS and Windows NT based distributed client/server system using IOtech DaqBoards with 256 channel capability. All post processing of the data was conducted at IOT using custom analysis software developed for open water testing. The final results were then imported into Microsoft Excel workbooks for plotting and comparison with the podded propeller results.

3.5 Instrumentation for Podded Propeller Experiments

The purpose of the podded propeller unit tests was to provide data about the performance of the model scale podded propeller configurations described in preceding sections. These experiments were conducted in the Ocean Engineering Research Center (OERC) towing tank at Memorial University of Newfoundland (MUN). This tank is approximately 58m in length, 4.5m in width and 2.2m in depth. The maximum speed capability of the towing carriage in this tank is 4.0 m/s. This carriage has two precision rails aligned with the towing direction, which are used to provide a secure mounting surface for the instrumentation as depicted in Figure 3.7.

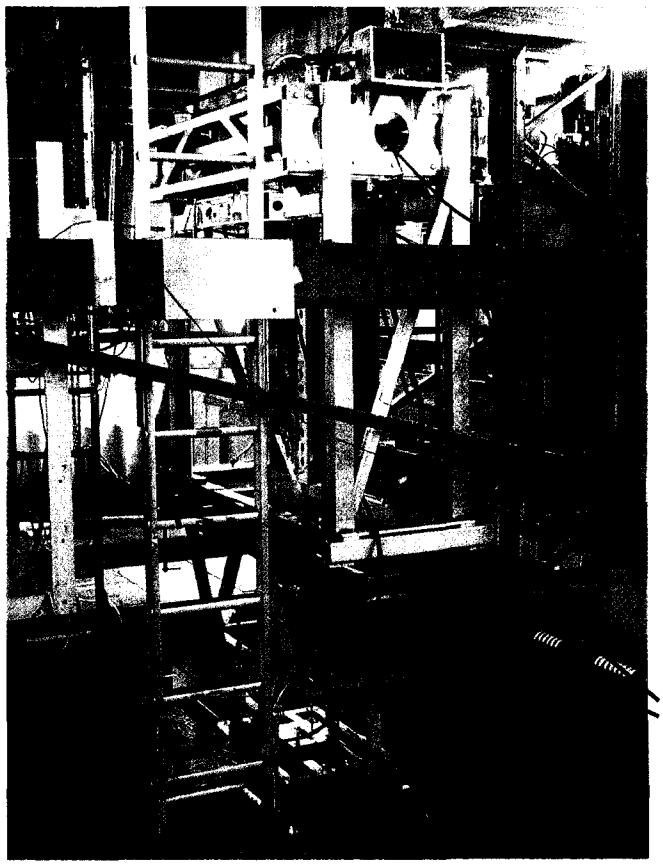

Figure 3.7: Instrumentation Mounted on Towing Carriage Rails

The test equipment required for these experiments was custom-designed to meet the specific needs of this project. A great deal of time and effort went into the design and fabrication of this instrumentation and the details of this design have been published by MacNeill et al. (2004). For completeness a brief explanation of the major components has been provided in Figure 3.8 below.

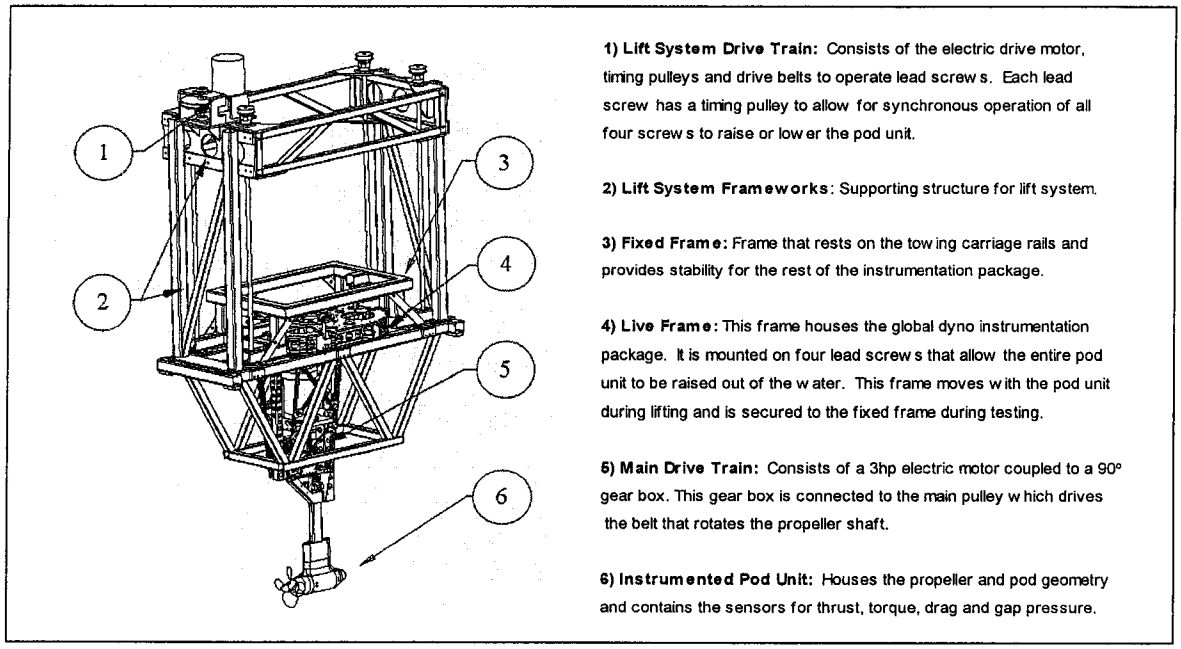

Figure 3.8: Podded Propeller Instrumentation Package - after MacNeill et al. (2004)

One of the main design features of this instrumentation package is its ability to easily raise and lower the instrumented pod unit, as illustrated in Figure 3.9, to allow for rapid changing of the propeller or pod geometry. Due to the large number of pod and propeller variations to be considered throughout the course of this project, this accessibility factor was specified early in the design process.

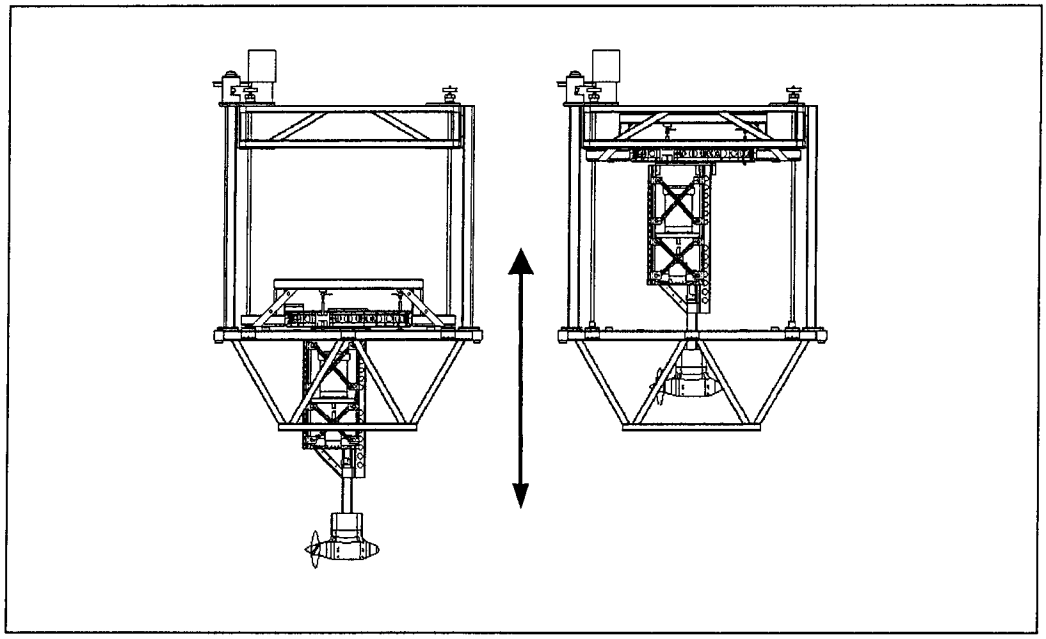

Figure 3.9: Lift System Feature of Podded Propeller Instrumentation – after MacNeill et al. (2004)

The voltage data outputs for these experiments were collected using an IOtech DaqBook data acquisition system connected to a laptop computer running DaqView software. For these tests the sensor voltage data was sampled at a frequency of 50 Hz and stored in raw form in .txt files. This data was post-processed by importing it into Microsoft Excel, plotting a time series of the data and cropping out the points from the desired operational range based on a graphical interpretation of the raw data. Average values for the data points were then calculated over the selected range and these averaged points were used in the final analysis. In the final analysis, calibration curves were applied to these average voltage values to express the measured signals in terms of the appropriate physical quantity. These physical quantities were then non-dimensionlized using the appropriate expressions, as discussed in Chapter 1. Analyzing and viewing the data in this manner was a very time consuming process and future developments should focus on ways to automate the analysis and checking procedures to make it easier to view results as they are obtained.

Chapter 4 - Methodology

4.1 Scope

The main purpose of this chapter is to describe the methods and procedures used while preparing and conducting the experiments considered in this investigation. This chapter may be most relevant to those interested in conducting similar experiments to those considered in this test program and as such, those most interested in the experimental results are advised to proceed to the next chapter. This chapter includes an overview of the calibration and installation procedures, as well as a brief description of the test methods used. The baseline tests were conducted according to standard open water propeller testing procedures and as such further detail may be obtained from the sources referenced in the sections below. Given the lack of operational experience with the podded propeller instrumentation, more emphasis has been placed on the calibration and installation procedures related to the podded propeller equipment rather than on the specific details of the procedures used to conduct the tests.

4.2 Instrumentation Calibration

Prior to testing it was necessary to calibrate all instrumentation components to characterize the conversion of the output voltage signals to the correct units for the physical quantity of interest. The calibration of the Kempf & Remmers dynamometer used for the baseline propeller experiments was carried out by technicians at IOT, using procedures compliant with IOT internal quality standards QP11.2 (1999). The procedures used by this facility for all propeller open water tests are standard and as such further discussion of the calibration techniques used for the baseline tests is not warranted.

Since the podded propeller instrumentation was a custom built piece of equipment, it was first necessary to develop the required calibration procedures. Since the tests conducted for this study did not use all measurement capabilities of the instrumentation package, only the required instrumentation components used in these tests were calibrated. Furthermore, several different calibration procedures were necessary to calibrate all appropriate measuring devices in this apparatus, as is outlined below.

NOTE: The procedures outlined in this thesis are only provisional procedures and should be revised for future test programs.

4.2.1 Unit Thrust Calibration

Due to time constraints, it was not possible to develop procedures, conduct tests and analyze the data necessary to calibrate all six components of the global force balance instrumentation. Given that the propulsion unit was fixed at a zero yaw angle throughout the test program and the side forces were not being considered, it was decided that calibrating the equipment in the x-direction was sufficient. It is noted that side forces are usually present, even for a zero yaw angle, due to the nature of the flow around the pod and strut. As indicated, characterization of these side forces was not considered in this study.

For the unit thrust calibration it has been assumed that there is negligible 'cross-talk' in the axial thrust measurement, since the flex links have been designed to offer very high ratios of axial stiffness to bending stiffness and it is assumed that fabrication errors are negligible. The degree of 'cross-talk' present in the system would need to be quantified if oblique flows were considered.

For this procedure, two steel cables and two precision pulleys were used to horizontally suspend an in-line load cell attached to the end of the main

structural strut of the pod unit. This was conducted in a manner that allowed the controlled application of axial forces, by vertically suspending calibration weights from the cable as illustrated in Figure 4.1.

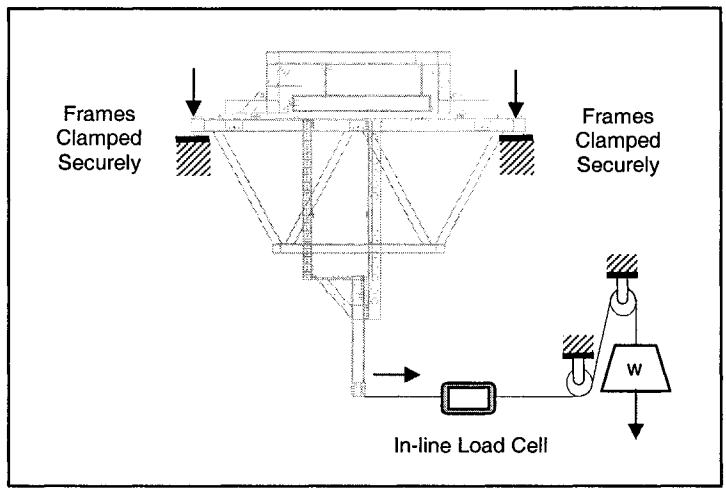

Figure 4.1: Pod Unit Mounted for Unit Thrust Calibration

The in-line load cell was factory calibrated and since the force was being measured in-line with the pulling direction, the losses through the calibration jig were eliminated from the applied force values. The horizontal alignment of both the instrumentation package and the cable direction were achieved using a high quality level, while the angular alignment of the cable in the horizontal plane was set to zero degrees by using a precision square to align the cable with a machined reference surface on the bottom of the strut. This ensured that the pulling force measured during calibration corresponded to an axially applied load during testing. This process was repeated in both axial directions to ensure the equipment was properly calibrated for both push and pull mode operation.

The known calibration forces were plotted against the voltage outputs of the x-direction load cell. The equation of the calibration line was determined using a first-order curve-fit in MS Excel. This equation was used to calculate the unit thrust from the x-direction load cell voltages collected during the open water experiments.

4.2.2 Propeller Thrust Calibration

The instrumentation package has been designed with the capability of measuring the thrust generated by the propeller using two separate sets of load cells: one in the hub of the propeller and one inside the pod unit. For the purpose of this study, only the instrumentation inside the pod unit has been used, since the hub instrumentation was of a new design and technical challenges during the test program prevented the results obtained from being used. For this reason, the propeller thrust discussed throughout this thesis represents the thrust measurement taken by the load cell in the pod unit.

The calibration of the propeller thrust was carried out by orienting the instrumented pod unit in the mounting frame such that the propeller shaft is in a vertical orientation, with the propeller end pointing up, as shown in Figure 4.2 below. Using a calibration fixture, a series of known weights were systematically suspended on the weight tray, applying a compression force to the propeller thrust load cell. The values of all weights used had been accurately measured prior to any calibrations using high-precision digital scales available at IOT to help reduce potential calibration errors.

Figure 4.2: Pod Unit Mounted in Calibration Fixture

These weights were then systematically removed and the orientation of the pod unit was rotated 180°, such that the propeller was pointing downward. The loading and unloading process was again repeated to simulate a tension loading cycle on the propeller shaft. Each time a weight was added or removed during this process, it was necessary to wiggle the propeller shaft by manually oscillating the main drive gear for approximately two seconds. This relieved any residual axial loading on the shaft due to static friction in the internal seals and bearings, which therefore allowed the load cell to return to its correct steady state position. Each weight was allowed to sit for approximately 10 seconds after the friction was relieved prior to adding or subtracting the next weight.

The known force values due to the application of the calibration weights were then plotted against the average thrust load voltage readings taken over each corresponding time interval. A linear curve-fit to this data yielded the equations for the calibration curves used to convert the voltage data collected during the testing phase to the force values obtained during the analysis of the results.

4.2.3 Propeller Torque Calibration

The propeller torque strain gauges were calibrated by installing a moment arm on the propeller hub while the podded propeller unit was installed in the horizontal orientation in the mounting frame, as shown in Figure 4.3 below. The end of this moment arm has a circular profile with radius equal to half the length of the arm. This helped reduce errors since any suspended weights always hung tangentially to this radius, thus providing a constant moment arm length regardless of the angular position of the arm, which would change as calibration loading was altered.

A weight tray was suspended from the side of the moment arm, necessary to provide a clockwise moment about the propeller shaft axis, as viewed from the front face of the propeller. The selected weights were then added and removed in ten second intervals to simulate torque loading. The weight tray was shifted to the other side of the moment arm and the process was repeated to collect data for the counterclockwise direction. The known torque values (calculated as the product of the applied weight and the known moment arm length) were plotted against the average voltage output data for the torque strain gauges for each time interval considered.

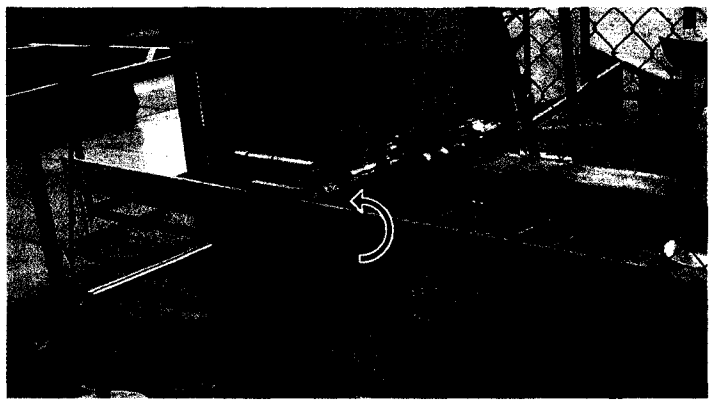

Figure 4.3: Arrangement for Calibration of Propeller Torque

This data was plotted in MS Excel and appropriate linear curve-fits were obtained to give the required torque calibration curves. It was assumed that negligible 'cross-talk' exists between thrust and torque measured on the shaft.

4.3 Testing Procedures

Upon completion of appropriate calibrations, the Kempf & Remmers dynamometer was installed by technicians at IOT according to standard procedures compliant with IOT internal quality standards. The testing procedures

used for the baseline open water propeller tests follow the methods detailed in IOT Standard Test Methods, 42-8595-S/TM-2 (2004) and the section on 'propeller only tests' in ITTC 7.5-02-03-01.3 (2002). Given that these are well-established methods, which have been described in detail in the above references, further discussion of these methods is not warranted.

Similarly for the podded propeller equipment, once it had been appropriately calibrated, it was then installed on the rails of the tow carriage of the OERC tank as described in Appendix B. The podded propeller experiments were conducted as per the provisional testing standard, ITTC 7.5-02-03-01.3 (2002). Unlike the 'propeller only' tests, the test procedures for podded units required more interpretation. As such, detailed description of the methodology used in this study is of limited value, since future testing would not likely attempt to replicate these results, but rather would incorporate the presented information to help guide the development of more standardized test methods for future experiments. For this reason, this following procedure is written as a descriptive overview of how the tests were conducted once the podded propeller instrumentation was calibrated and installed in the towing tank.

From a testing point of view, one of the most important pieces of information required in order to proceed with experiments was the test plan. For all experiments considered in this study the test plan was based on the same standard methods used for planning open water propeller experiments. From a high level, the tests conducted in this study simply required the propeller to be operated at some fixed value of rotational speed while the instrumented pod unit was towed down the tank at the specified advance speeds required to attain data at pre-determined advance coefficients. The value of the shaft speed remained constant for all experiments and the value selected was 9 rps. This shaft speed was determined to be the optimal speed to allow for minimal Reynolds effects, while keeping loading levels on the sensors within a safe range as discussed further in Chapter 5.

The advance coefficient range was assessed based on baseline tests and the maximum expected J value required to obtain at least one point with negative thrust was determined to be J = 1.2. This range was then divided into increments of 0.10 and since both the shaft speed and propeller diameter were constant, the required advance speeds were calculated as shown in Table 4.1 below.

J	rps	V_A(m/s)
0.00	9	0.000
0.10	9	0.243
0.20	9	0.486
0.30	9	0.729
0.40	9	0.972
0.50	9	1.215
0.60	9	1.458
0.70	9	1.701
0.80	9	1.944
0.90	9	2.187
1.00	9	2.430
1.10	9	2.673
1.20	9	2.916

$J = V_A/(nD)$

Therefore:

$V_A = J\,(nD)$

Where:

J = Advance Coefficient

V_A = Advance Speed

n = Shaft Speed

D = Propeller Diameter

Table 4.1: Experimental Test Plan

Using this information, the shaft speed could be set on the instrumentation controller and the carriage speed set to desired value so as to give measured results at the above specified advance coefficient points.

To help ensure steady state operational behavior of all mechanical components, such as water lubricated bearing, gears, belts and other internal mechanisms the propeller controller was set to 3Hz and the propeller was allowed to run for about 10 minutes prior to starting testing each day. This also helped ensure that the temperature of the pod unit was allowed to lower from the ambient air temperature to the water temperature after the unit was initially placed in the tank.

Once the equipment was finally ready to test, each individual test run was completed by following the basic steps shown below:

- Set the carriage controller to the desired advance speed for the selected data point, but do not start yet.
- Set the main drive motor controller to the lowest possible smooth-operating RPM setting (this was determined to correspond to a controller input setting of 3 Hz).
- Run the podded propeller unit at the above RPM setting for approximately ten minutes to ensure steady state operating conditions.
- Stop the propeller from turning
- Start recording data into the data acquisition system
- Start the main drive motor at 3Hz for approximately 10 seconds (this was collected to use as the tare thrust point)
- Change the controller input speed to 36.61 Hz (this corresponded to the desired shaft speed of 9 rps)
- As the propeller shaft speed accelerates, watch the speed indicator and once the propeller reaches approximately 75% of the set shaft speed (which was approximately 28 Hz), start accelerating the carriage to the preset advance speed. (This was done to help reduce loading on the instrumentation, since the bollard loading condition was not reached every time a test run was completed)
- Run at the set carriage speed for approximately 10 seconds to ensure a good data stream is obtained. (For high speed runs, it was not always possible to get 10 seconds of data – in these instances the set speed was maintained for the longest safe amount of time before decelerating, which was never less than 5 seconds of data)
- Stop the carriage

- Decelerate the propeller as the carriage slows down (this was done to reduce high loading on the instrumentation at the end of the test run).
- Stop recording data into the data acquisition system
- Wait for the water in the tank to settle
- Start the propeller at a speed of 3 Hz
- Reverse the carriage at a speed of 0.5 m/s (or less)
- Repeat the entire process until data is collected for all required test conditions

Using the above methods for calibrating, installing and operating the required instrumentation, all necessary results were collected for the selected test configurations, as discussed in the next chapter.

Chapter 5 - Results

5.1 Scope

This chapter focuses on the results of the two series of experiments: baseline propeller open water test results and podded propeller open water experimental results. A discussion of considerations regarding Reynolds number and speed selection is presented along with descriptions of the results of the two series of open water experiments. The results of these tests have been non-dimensionalized and plotted in the form of K_T, $10K_Q$, η versus J performance curves. The baseline propeller data and the podded propeller data are both discussed in terms of the influence of propeller hub taper angle on the considered performance characteristics. Furthermore, the data for the propellers operating in push mode are compared with the data for the propellers operating in pull mode for both baseline and podded configurations.

5.2 Assessment of the Influence of Reynolds Number

To maximize available test time, the custom-made podded propeller instrumentation was originally designed to accommodate testing in the tow tank facilities at both the Institute for Ocean Technology (IOT) and Memorial University of Newfoundland (MUN). The reason for making this decision was based on the fact that the high demand for time in these test facilities would present challenges for planning experiments. By having equipment that could operate in both facilities, it was hoped that this would maximize the availability of the equipment for testing since it could be used at whichever facility had available tank time.

The range of towing carriage speeds, which is representative of the advance speed of the model propeller, is much larger for the IOT tank than for the MUN facility. Based on this fact, it was reasoned that by running all experiments in the IOT tank, the tests could be run at a higher shaft speed and therefore higher Reynolds numbers. This in turn would result in larger loads, which typically result in lower relative uncertainty levels. Furthermore, operating at higher shaft speeds helps ensure fully turbulent flow over the propeller blades, thereby minimizing the dependency of results on the Reynolds number. As such, all of the initial planning for both the baseline and podded propeller experiments had been based on the capabilities of the IOT tow tanks.

While it was possible to conduct the baseline propeller tests at the IOT deepwater towing tank, these facilities were in very high demand, making it difficult to schedule sufficient time for the podded propeller experiments. Since the MUN tank offered much more flexibility and could provide a satisfactory range of carriage speeds it was decided that the podded propeller experiments would be conducted in this tank.

The plans for the IOT tow carriage specified a shaft speed of 15 rps, which was the shaft speed used during the baseline propeller experiments. Given that the podded propeller experiments had to be conducted in the MUN tank, the shaft speed selected for this tank facility was 9 rps. This shaft speed was selected to minimize the loading on the new instrumentation during this first set of tests.

To assess the dependence of the results on shaft speed, and therefore Reynolds number, a series of baseline open water experiments were conducted at 9, 12 and 15 rps. The results of these tests are presented in Figure 5.1 below. Sample Reynolds number values corresponding to each of the three shaft speeds considered are also provided. As observed in this plot, it appears that increasing the shaft speed increases the torque coefficient and the thrust coefficient by a small amount. While this observed trend was not expected, it is important to recognize the levels of uncertainty in the data.

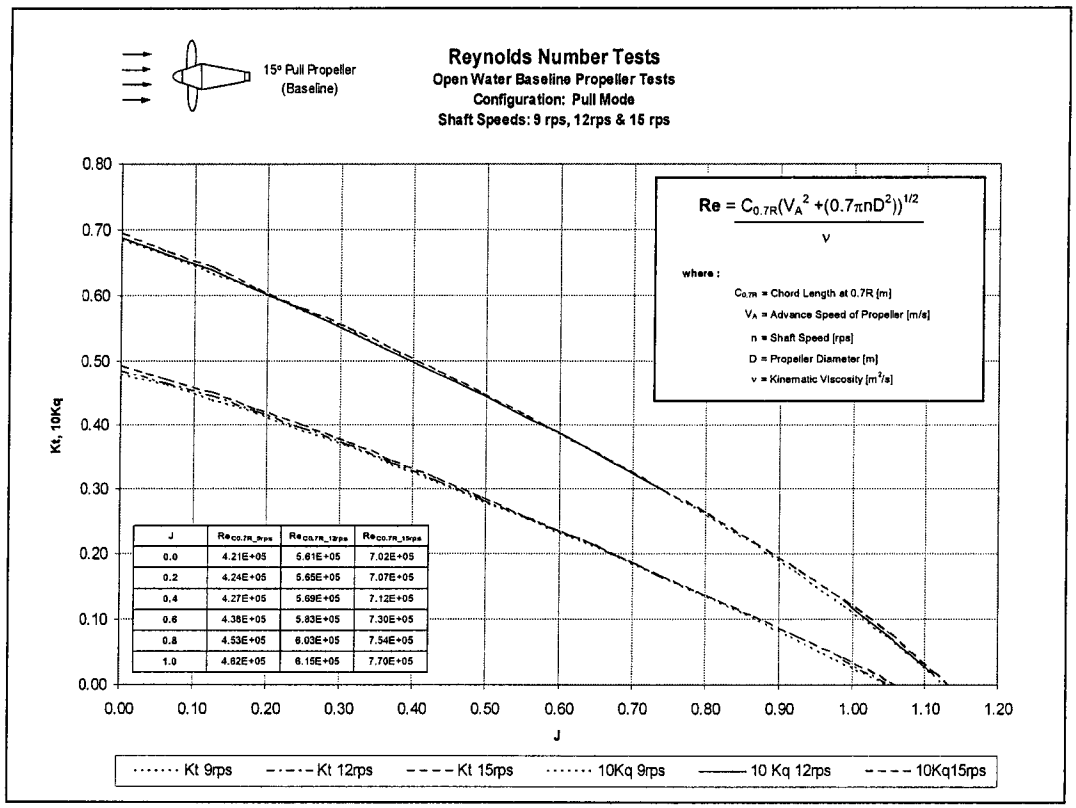

J	$Re_{C0.7R\_9rps}$	$Re_{C0.7R\_12rps}$	$Re_{C0.7R\_15rps}$
0.0	4.21E+05	5.61E+05	7.02E+05
0.2	4.24E+05	5.65E+05	7.07E+05
0.4	4.27E+05	5.69E+05	7.12E+05
0.6	4.38E+05	5.83E+05	7.30E+05
0.8	4.53E+05	6.03E+05	7.54E+05
1.0	4.62E+05	6.15E+05	7.70E+05

Figure 5.1: Comparison of Baseline Propeller Data at 9rps, 12rps and 15rps

Table 5.1 presents a summary of the calculated uncertainty levels in the baseline propeller test results. As seen from this table, the uncertainty levels are such that the above differences due to Reynolds effects are within the error bars of the data. This is illustrated graphically in Figure 5.2 below. The details of how these values were calculated are presented in Chapter 6.

	Advance Coefficient Value	Thrust Coefficient K_T (+/-)	Percentage Error in K_T (+/-)	Torque Coefficient K_Q (+/-)	Percentage Error in K_Q (+/-)	Advance Coefficient Error (+/-)
9 rps	0.1	0.00205	0.5%	0.00104	1.7%	0.00148
	0.4	0.00153	0.5%	0.00102	2.1%	0.00164
	0.7	0.00105	0.6%	0.00101	3.1%	0.00195

Table 5.1: Overall Error in Thrust, Torque and Advance Coefficients for Baseline Results

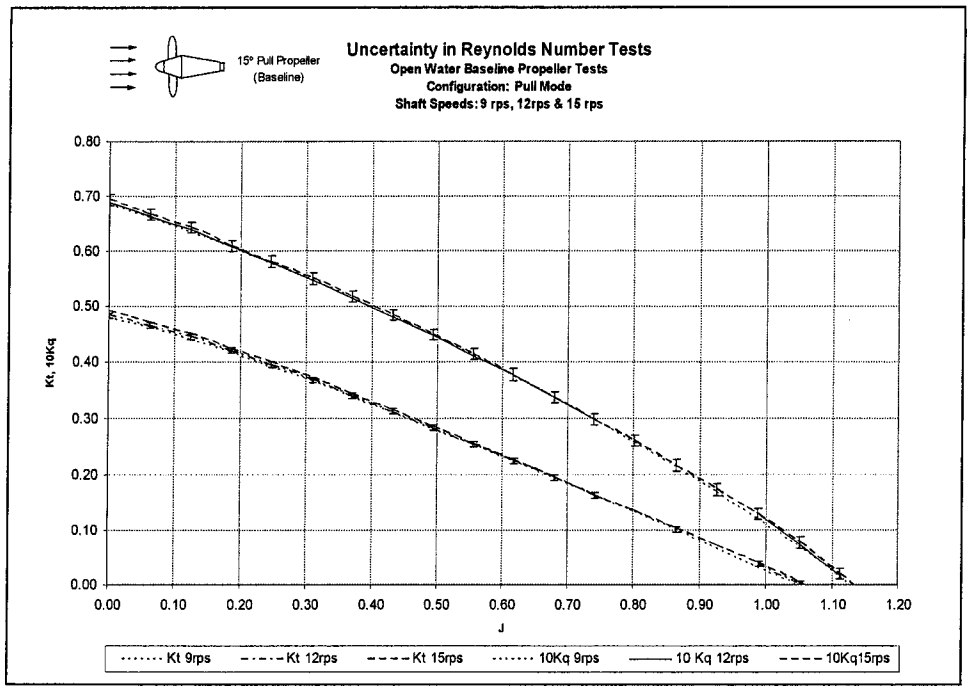

Figure 5.2: Consideration of Uncertainty in Baseline Propeller Data for 9rps, 12rps and 15rps

Given that the podded propeller results had similar uncertainty levels, as illustrated in Table 5.2 below and that the observed results show that the Reynolds number effects are within the bounds of these limits, it has been assumed that the influence of Reynolds number on these experiments is not significant.

	Advance Coefficient Value	Prop Thrust Coefficient K_{Tprop} (+/-)	Percentage Error in K_{Tprop} (+/-)	Unit Thrust Coefficient K_{Tunit} (+/-)	Percentage Error in K_{Tunit} (+/-)	Torque Coefficient K_Q (+/-)	Percentage Error in K_Q (+/-)	Advance Coefficient Error (+/-)
9 rps	0.1	0.00829	1.9%	0.00257	0.6%	0.00113	1.8%	0.00246
	0.4	0.00816	2.5%	0.00207	0.7%	0.00111	2.2%	0.00269
	0.7	0.00802	4.1%	0.00149	1.0%	0.00120	3.7%	0.00313

Table 5.2: Overall Error in Propeller Thrust, Unit Thrust, Torque and Advance Coefficients for Podded Propeller Tests

5.3 Baseline Propeller Open Water Test Results

As explained in Chapter 3, to allow for smooth flow through the propeller during testing the conical hub propellers required adapters to smoothly fair the propeller geometry in with the shaft of the instrumentation. These adapters included a nose cone and a tail cone to provide smooth flow transitions. While the details of the configurations of these adapters are described in previous chapters, for graphical purposes it is important to clarify which propeller configurations correspond to which sets of data. As such, the graphical indicators shown in Figure 5.3 below have been used on the performance plots to make it clear which propellers and adapter are being considered.

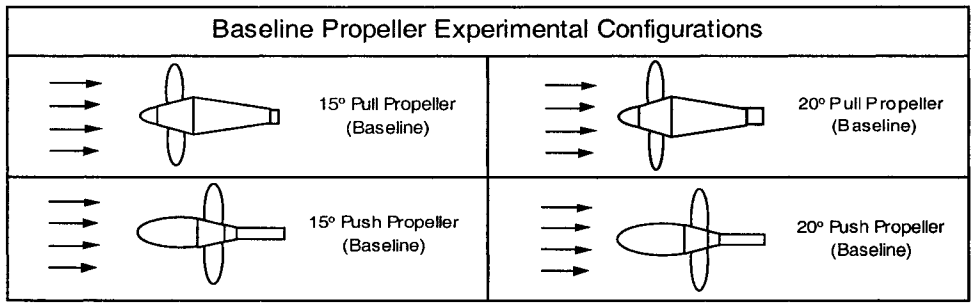

Figure 5.3: Graphical Indicators for Baseline Propeller Configurations

To illustrate the open water performance characteristics of these various propellers in baseline mode the K_T, $10K_Q$, η vs. J plots have been generated for each of the above configurations. While the efficiency curves have been plotted for completeness, these curves tend to be more sensitive to errors than either the thrust or torque coefficients. As a result, it is difficult to make conclusive observations about performance trends based strictly on the efficiency curves, and as such focus has been placed primarily on observations in the thrust and torque coefficient data for this section. The experimental data used to generate the performance plots given below is presented in Appendix C.

The 15° pull propeller was the first propeller tested. These experiments were conducted using the methods described in Chapter 4 and the results are shown in Figure 5.4 below.

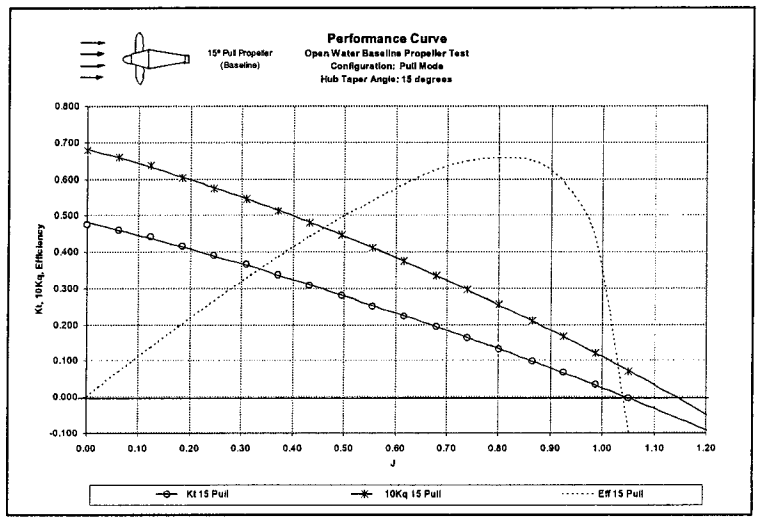

Figure 5.4: Performance Curve for Baseline 15° Pull Propeller

Comparing the above plot for the 15° pull propeller with the performance curve for the 15° push propeller shown in Figure 5.5, it is observed that the pull propeller has higher bollard thrust and torque coefficients than its pull counterpart.

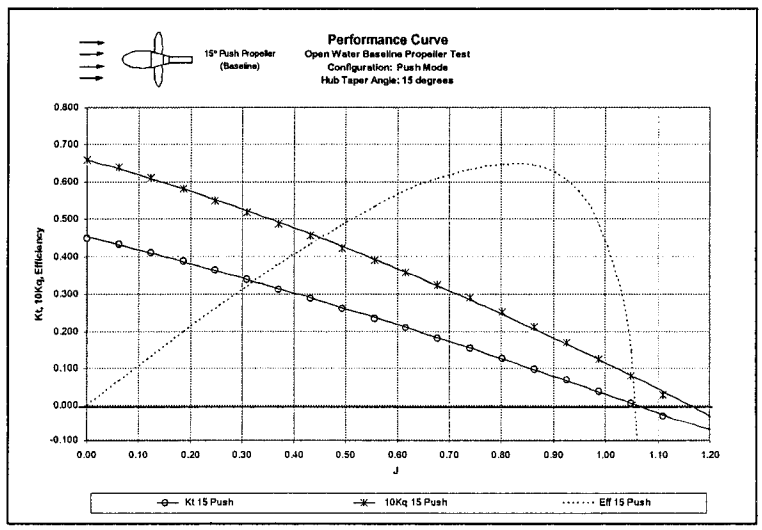

Figure 5.5: Performance Curve for Baseline 15° Push Propeller

For the 20° pull propeller, manufacturing defects were discovered after the baseline tests had been conducted, and therefore it was necessary to discard the original test data obtained for this propeller. To correct these defects, a new 20° pull propeller was manufactured. As there was no opportunity to conduct baseline propeller tests with this new propeller in the IOT towing tank facility, it was decided that a set of open water experiments would be conducted in the water tunnel at IOT. Since the pumping effect of the propeller in the water tunnel creates circulation through the test section even when the tunnel pumps are shut down it is impossible to get test data in the low range of advance coefficients. This explains the limited data set available for the performance curve of this propeller shown in Figure 5.6.

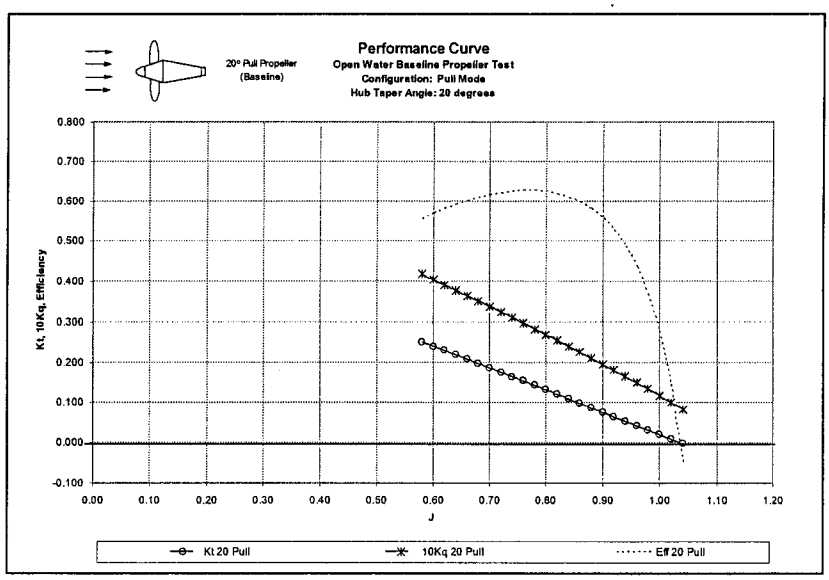

Figure 5.6: Performance Curve for Baseline 20° Pull Propeller

Given the limited data available for the above plot, it is impossible to draw conclusions about the bollard performance of this propeller in baseline mode. Future baseline propeller test programs should include more thorough testing of this model propeller to provide additional data for the full range of advance coefficients.

The final propeller in this series of experiments was the 20° push propeller. The data for this propeller was plotted as shown in Figure 5.7 below.

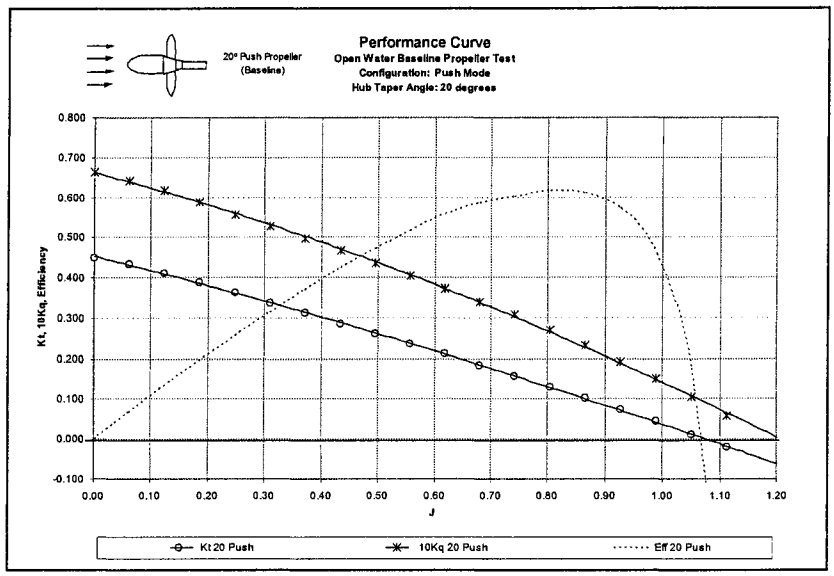

Figure 5.7: Performance Curve for Baseline 20° Push Propeller

The K_T and $10K_Q$ values at the bollard condition, which corresponds to an advance coefficient of J = 0, for each of these above baseline 15° and 20° propellers is provided in Table 5.3.

Baseline Propeller Open Water Tests - Bollard Condition

Propeller	J	K_T	$10K_Q$
15° Pull	0.00	0.475	0.679
15° Push	0.00	0.449	0.660
20° Pull	0.00	-	-
20° Push	0.00	0.449	0.665

Table 5.3: Bollard Condition Results for Baseline Propeller Tests

While sufficient data is not available to make comparisons between the two pull propellers, it is observed from the above data that the 15° and 20° push propellers generate the same bollard K_T values, but the 20° version requires more torque to generate the same amount of thrust. Comparing the two 15° propeller results, it may also be observed that the pull propeller has a higher bollard thrust and torque coefficients than the push counterpart.

The complex flow around the propellers and the influence of the hub adapters on the flow makes it difficult to identify the cause of these observed trends. Additional research into the details of the flow around these propellers using techniques such as Laser Doppler Velocimetry (LDV) or Particle Image Velocimetry (PIV) with these propellers may help provide further insight into the observed phenomena.

Furthermore, since the geometry of the propeller hubs require large fairing adapters to ensure smooth flow through the propeller, it is also possible that these adapters influence the measured result. This is especially the case for the large, bulbous nose cone that is required for push mode propellers. As described previously, the current test methods require the use of a dummy hub for the purpose of quantifying and correcting for the influence of shaft friction on the torque reading. While this is useful in accounting for the influence of friction on the torque reading, it does not account for the drag acting on the fairing adapters which affects the measured thrust.

To this end, it is recommended that any future tests which consider the performance of baseline conical hub propellers include an additional series of dummy hub experiments to test for the influence of the fairing adapter drag on the measured thrust. Unlike the 'torque dummy hub tests', which use a dummy hub that is cylindrical in shape and of equal mass to the model propeller, the 'thrust dummy hub tests' should use a dummy hub that is of identical geometry to the hub of the propeller being tested, regardless of the mass. This 'thrust dummy hub' should be mounted on the instrumentation, exactly as the propeller would

be, and tested over the exact range of shaft speeds and advance speeds expected to be covered during the regular test program.

The thrust measurement data collected during these 'thrust dummy hub tests' is in effect the fairing adapter drag. This could be plotted as a function of advance coefficient and then subtracted from the propeller thrust measured during baseline propeller tests. This would make it possible to more accurately assess which components of the performance are caused by the design of the actual propeller, and which components are influenced by the large fairing adapters.

Performance data for the above plots corresponding to an advance coefficient of J = 0.7 is given in Table 5.4 below. As observed above, the thrust coefficients for both pull propellers are approximately the same, but the 20° propeller has a higher torque coefficient. Similarly for the push propellers, the thrust coefficients are very close to the same value, but the 20° version requires more torque than the 15° version to attain the same thrust. The corresponding effect on open water efficiency is that pull propellers tend to have a higher efficiency than push propellers, and that increasing the propeller hub taper angle decreases the efficiency. Further discussions of these results are provided in subsequent sections.

Baseline Propeller Open Water Tests - Performance Data at J = 0.7

Propeller	J	K_T	$10K_Q$	η
15° Pull	0.70	0.186	0.323	64.0%
15° Push	0.70	0.176	0.313	62.4%
20° Pull	0.70	0.187	0.338	61.5%
20° Push	0.70	0.178	0.331	59.7%

Table 5.4: Baseline Propeller Open Water Efficiencies at J = 0.7

5.4 Podded Propeller Open Water Test Results

To help ensure the information for each podded propeller is clearly presented, an additional set of graphical indicators has been included as shown in Figure 5.8 below. These indicators have been used on the performance plots to make it clear which propulsor configurations are being compared.

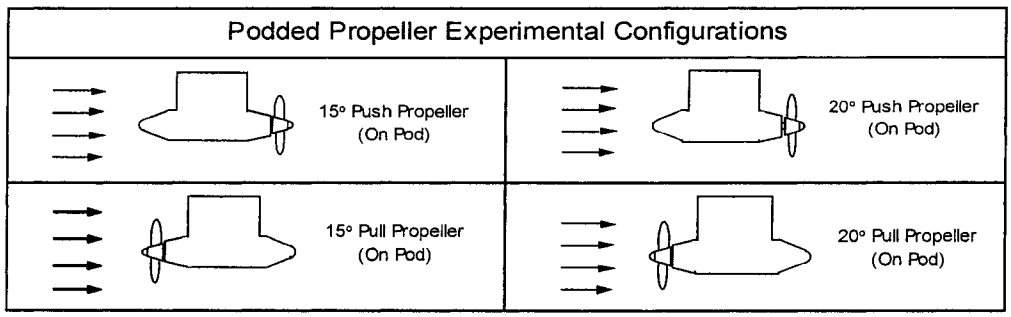

Figure 5.8: Graphical Indicators for Podded Propeller Configurations

The data for the open water performance characteristics of each of these podded propellers are plotted in the form of K_{Tprop}, K_{Tunit} $10K_Q$, η_{prop}, η_{unit} vs. J plots. As noted in previous chapters, the propeller thrust data considered in this study was measured using the thrust instrumentation located inside the pod body, not using the hub instrumentation. The experimental data used to generate the plots given in this section is presented in Appendix D.

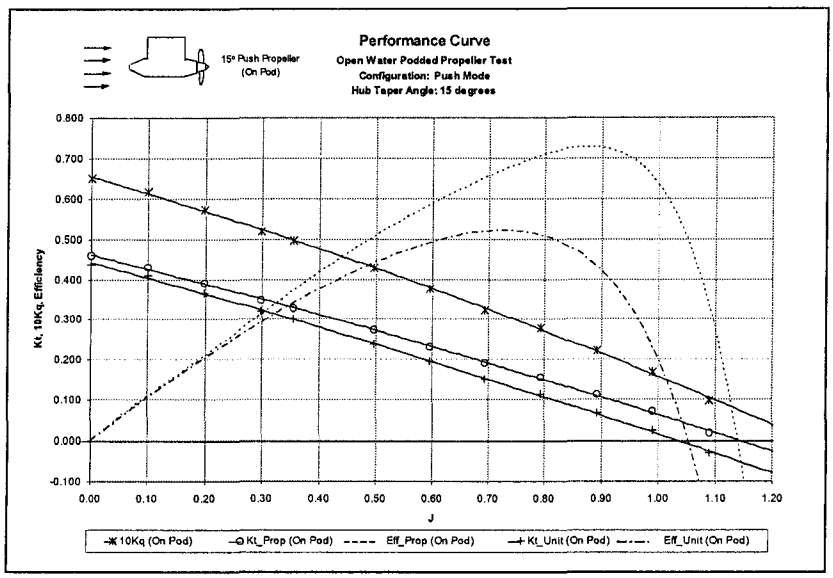

Figure 5.9: Performance Curve for 15° Push Podded Propeller

From Figure 5.9 it can be seen that for the 15° push podded propeller the bollard unit thrust is below the bollard propeller thrust. A possible explanation for this may be found by considering the acceleration of inflowing fluid as it approaches the propeller race. In this instance a push pod is being considered, meaning that the pod body is located such that the suction of fluid into the propeller creates an induced velocity over the surface of body. This in turn would produce a drag force on the pod unit, since the local fluid velocity around the pod unit is non-zero, despite having a zero advance speed. This induced drag force would oppose the thrust force generated by the propeller resulting in a bollard unit thrust force that is smaller than the bollard propeller thrust.

Furthermore, it is observed that the unit thrust tends to decrease faster than the propeller thrust for increasing advance coefficient. This steeper slope for the unit thrust is expected, since the unit thrust measurement consists of components of the propeller thrust in addition to the drag acting on the body of the pod. Since the drag on the pod body would be expected to increase with increasing advance speed, the unit thrust measurement should correspondingly

decrease at a faster rate. This is reflected in the unit efficiency, which is observed to have a much lower maximum value and occurs at a lower advance coefficient than is the case for the propeller efficiency.

A similar plot for the 15° pull podded propeller was generated as shown below in Figure 5.10. Unlike the previous case, in this instance the bollard unit thrust exceeds the bollard propeller thrust. The higher bollard unit thrust would indicate that in addition to the thrust generated by the propeller, an additional forward acting force may be acting on the body of the pod.

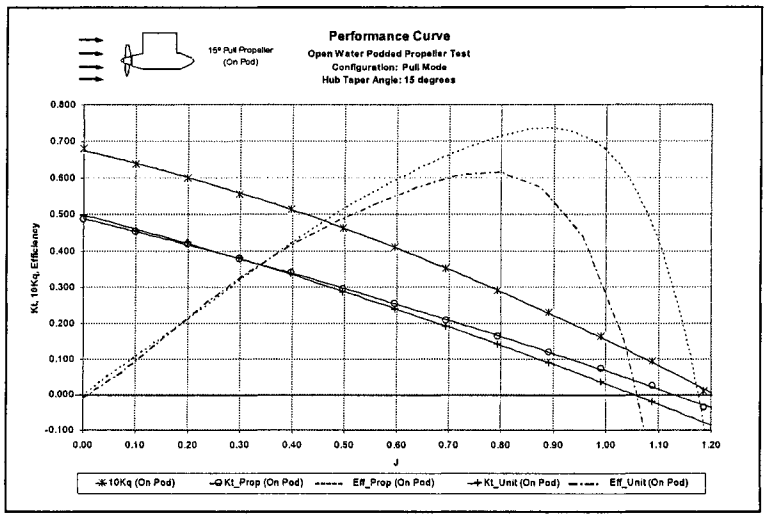

Figure 5.10: Performance Curve for 15° Pull Podded Propeller

One possible way to explain this observation may be found by considering the work of Halstensen and Leivdal (1990). As indicated in this paper, depending on the geometry it is possible for the strut and body to recover some of the rotational energy in the propeller slipstream, by acting as lifting bodies which generate a force with a forward acting component. If this forward force component were greater than the induced drag on the pod, it may be possible for the unit thrust to exceed the propeller thrust. However, as discussed in the following chapter, due to uncertainty levels in the data, it is possible that the

observed behavior may be related to error in the data and as such further testing is required to provide conclusive evidence of such phenomena.

For the 15° pull podded propeller, it is observed that the unit thrust decreases faster with increasing advance coefficient than does the propeller thrust and that the maximum unit efficiency is much lower than the maximum propeller efficiency.

The performance results for the 20° push podded propeller and the 20° pull podded propeller are given in Figure 5.11 and Figure 5.12 respectively. For the 20° push podded propeller, the bollard unit thrust and bollard propeller thrust are equal, meaning that in this instance the pod body neither increases nor decreases the thrust generated by the propeller. As with the 15° push propeller, the unit thrust decreases faster than the propeller thrust with increasing advance coefficient, and the maximum unit efficiency is significantly lower than the propeller efficiency.

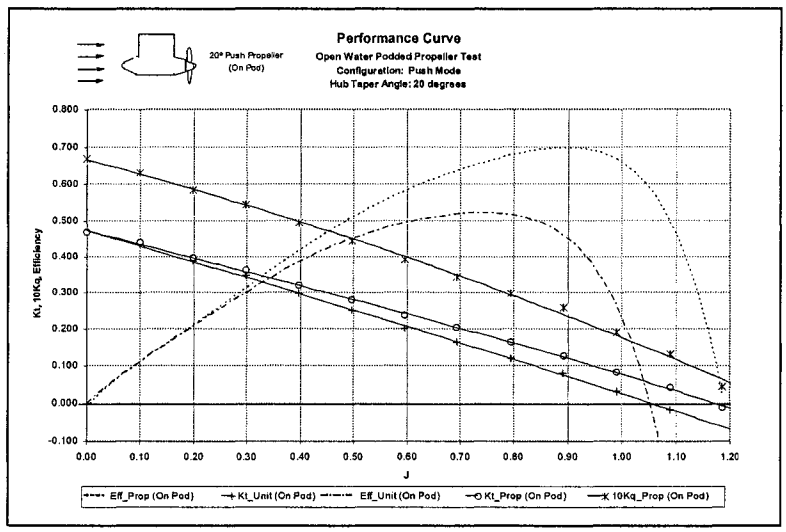

Figure 5.11: Performance Curve for 20° Push Podded Propeller

Figure 5.12 shows that the bollard unit thrust equals the bollard propeller thrust for the 20° pull podded propeller, while the unit thrust, as with the other pod units decreases at a faster rate than the propeller thrust for increasing advance

coefficient, resulting in an overall unit efficiency that is lower than the propeller efficiency.

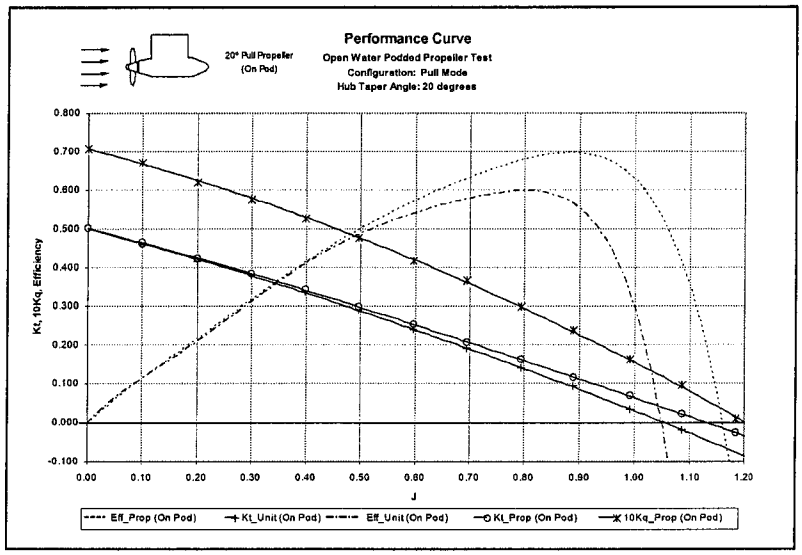

Figure 5.12: Performance Curve for 20° Pull Podded Propeller

As for the baseline propellers, the K_T and $10K_Q$ values at the bollard condition have been summarized in Table 5.5.

Podded Propeller Open Water Tests - Bollard Condition

Propeller	J	K_{T_UNIT}	K_{T_PROP}	$10K_Q$
15° Pull	0.0	0.4972	0.4866	0.6787
15° Push	0.0	0.4375	0.4596	0.6517
20° Pull	0.0	0.5002	0.5016	0.7070
20° Push	0.0	0.4670	0.4681	0.6696

Table 5.5: Bollard Condition Results for Podded Propeller Tests

Considering data from Table 5.4 and Table 5.5, it may be observed that baseline 'propeller only' tests serve as a useful tool for evaluating the performance of conical hub propellers in relative terms, but there is a large

difference in the actual magnitudes of the performance characteristics for thrust and torque in absolute terms. As discussed in later sections of this chapter, the propeller thrust and efficiency trends observed in the baseline tests provide strong supporting evidence for the trends predicted by the podded propeller unit tests, but it is important to recognize the differences and limitations of each testing approach. Specifically, baseline propeller tests reflect general propeller performance trends for comparative purposes, but do not accurately predict the magnitudes of performance characteristics and overall system performance for podded propeller units. Podded propeller unit tests are inherently more complex than standard open water tests and require specialized instrumentation, which generally increases testing time and cost.

As observed in Table 5.5, it is difficult to characterize specific trends based on these results and as such further comparisons are considered in subsequent sections of this chapter.

5.5 Influence of Propeller Hub Taper Angle

One key factor considered in this study is the influence of the hub taper angle on the performance of these propellers. The plot shown in Figure 5.13 provides a comparison of the open water results for baseline tests with the 15° pull propeller and the 20° pull propeller. As noted, data for the 20° pull propeller was obtained from tests conducted in the IOT water tunnel at atmospheric conditions. This is why the data does not extend below J = 0.58.

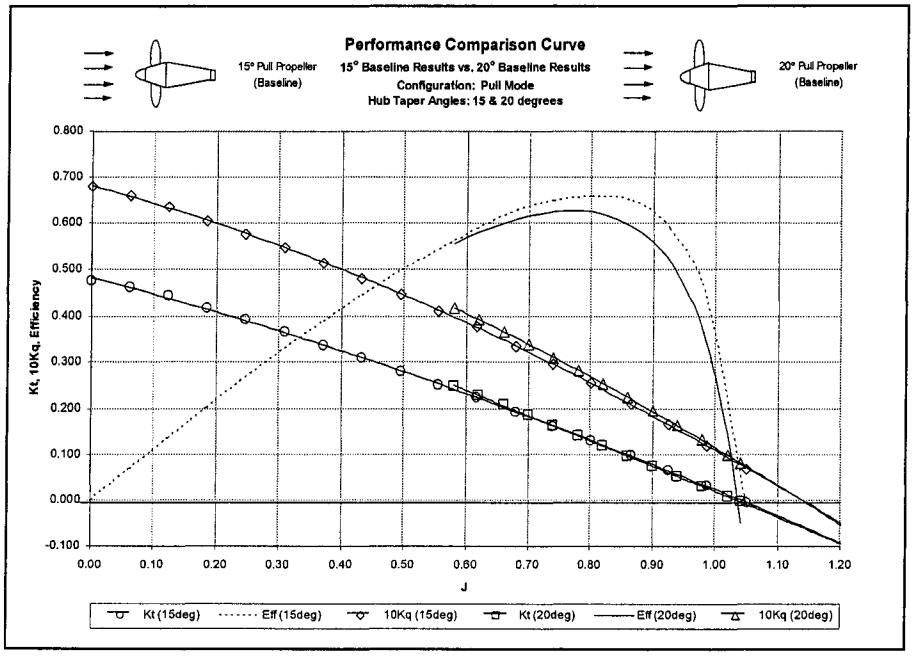

Figure 5.13: Performance Plot - 15° and 20° Pull Propellers

Data points over the higher range of advance coefficients are compared by calculating the percent difference of the 20° pull propeller compared to 15° pull propeller as shown in Table 5.6.

20° vs. 15° Pull 'Baseline' Open Water Test Results

J	% Diff $10K_Q$	% Diff K_T	% Diff η
0.0	-	-	-
0.2	-	-	-
0.4	-	-	-
0.6	4.3 %	2.5 %	-0.7 %
0.7	4.9 %	1.0 %	-2.4 %
0.9	6.6 %	-1.4 %	-5.3 %

Table 5.6: Percent Difference in 20° Pull Propeller Results Compared to 15° Pull Propeller Results

From the above table it is observed that for baseline pull propellers, increasing the hub taper angle increases the torque, and for advance coefficients below the design point (J = 0.8) it produces an increase in thrust coefficient. Since the effect on torque increases with advance coefficient, while the effect on thrust decreases with advance coefficient, the net result is that efficiency is lower for the larger hub taper angle and this difference in efficiency gets larger with increasing advance coefficient.

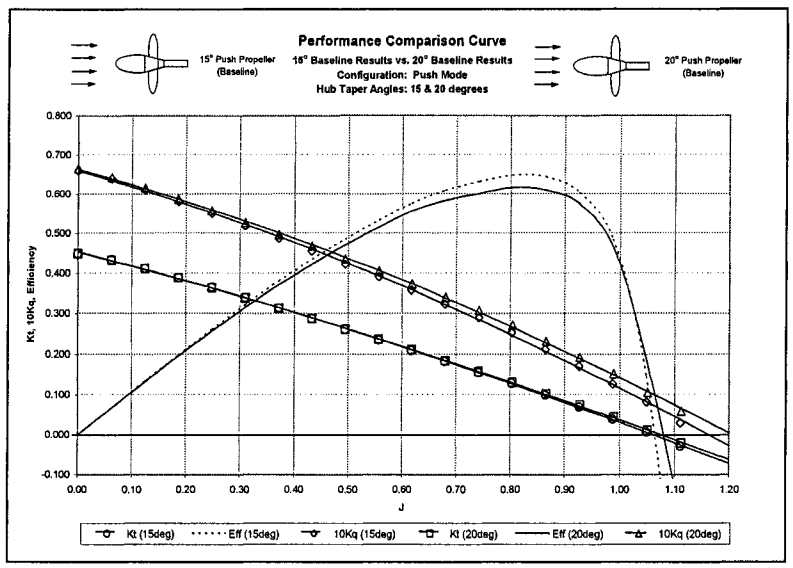

Figure 5.14: Performance Plot - 15° and 20° Push Propellers

The data plotted in the performance curve shown in Figure 5.14 compares the 'propeller only' open water data for the 15° push propeller and the 20° push propeller. The percent differences for selected data points are summarized in Table 5.7 below. As previously, the percent difference calculations are based on the difference of the 20° propeller compared with the 15° propeller to show the effect of increasing the hub taper angle.

20° vs. 15° Push 'Baseline' Open Water Test Results			
J	% Diff $10K_Q$	% Diff K_T	% Diff η
0.0	0.8 %	0.1 %	0.0 %
0.2	1.2 %	-0.5 %	-0.4 %
0.4	2.6 %	-0.1 %	-1.0 %
0.6	3.6 %	0.3 %	-1.7 %
0.8	6.8 %	1.7 %	-3.0 %

Table 5.7: Percent Difference in 20° Push Propeller Results Compared to 15° Push Propeller Results

Based on the data in this table, it may be observed that for the push propeller results, increasing the hub taper angle increases the torque, and this effect increases with advance coefficient. For thrust, increasing the taper angle does not show a great effect in the low J range, but slight increases in thrust are observed for high J. The net effect on the propeller efficiency is that the efficiency decreases for larger hub angles and this effect is more pronounced for higher advance coefficients.

The results of the 'podded propeller unit' experiments were collected and analyzed in a manner similar to the 'propeller only' tests. The major difference with these tests is that one extra variable was measured, the 'unit thrust'. Correspondingly, two additional performance characteristics, unit thrust coefficient, K_{Tunit}, and unit efficiency, η_{unit}, were calculated, in addition to the standard performance characteristics. The plot shown in Figure 5.15 provides a comparison of the open water results for 'podded propeller unit' tests with the 15° pull podded propeller and the 20° pull podded propeller.

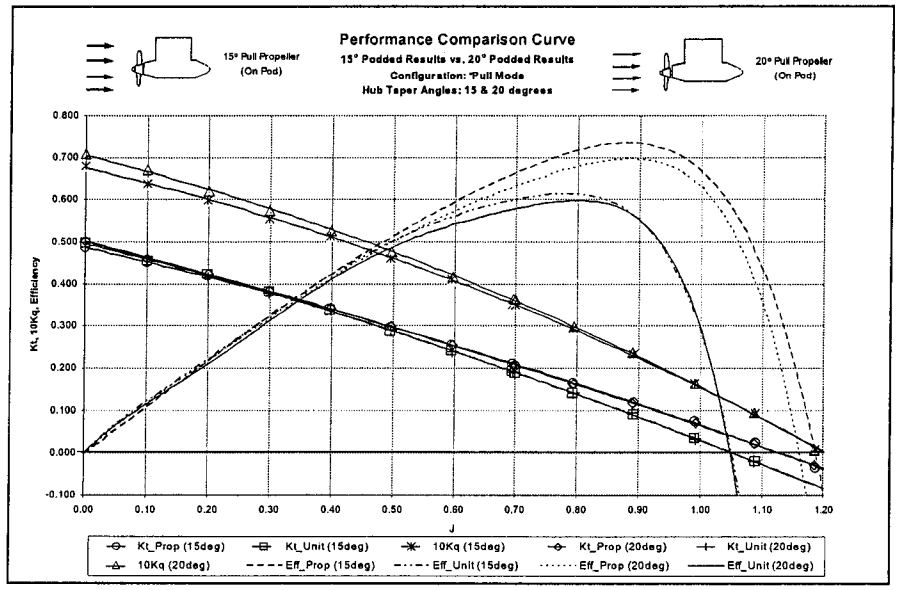

Figure 5.15: Performance Plot - 15° and 20° Pull Podded Propellers

To assess the influence of the hub taper angle on the podded propeller units, the percent difference of the 20° pull podded propeller relative to the 15° pull podded propeller is shown in Table 5.8.

20° vs. 15° Pull 'Podded Propeller' Open Water Test Results

J	% Diff $10K_Q$	% Diff K_{T_PROP}	% Diff η_{PROP}	% Diff K_{T_UNIT}	% Diff η_{UNIT}
0.0	4.2%	3.1%	0.0%	0.6%	0.0%
0.2	3.6%	1.4%	-0.4%	-1.7%	-1.1%
0.4	2.7%	0.7%	-0.7%	0.0%	-1.0%
0.6	1.6%	-0.4%	-1.0%	-0.6%	-1.0%
0.8	2.0%	-2.2%	-2.7%	-1.1%	-1.7%

Table 5.8: Percent Difference in 20° Pull Podded Propeller and 15° Pull Podded Propeller Results

From the table above, it may be observed that for a 'podded propeller unit' case with a pull podded propeller, increasing the hub taper angle increases the torque and this effect decreases with increasing advance coefficient. Increasing hub angle tends to cause higher propeller thrust at low J (i.e. greater bollard pull) but this comes at the cost of lower propeller thrust in the higher J range. The net

effect on propeller efficiency is a decrease in efficiency for increased hub taper angle, which becomes more pronounced for higher J. The overall unit thrust does not appear to have a distinct trend, though the overall unit efficiency data are consistently lower when hub taper angle is increased.

The data plotted in Figure 5.16 provides a comparison of 'podded propeller unit' open water test results for a 15° push podded propeller and a 20° push podded propeller.

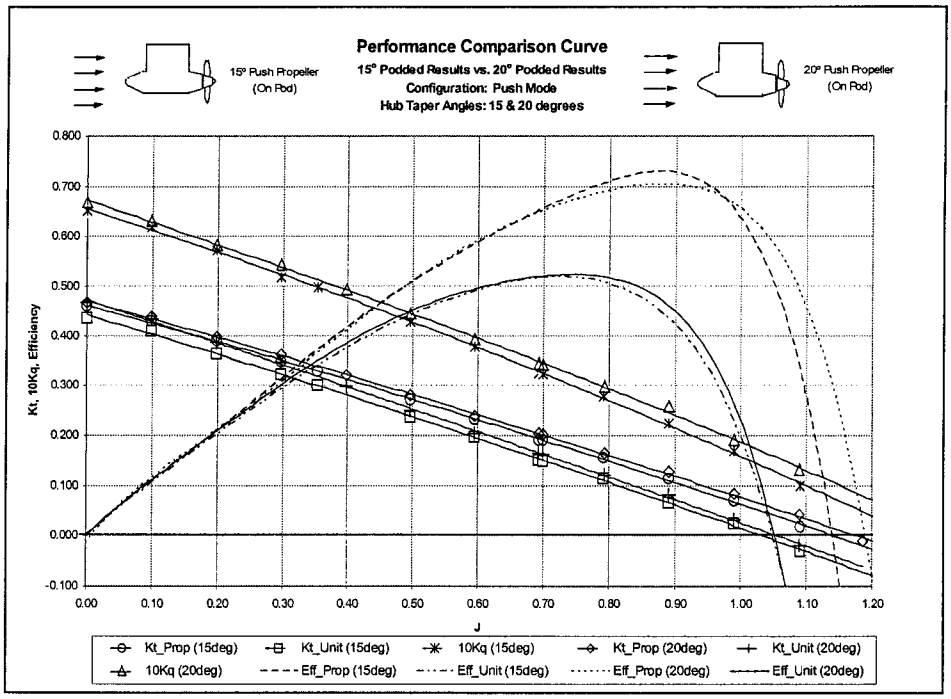

Figure 5.16: Performance Plot - 15° and 20° Push Podded Propellers

As with the previous plots, the percent difference is calculated to illustrate how the larger hub angle of the 20° push podded propeller caused the performance characteristics to differ from the 15° push podded propeller. This data is shown in Table 5.9.

20° vs. 15° Push 'Podded Propeller' Open Water Test Results					
J	% Diff $10K_Q$	% Diff K_{T_PROP}	% Diff η_{PROP}	% Diff K_{T_UNIT}	% Diff η_{UNIT}
0.0	2.7%	1.8%	0.0%	6.7%	0.0%
0.2	2.0%	2.0%	0.0%	6.2%	0.8%
0.4	3.7%	3.0%	-0.1%	6.5%	1.3%
0.6	4.0%	2.6%	-0.9%	3.6%	-0.2%
0.8	6.8%	6.1%	-0.3%	6.2%	-0.2%

Table 5.9: Percent Difference in 20° Push Podded Propeller and 15° Push Podded Propeller Results

From the above data it can be seen that for a push podded propeller tested using the 'podded propeller unit' approach, increasing the hub taper angle increases the torque and this effect increases for higher advance coefficients. Similarly the propeller thrust is higher when a larger hub angle is used, and this effect increases with advance coefficient. The overall effect on the propeller efficiency is a slight decrease in efficiency for increased hub taper angle, which is more pronounced for higher J. For the push mode podded propellers, the overall unit thrust appears to be significantly greater over the entire range of advance coefficient when hub angle is increased. This causes slightly higher overall unit efficiency for low J, but for higher advance coefficients, the hub taper angle does not appear to greatly affect the overall unit efficiency.

Based on the above observations, it may be concluded that in general, increasing the hub taper angle on a conical hub propeller will decrease the efficiency of the propeller in the higher advance coefficient range. Furthermore, for podded propellers, the performance of the pull mode configuration appears to be more sensitive to variations in hub taper angle than the push mode units.

5.6 Comparison of Push and Pull Configurations

Another objective of this experimental study was to investigate the dependence of propulsion performance on the mode of operation for which that

propeller was designed: push or pull. To this end, comparisons of the performance of push configurations relative to their pull counterparts are presented for both hub taper angles and are given for both the baseline and podded propeller series of experiments.

Figure 5.17 shows a plot comparing the performance characteristics of the baseline 15° pull and push propellers.

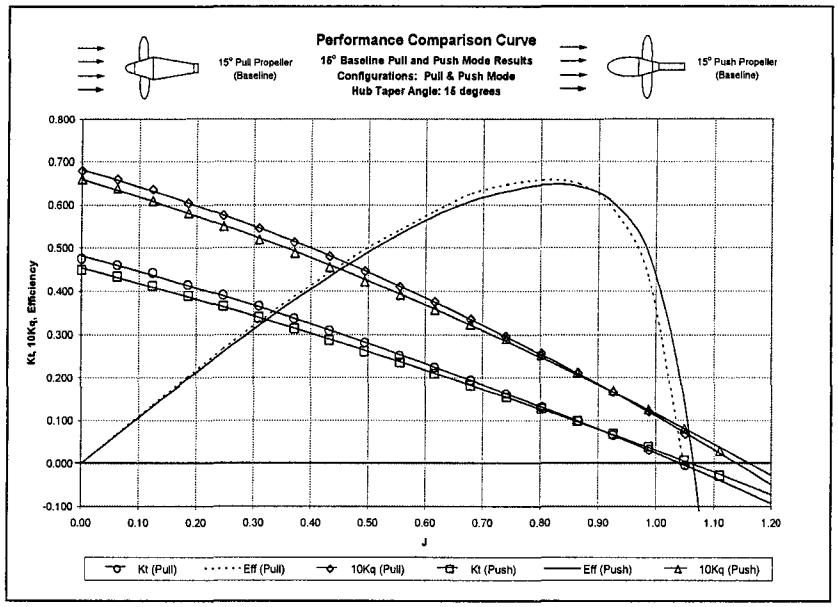

Figure 5.17: Comparison of Push and Pull Mode - 15° Baseline Propellers

To more clearly illustrate the trends present in the above plot, percent differences have been calculated and are summarized in Table 5.10. This table provides a comparison of the thrust coefficients, torque coefficients and efficiencies over a range of advance coefficients for the 15° push and pull configuration propellers.

15° Push vs. Pull 'Baseline' Open Water Test Results			
J	% Diff $10K_Q$	% Diff K_T	% Diff η
0.0	-2.9 %	-5.6 %	0.0 %
0.2	-3.8 %	-6.3 %	-0.4 %
0.4	-4.8 %	-6.8 %	-0.7 %
0.6	-4.8 %	-6.5 %	-1.1 %
0.8	-1.3 %	-2.9 %	-1.0 %

Table 5.10: Comparison of Data for 15° Pull Propeller (Baseline) and 15° Push Propeller (Baseline)

Based on the above data it can be seen that the push configuration propeller consistently has lower torque and thrust coefficients than its pull counterpart tested under the same conditions. The overall effect on the propeller efficiency is a slight decrease in efficiency, particularly for the lightly loaded condition (i.e. higher advance coefficients).

The 20° baseline propeller data for both push and pull configurations is plotted in Figure 5.18. A comparison of the thrust coefficients, torque coefficients and efficiencies is summarized in Table 5.11. As can be seen in this table, the limited data available for the 20° pull propeller in baseline mode limits the conclusions that may be drawn about this propeller at the bollard condition.

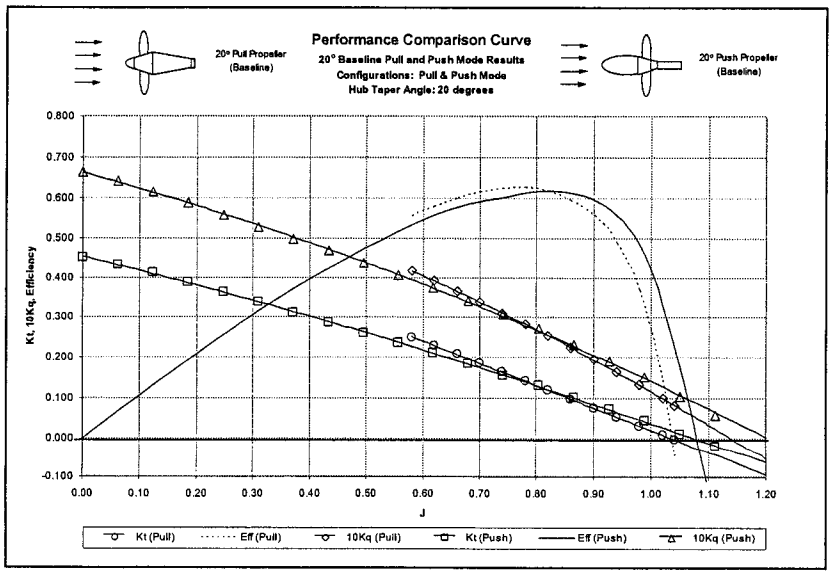

Figure 5.18: Comparison of Push and Pull Mode - 20° Baseline Propellers

Based on the available data for these particular propellers, it is observed that the push mode propellers appear to have lower torque, thrust and corresponding propeller efficiency for advance coefficients below the design point (J = 0.8).

20° Push vs. Pull 'Baseline' Open Water Test Results			
J	% Diff $10K_Q$	% Diff K_T	% Diff η
0.0	-	-	-
0.2	-	-	-
0.4	-	-	-
0.6	-4.7 %	-7.9 %	-2.1 %
0.7	-0.8 %	-4.5 %	-2.2 %
0.9	4.6 %	7.3 %	1.5 %

Table 5.11: Comparison of Data for 20° Pull Propeller (Baseline) and 20° Push Propeller (Baseline)

A possible explanation for this observation has been reported by Islam et al. (2004), who proposed that the cause of the observed differences in performance for the push and pull baseline propellers is due to the variance in the inflow conditions, as well as the differences in the blade root intersection geometry for push and pull propellers with the conical hubs. These differences in root geometry were reported to cause variation in the numerically predicted root hub pressure distributions, which in turn impact the overall propeller performance.

The results of the podded propeller experiments yield more significant differences in performance as a function of the propeller mode than was observed in the baseline tests. The results presented in Figure 5.19 show a comparison of the performance of the 15° push and pull mode podded propellers.

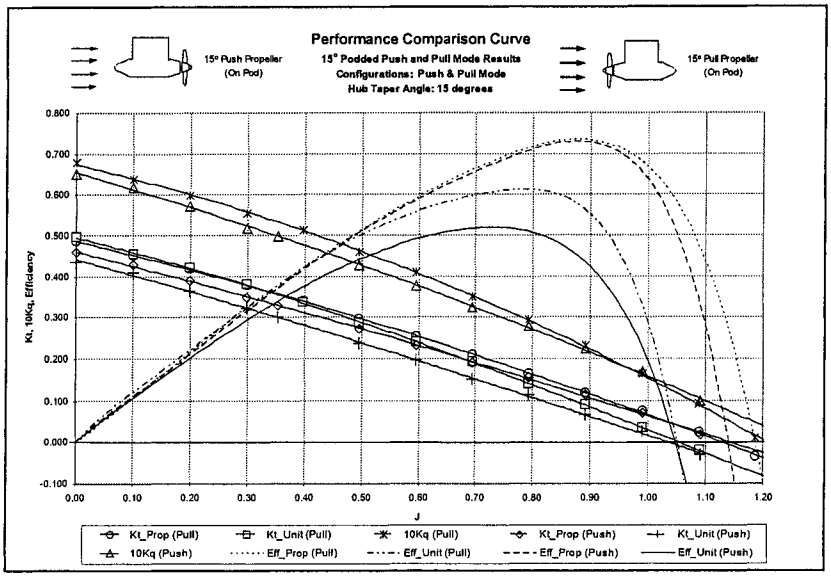

Figure 5.19: Comparison of Push and Pull Mode - 15° Podded Propellers

The percent differences of the unit thrust coefficients, propeller thrust coefficients, torque coefficients and efficiencies over a range of advance coefficients are summarized in Table 5.12.

15^0 Push vs. Pull 'Podded Propeller' Open Water Test Results					
J	% Diff $10K_Q$	% Diff K_{T_PROP}	% Diff η_{PROP}	% Diff K_{T_UNIT}	% Diff η_{UNIT}
0.0	-4.0 %	-5.5 %	0.0 %	-12.0 %	0.0 %
0.2	-4.4 %	-6.8 %	-0.5 %	-13.8 %	-2.2 %
0.5	-7.1 %	-8.1 %	-0.5 %	-17.1 %	-5.3 %
0.6	-8.1 %	-9.0 %	-0.5 %	-18.5 %	-6.3 %
0.8	-4.6 %	-6.3 %	-1.2 %	-19.9 %	-9.8 %

Table 5.12: Comparison of Data for 15° Pull Propeller (Podded) and 15° Push Propeller (Podded)

From the above data, it may be observed that the torque coefficient and the propeller thrust are consistently lower for a push mode podded propeller unit than for a pull mode podded propeller unit, with the overall effect being slightly lower propeller efficiency for push mode than for pull mode. A much more

significant difference in the propeller thrust coefficient is observed for push units than for pull units, resulting in significantly lower overall unit efficiency.

The results of the 20° podded propeller tests shown in Figure 5.20 show very similar trends, with the propeller efficiencies being very close for both modes, while the pull mode unit efficiency exceeds the push mode unit efficiency by a large amount.

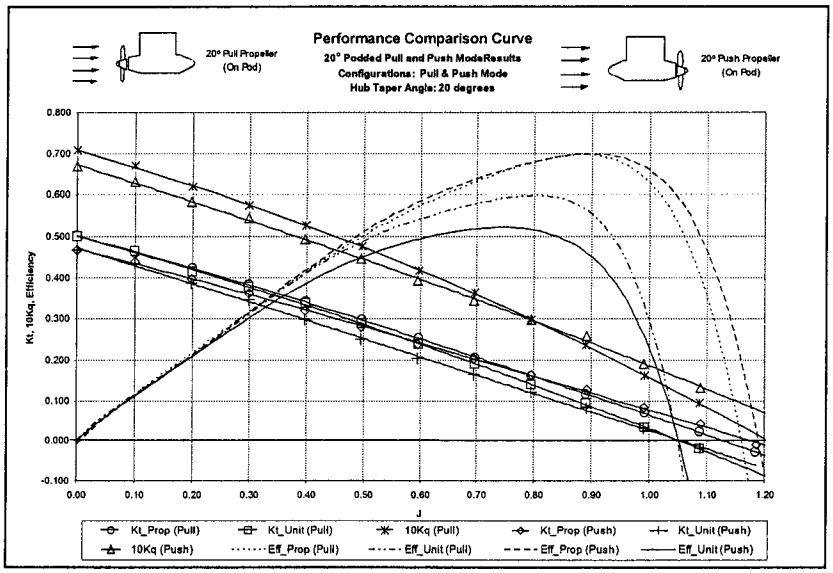

Figure 5.20: Comparison of Push and Pull Mode - 20° Podded Propellers

The percent difference calculations for these two podded propeller units are presented in Table 5.13 below. As observed, the torque coefficient and propeller torque are lower for the 20° push mode podded propeller unit than for its pull mode counterpart, resulting in slightly lower propeller efficiency for push mode than for pull mode. The unit thrust coefficient is observed to be significantly lower for push units than for pull units, which in turn seems to have a net effect of producing an overall unit efficiency which is lower for push units than for pull units.

20° Push vs. Pull 'Podded Propeller' Open Water Test Results					
J	% Diff $10K_Q$	% Diff K_{T_PROP}	% Diff η_{PROP}	% Diff K_{T_UNIT}	% Diff η_{UNIT}
0.0	-5.3%	-6.7%	0.0%	-6.6%	0.0%
0.2	-5.9%	-6.2%	-0.2%	-6.9%	-0.3%
0.4	-6.2%	-6.3%	-0.2%	-11.2%	-2.3%
0.6	-5.9%	-6.2%	-0.4%	-15.0%	-5.5%
0.8	-0.1%	1.6%	1.1%	-14.0%	-8.3%

Table 5.13: Comparison of Data for 20° Pull Propeller (Podded) and 20° Push Propeller (Podded)

Based on these observations it may be concluded that both sets of experiments indicate that pull mode propellers perform slightly better in terms of propeller thrust coefficient, torque coefficient and propeller efficiency than their push mode counterparts. Therefore, in terms of propeller performance in open water conditions, pull mode propellers perform slightly better than push mode propellers.

For the podded propeller unit performance, it may be concluded that the unit thrust for a pull mode podded propulsor is consistently higher than for a push mode unit. This in turn results in higher unit efficiency for the pull mode case. Therefore, in terms of podded propeller unit performance in open water conditions, pull mode podded propellers perform significantly better than push mode pod units.

Based on these two points, it may also be concluded that the mode of operation has a greater influence on the overall unit performance than on the propeller performance.

The relative differences predicted by both the baseline and podded propeller unit series of experiments for push and pull mode propellers in terms of propeller thrust coefficient, torque coefficient and propeller efficiency are in very close agreement. This indicates that the unit performance as a function of mode of operation is primarily influenced by hydrodynamic forces acting on the pod shell and strut, not by a change of the propeller performance due to the presence

of the pod body in the flow. If the loss of propeller performance due to poor inflow were the cause of the difference in the overall unit performance, this would be reflected in the propeller thrust measurements, as well as the calculated propeller efficiency. Since the relative propeller performance is the same whether the pod is present or not, the results indicate that the key to improving push podded propeller unit performance lies in obtaining a better understanding of the hydrodynamic forces acting on the pod body and how they impact the performance of the podded propeller as a complete unit.

The presence of the pod and strut will result in notably different inflow for the propellers of the push and pull mode podded propulsors. However, this difference in inflow did not appear to greatly impact the relative propeller performance of the push and pull mode propulsors. Since a significant difference in unit performance was observed for both modes of operation, while the relative propeller performance was not significantly affected by the presence of the pod body and strut, this indicates that differences in the unit performance may be attributed primarily to hydrodynamic forces on the pod body and strut, not as a result of effects due to variation in inflow conditions.

As discussed previously, a proposed explanation for the major difference in the push and pull mode units, is that the strut and body to recover some of the rotational energy in the propeller slipstream, by acting as lifting bodies which generate a force with a forward acting component, which effectively reduces the overall resistance component of the pull unit when compared with the push unit, Halstensen and Leivdal (1990). Further testing is recommended to validate the observed results and to assess ways to characterize and optimize these effects.

While the experimental results presented above provide useful insight into the performance of podded propellers, it is important to recognize that uncertainty levels in the results obtained may impact the corresponding conclusions. As with any set of experiments, uncertainties exist. Based on this understanding, a detailed uncertainty analysis was completed, as presented in Chapter 6.

Chapter 6 - Uncertainty Analysis

6.1 Scope

This chapter examines the uncertainty levels of both the baseline propeller open water test results and podded propeller open water experimental results. A brief overview of the analysis methodology has been provided, with a particular focus on specific elements that are unique to these experiments. Results of both the baseline propeller and podded propeller uncertainty analysis are included. Based on these findings, a series of recommendations of possible ways to reduce the overall uncertainty levels are made.

6.2 Uncertainty Analysis Methodology

Many standards organizations offer general recommendations and guidelines for uncertainty analysis, but it is the work of the International Towing Tank Conference (ITTC) which is most closely aligned with the testing techniques used in this study. The methodology used in this analysis follows the recommended guidelines set out by the ITTC in combination with approaches described by Bose and Luznik (1996), as well as Coleman and Steele (1999). The details of the exact methodology used in this chapter have been included in Appendix E for the baseline tests and Appendix F for the podded propeller tests.

As detailed by Coleman and Steele (1999), overall uncertainty estimates consist of a combination of two categories of error: bias errors and precision errors. The bias components are fixed errors inherent in the system or process, which may be reduced through calibration. The precision errors are variable errors which can be reduced through the use of multiple readings.

Given that the objective of this analysis was to determine the overall uncertainty in the non-dimensional performance coefficients, it was first essential to identify all of the variables contained within the data reduction expressions of

interest. Recall the data reduction equations used in this study, shown again in Table 6.1, are adapted from the generalized forms, as discussed in Chapter 1.

Baseline Propeller Open Water Tests	
Performance Chararcteristic	Data Reduction Equation
K_T - Thrust Coefficient	$T/(\rho n^2 D^4)$
K_Q - Torque Coefficient	$(Q-Q_o)/(\rho n^2 D^5)$
J - Advance Coefficient	$V/(nD)$
η_o - Baseline Efficiency	$(K_T J)/(2\pi K_Q)$
Where:	
T = thrust	n = shaft speed
Q = torque	D = propeller diameter
Q_o = frictional torque	V = advance speed
ρ = density	

Podded Propeller Open Water Tests	
Performance Chararcteristic	Data Reduction Equation
K_{Tprop} - Propeller Thrust Coefficient	$T_{PROP}/(\rho n^2 D^4)$
K_{Tunit} - Unit Thrust Coefficient	$T_{UNIT}/(\rho n^2 D^4)$
K_Q - Torque Coefficient	$Q/(\rho n^2 D^5)$
J - Advance Coefficient	$V/(nD)$
η_{PROP} - Propeller Efficiency (on Pod)	$(K_{Tprop} J)/(2\pi K_Q)$
η_{UNIT} - Unit Efficiency (on Pod)	$(K_{Tunit} J)/(2\pi K_Q)$
Where:	
T_{PROP} = propeller thrust	n = shaft speed
T_{UNIT} = unit thrust	D = propeller diameter
Q = torque	V = advance speed
ρ = density	

Table 6.1: Data Reduction Equations

The variables of interest from the above equations are grouped according to each set of tests. For the baseline propeller tests, thrust, torque, frictional torque, shaft speed, advance speed, density and propeller diameter were the variables considered in the analysis. The variables included in the podded propeller uncertainty analysis were propeller thrust, unit thrust, torque, shaft speed, advance speed, density and propeller. In addition, it should be noted that since density is dependent on temperature, this relationship must be included

and thus, temperature was also a variable included in the uncertainty analysis of both sets of experiments.

The measurement systems and processes used to obtain the data for each of these variables were influenced by a variety of elemental sources of error. These elemental sources were estimated, as detailed in Appendices E and F, and combined using the root-sum-square (RSS) method to give the bias and precision limits for each of the variables. While it was often possible to identify many elemental error sources for the bias limits, for the precision error estimates of most variables, only one source of error was considered significant.

The error estimates used in the determination of the bias and precision limits in this study were taken to represent 95-percent confidence interval estimates. These limits were combined using the general equation shown below to provide estimates of overall uncertainty levels in these variables using the equation given below.

$$U_r = [B_r^2 + P_r^2]^{1/2}$$

The final step in the analysis methodology was to determine how uncertainties in each of the variables propagate through the data reduction equations. Using the approaches described by Bose and Luznik (1996), and Coleman and Steele (1999) the uncertainty expressions for each set of experiments were developed. In the expressions for the baseline propeller tests shown below, it should be noted that for thrust coefficient uncertainty, the tare thrust is imbedded in the thrust measurement.

$$(U_{Kt}/K_T)^2 = (U_T/T)^2 + (U_\rho/\rho)^2 + 4(U_n/n)^2 + 16(U_D/D)^2$$

$$(U_{Kq}/K_Q)^2 = (U_Q/Q\text{-}Q_o)^2 + (U_{Qo}/Q\text{-}Q_o)^2 + (U_\rho/\rho)^2 + 4(U_n/n)^2 + 25(U_D/D)^2$$

$$(U_J/J)^2 = (U_V/V)^2 + (U_n/n)^2 + (U_D/D)^2$$

Since the tare thrust is part of the same data stream as the thrust reading, it has not been treated as an independent contributor of error to the thrust coefficient, but rather has been treated as a bias error on the static-zero value of the thrust measurement. As shown below, for the purposes of the uncertainty analysis, both podded propeller thrust measurements were treated in the same manner as the thrust for the baseline tests.

$$(U_{KTprop}/K_{Tprop})^2 = (U_{Tprop}/T_{prop})^2 + (U_\rho/\rho)^2 + 4(U_n/n)^2 + 16(U_D/D)^2$$

$$(U_{KTunit}/K_{Tunit})^2 = (U_{Tunit}/T_{unit})^2 + (U_\rho/\rho)^2 + 4(U_n/n)^2 + 16(U_D/D)^2$$

$$(U_{KQ}/K_Q)^2 = (U_Q/Q)^2 + (U_{Qo}/Q)^2 + (U_\rho/\rho)^2 + 4(U_n/n)^2 + 25(U_D/D)^2$$

$$(U_J/J)^2 = (U_V/V)^2 + (U_n/n)^2 + (U_D/D)^2$$

As discussed previously the instrumentation for the baseline propeller experiments was such that it required frictional torque to be subtracted from the measured torque. Since the frictional torque necessitated a set of separate tests, this data stream was subject to the same possible errors as the actual test condition torque measurement. Based on this observation it was determined that from an uncertainty analysis point of view, the frictional and test torque data should both be included as two separate variables, each of which contributes to the overall error in the torque coefficient. This additional term for frictional torque was not required for the podded propeller instrumentation, as it was designed such that the torque reading was not influenced by friction.

The uncertainty analysis results for both series of tests, using the above outlined methodology, are found in a subsequent section of this chapter.

6.3 Uncertainty Estimates for Baseline Tests

Each of the variables identified in the above data reduction expressions has been either directly or indirectly obtained through measurements. As such, each one of these variables had to be examined in detail to determine the overall

levels of uncertainty. Using the approach detailed in Appendix E, the bias and precision limit estimates for the baseline propeller tests were estimated as summarized in Table 6.2.

Variable	Bias Errors		Bias Limit		Precision Errors		Precision Limit	
Temperature	Calibration:	+/- 0.5 °C.	Fossilized into +/- 0.714 °C for Temperature		Scale: Range:	+/- 0.5 °C. +/- 0.10 °C.		
Density	Temp Related Errors: Density Eqn Errors:	+/- 0.017 kg/m^3 +/- 0.112 kg/m^3	Overall Limit:	+/- 0.113 kg/m^3				
Propeller Diameter	CNC Machining Errors: Hand Polishing Errors:	+/- 0.0001 m +/- 0.0002 m	Overall Limit:	+/- 0.000224 m				
Shaft Speed	Calibration:	+/- 0.0167 rps	Overall Limit:	+/- 0.0167 rps	Scale:	+/- 0.0167 rps	Overall Limit:	+/- 0.0167 rps
Advance Speed	Measurement Errors: Tide Effects:	+/- 0.00586 m/s +/- 0.001 m/s	Overall Limit:	+/- 0.00595 m/s			J = 0.1 J = 0.4 J = 0.7	+/- 0.00014 m/s +/- 0.00043 m/s +/- 0.00106 m/s
PropellerThrust	Weights: Loading Angle: Load Cell Align: Static Zero: A/D Error: Curve Fit:	+/- 0.00277 N +/- 0.01378 N +/- 0.00344 N +/- 0.08900 N +/- 0.04063 N +/- 0.66823 N	*Calibration Data Errors* Overall Limit:	+/- 0.68257 N			J = 0.1 J = 0.4 J = 0.7	+/- 0.21688 N +/- 0.19794 N +/- 0.40813 N
	Equipment Angle: Load Cell Align: Static Zero: A/D Error:	+/- 0.00067 N +/- 0.00344 N +/- 0.08900 N +/- 0.04063 N	*Testing Data Errors*					
Torque	Weights: Lever Angle: A/D Error: Static Zero: Curve Fit: Static Zero: A/D Error:	+/- 0.11768 Nm +/- 0.01200 Nm +/- 0.04733 Nm +/- 0.01200 Nm +/- 0.17851 Nm +/- 0.01200 Nm +/- 0.04733 Nm	*Calibration Data Errors* Overall Limit: *Testing Data Errors*	+/- 0.22501 Nm			J = 0.1 J = 0.4 J = 0.7	+/- 0.00931 Nm +/- 0.00592 Nm +/- 0.00269 Nm
Frictional Torque	Weights: Lever Angle: A/D Error: Static Zero: Curve Fit: Static Zero: A/D Error:	+/- 0.11768 Nm +/- 0.01200 Nm +/- 0.04733 Nm +/- 0.01200 Nm +/- 0.17851 Nm +/- 0.01200 Nm +/- 0.04733 Nm	*Calibration Data Errors* Overall Limit: *Testing Data Errors*	+/- 0.22501 Nm			+/- 0.0033752 Nm	

Table 6.2: Baseline Propeller Test Bias and Precision Limits

Combining these bias and precision limits as described in the preceding section, each of the overall uncertainty estimates shown in Table 6.3 was calculated for the variables of interest.

	J = 0.1	J = 0.4	J = 0.7
U_p	0.11308	0.11308	0.11308
U_D	0.00022	0.00022	0.00022
U_n	0.02357	0.02357	0.02357
U_V	0.00595	0.00596	0.00604
U_T	0.71619	0.71069	0.79528
U_Q	0.22520	0.22508	0.22502
U_{Qo}	0.22503	0.22503	0.22503

Table 6.3: Overall Uncertainty Estimates for Baseline Propeller Variables

Substituting these values into the uncertainty expressions for the data reduction equations gives the overall uncertainty levels for the thrust, torque and advance coefficients as summarized in Table 6.4 below.

	Advance Coefficient Value	Thrust Coefficient K_T (+/-)	Percentage Error in K_T (+/-)	Torque Coefficient K_Q (+/-)	Percentage Error in K_Q (+/-)	Advance Coefficient Error (+/-)
9 rps	0.1	0.00205	0.5%	0.00104	1.7%	0.00148
	0.4	0.00153	0.5%	0.00102	2.1%	0.00164
	0.7	0.00105	0.6%	0.00101	3.1%	0.00195

Table 6.4: Overall Error in Thrust, Torque and Advance Coefficients

Comparing the above uncertainty estimates with those published by Bose and Luznik (1996) for a series of propeller open water experiments, one can conclude that for the baseline propeller open water tests, the overall levels of uncertainty are reasonable. It should be noted that some opportunities exist for improvement, as explored in further detail in the last section of this chapter.

Applying the above uncertainty limits to the performance curves in the form of error bars results in a plot as shown in Figure 6.1 below.

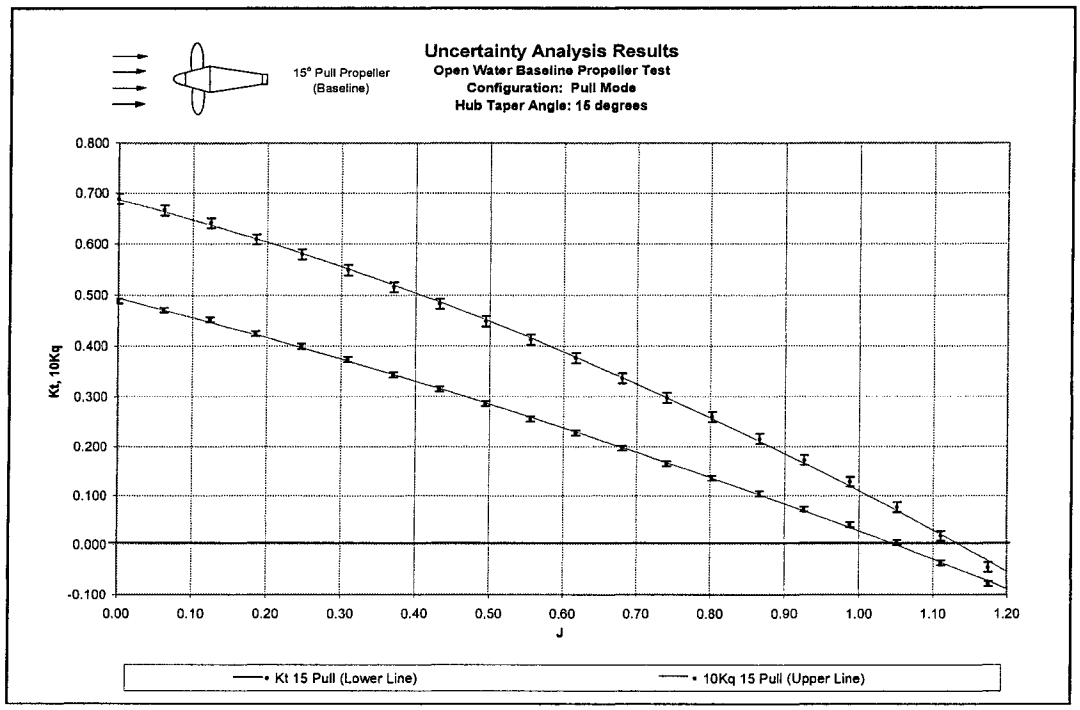

Figure 6.1: Uncertainty Analysis Results for Baseline Propeller Tests

This plot illustrates that the curve fitted to the above data set is within the error bars representing the 95-percent confidence interval estimate of the uncertainty in the data. Based on this finding, it can be concluded that this curve fit provides a good representation of the trends indicated by the experimental results.

6.4 Uncertainty Estimates for Podded Propeller Tests

As for the baseline propeller uncertainty analysis, it was necessary to identify and examine each of the variables in the above data reduction expressions to determine the appropriate bias and precision limits. Table 6.5 below summarizes the bias and precision limit estimates for the podded propeller tests obtained using the approach detailed in Appendix F.

Variable	Bias Errors		Bias Limit		Precision Errors		Precision Limit	
Temperature	Calibration:	+/- 0.5 °C.	Fossilized into +/- 0.745 °C for Temperature		Scale: Range:	+/- 0.05 °C. +/- 0.55 °C.		
Density	Temp Related Errors: Density Eqn Errors:	+/- 0.122 kg/m^3 +/- 0.108 kg/m^3	Overall Limit:	+/- 0.162 kg/m^3				
Propeller Diameter	CNC Machining Errors: Hand Polishing Errors:	+/- 0.0001 m +/- 0.0002 m	Overall Limit:	+/- 0.000224 m				
Shaft Speed	Calibration:	+/- 0.0167 rps	Overall Limit:	+/- 0.0167 rps	Scale:	+/- 0.0167 rps	Overall Limit:	+/- 0.0167 rps
Advance Speed	Measurement Errors: Tide Effects:	+/- 0.00586 m/s +/- 0.001 m/s	Overall Limit:	+/- 0.00595 m/s			J = 0.1 J = 0.4 J = 0.7	+/- 0.00014 m/s +/- 0.00043 m/s +/- 0.00106 m/s
PropellerThrust	Weights: Loading Angle: Load Cell Align: Static Zero: A/D Error: Curve Fit: Equipment Angle: Load Cell Align: Static Zero: A/D Error:	+/- 0.00276 N +/- 0.00525 N +/- 0.00131 N +/- 0.14110 N +/- 0.23904 N +/- 3.38951 N +/- 0.00525 N +/- 0.00131 N +/- 0.14110 N +/- 0.23904 N	*Calibration Data Errors* Overall Limit: *Testing Data Errors*	+/- 3.40696 N			J = 0.1 J = 0.4 J = 0.7	+/- 0.1798 N +/- 0.3959 N +/- 0.5018 N
Unit Thrust	Weights: Loading Angle: Load Cell Align: Static Zero: A/D Error: Curve Fit: Equipment Angle: Load Cell Align: Static Zero: A/D Error:	+/- 0.00276 N +/- 0.01905 N +/- 0.00119 N +/- 0.10643 N +/- 0.22567 N +/- 2.36918 N +/- 0.01905 N +/- 0.00119 N +/- 0.10643 N +/- 0.22567 N	*Calibration Data Errors* Overall Limit: *Testing Data Errors*	+/- 2.41523 N			J = 0.1 J = 0.4 J = 0.7	+/- 0.59463 N +/- 0.6879 N +/- 0.5656 N
Torque	Weights: Static Zero: A/D Error: Curve Fit: Static Zero: A/D Error:	+/- 0.00935 Nm +/- 0.03522 Nm +/- 0.0671 Nm +/- 0.0598 Nm +/- 0.03522 Nm +/- 0.0671 Nm	Overall Limit:	+/- 0.12311 Nm			J = 0.1 J = 0.4 J = 0.7	+/- 0.0034 Nm +/- 0.0188 Nm +/- 0.0641 Nm

Table 6.5: Podded Propeller Test Bias and Precision Limits

These bias and precision limits were combined using RSS to determine the overall uncertainty estimates for each of the variables of interest. These uncertainty estimates are summarized in Table 6.6.

	J = 0.1	J = 0.4	J = 0.7
U_ρ	0.16242	0.16242	0.16242
U_D	0.00022	0.00022	0.00022
U_n	0.02357	0.02357	0.02357
U_V	0.00595	0.00596	0.00604
U_{TPROP}	3.41697	3.43512	3.44893
U_{TUNIT}	0.17977	0.39589	0.50176
U_Q	2.48736	2.51129	2.48058
U_{Qo}	0.12316	0.12455	0.13878

Table 6.6: Overall Uncertainty Estimates for Podded Propeller Variables

Substitution of the above values into the appropriate uncertainty expressions gave the overall uncertainty levels for the propeller thrust, unit thrust, torque and advance coefficients as summarized in Table 6.7 below.

	Advance Coefficient Value	Prop Thrust Coefficient K_{Tprop} (+/-)	Percentage Error in K_{Tprop} (+/-)	Unit Thrust Coefficient K_{Tunit} (+/-)	Percentage Error in K_{Tunit} (+/-)	Torque Coefficient K_Q (+/-)	Percentage Error in K_Q (+/-)	Advance Coefficient Error (+/-)
9 rps	0.1	0.00829	1.9%	0.00257	0.6%	0.00113	1.8%	0.00246
	0.4	0.00816	2.5%	0.00207	0.7%	0.00111	2.2%	0.00269
	0.7	0.00802	4.1%	0.00149	1.0%	0.00120	3.7%	0.00313

Table 6.7: Overall Uncertainty for Propeller Thrust, Unit Thrust, Torque and Advance Speed

From the above table it can be seen that the uncertainty levels of the propeller thrust coefficient are significantly higher than those of the unit thrust coefficient. In addition, the torque uncertainty is comparable with that of the baseline tests. Further investigation assisted with the identification of the major contributing factors in the overall uncertainty estimates, which resulted in the recommendations discussed in the next section.

Applying the above uncertainty limits to the performance curves in the form of error bars results in a plot as shown in Figure 6.2 below.

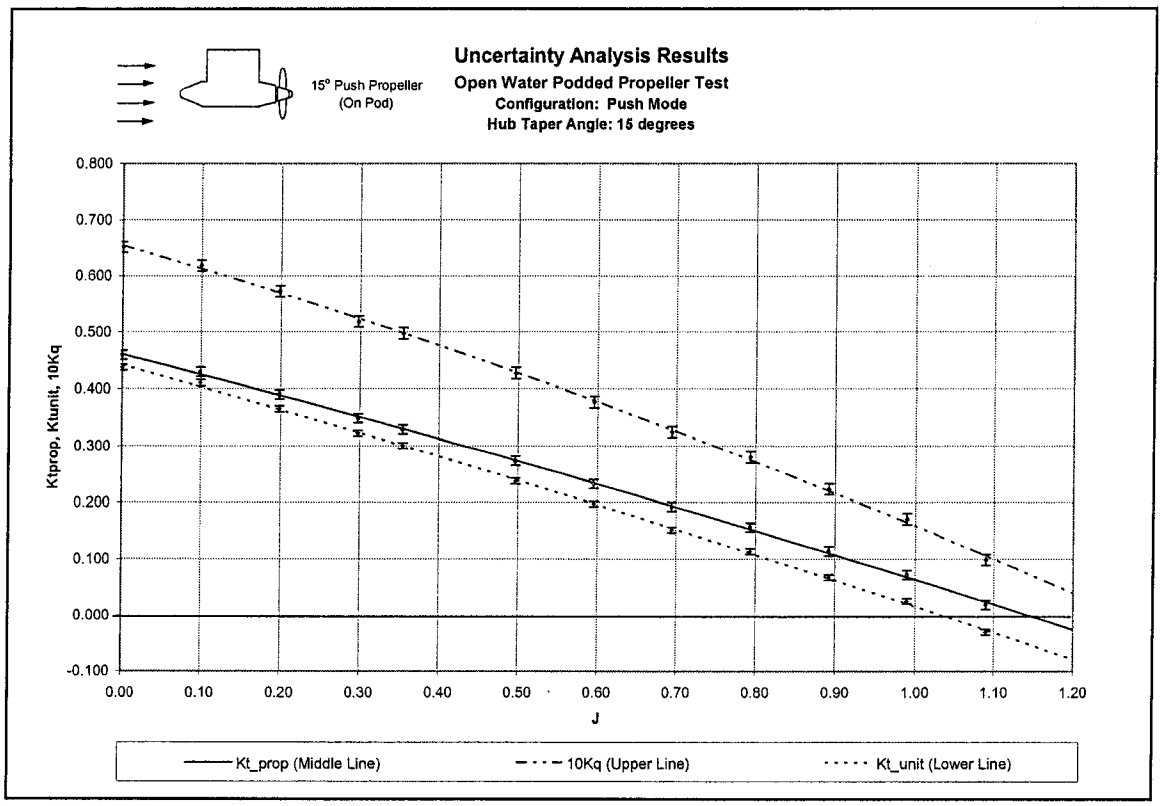

Figure 6.2: Uncertainty Analysis Results for Podded Propeller Test

From the above figure it can be observed that the curve fitted to this data lies within the error bars. Therefore this curve provides a good representation of the trends indicated by the results.

6.5 Discussion

As explained in Chapter 3, the baseline propeller tests were conducted using very high quality, well-established equipment, whereas the podded propeller tests were conducted using new, custom built instrumentation. For this reason, the uncertainty analysis results for the baseline propeller tests provided a good benchmark to compare with the uncertainty levels in the new podded propeller instrumentation. Comparison of the overall uncertainty levels given in

Table 6.4 and Table 6.7, show that the new instrumentation provides levels of accuracy comparable with the established equipment. The uncertainty levels observed in the propeller thrust and unit thrust in the pod tests were found to be higher than the thrust uncertainty for the baseline tests, but as discussed below, it is likely that procedural modifications will isolate and reduce these errors.

Given the objective of trying to reduce the overall error in the final results, each individual variable in Table 6.2 and Table 6.5 has been examined for possible ways to improve the accuracy. Given the high degree of accuracy presently found in the temperature, density, propeller diameter, shaft speed and advance speed, these variables have not been given any further consideration for improvement. Table 6.8 summarizes the major factors identified as influencing the uncertainty levels of thrust, torque and frictional torque for the baseline tests, in addition to the propeller thrust, unit thrust and torque for the podded propeller tests.

Variable	Major Factor(s) Influencing Uncertainty
Thrust	Curve-Fit Error
Torque	Weight Error, Curve-Fit Error
Frictional Torque	Weight Error, Curve-Fit Error
Propeller Thrust	Curve-Fit Error
Unit Thrust	Curve-Fit Error
Torque	Low Magnitude Reading

Table 6.8: Major Factors Influencing Uncertainty

From the above table we see that there are three major factors influencing the measurement variables: curve-fit error, weight error, and the low magnitude of the measurements.

The first of these, curve-fit error, is the main contributor to the overall levels of uncertainty. The recommended approach to reduce curve-fit error is to incorporate a standard error estimate (SEE) analysis into the calibration procedure. Error identification and reduction at the calibration stage may help

reduce error in the testing phase and in the final result, as one can determine whether or not a curve-fit is acceptable and ascertain the functionality of the equipment.

The existing procedure included plotting the calibration curve, and checking the R^2 coefficient to ensure the data was linear. While this gave an indication of the linearity of the data set, it did not provide a good measure of the error in the curve fit. Using the SEE as an evaluation technique one can refine techniques, instrumentation and analysis procedures until satisfactory calibration data and curve-fits are obtained.

This aspect of the calibration and curve-fitting was not considered until the overall uncertainty analysis was carried out. This may be several months after the fact, at which point it is not valid to simply set up equipment and re-calibrate if the data has an undesirably high SEE. Test equipment often undergoes changes between test programs, including minor repairs and changes in set-up procedures, which may have a significant impact on the calibration results. It is therefore vital to ensure that high quality calibration data, with a low SEE curve-fit has been obtained prior to proceeding to the testing phase. Furthermore, the inclusion of similar procedures for post-testing calibrations is recommended.

The uncertainty resulting in the torque coefficient for the baseline propeller tests due to errors in the weights is actually also in part influenced by the tolerance on the length of the moment arm used to balance the weights on the propeller shaft during calibration. Reducing this tolerance and improving the accuracy of the weights considered would help reduce these uncertainty levels. In addition, the range of weights selected for the calibration should more closely reflect the range of loads expected during testing.

Another possible approach to improve accuracy is to simply run future experiments at higher shaft speeds. As identified above, for the torque readings of the podded propeller experiments, there is no one dominant factor influencing the overall uncertainty. Despite low error levels in the variables in this uncertainty expression, the magnitudes of the actual test measurements are small and as

such the overall error is relatively larger. At higher shaft speeds, higher advance speeds will be required to achieve the desired advance coefficients. Under these conditions the magnitudes of the thrust and torque will be larger relative to the uncertainty levels. Correspondingly, the percent error for each of these measured variables would be reduced, which results in less overall uncertainty in the thrust and torque coefficients. As discussed previously, the main reason why these experiments were conducted at such low shaft speeds was to try to prevent damage to the instrumentation, as this was the first large scale series of tests completed with this new equipment.

Similar effects could be achieved if the torque strain gauge signals were amplified prior to digitization. This would boost the signal to noise ratio and reduce errors in the signal. By adjusting the amplification levels, it would allow the signal to noise ratio to be optimized based on the expected loading conditions, resulting in reduced error levels in the torque readings.

An additional route to pursue to improve uncertainty levels may be through modification of instrumentation. Examination of the torque coefficient uncertainty expression for the baseline propeller tests has revealed that the frictional torque component contributed approximately thirty-percent of the overall error estimate. While it was appropriate to include frictional torque in these calculations, it is possible for equipment to be designed such that no bearings and seals are located between the instrumentation and the propeller. This principle was employed in the design of the podded propeller instrumentation and as such torque measurements taken by this equipment were not influenced by friction. Modification of the equipment used for the baseline propeller tests to eliminate frictional torque may help reduce the overall uncertainty levels in the torque coefficient.

Based on experience gained from these experiments, speeds could be adjusted in future test plans to better avail of the full safe-loading range of the instrumentation. In addition, the range of calibration weights should be selected as to provide adequate resolution over the expected loading range. This may

have contributed to the error in the calibration curve obtained for the propeller thrust readings in the podded propeller series of tests. For this test series in particular, the instrumentation had been calibrated to a maximum load of approximately 600N, which was the loading estimated for a shaft speed of fifteen revolutions per second. From the test results it was discovered that, for the selected shaft speed of nine revolutions per second, a maximum calibration load of 250N with a finer resolution of calibration data points would have likely produced a better set of calibration data.

A final factor to consider is the degree to which inexperience in using this new equipment and in dealing with experimental uncertainty contributed to error in the results obtained. This combined with a compressed time schedule, due to limited towing tank availability, may have contributed to the overall error in the results. Through implementation of the above recommendations, and careful planning of future experiments, it is likely that significant reductions in uncertainty can be achieved.

As an aside, one must be aware of the implications that identifying and reducing the most significant sources of error will have on the uncertainty model that is used for the analysis. In reducing the obvious sources of error, elemental components, which previously may have appeared negligible, would become relatively larger contributors to the remaining total error. For instance if the curve-fit error, which is presently a predominant factor in the overall error, is greatly reduced through instrumentation and procedural modifications, it is possible that this new total error estimate may be dominated by another factor, which previously seemed negligible. As shown above, many small errors, which by themselves appear to be negligible, when combined result in significant errors in the variables. Therefore, one must exercise caution in prematurely stating that elemental error components are negligible and eliminating them from the analysis, as changes through the life cycle of a testing program may in fact change their relative significance.

For practical purposes, it is recognized that not every factor can or should be included in each uncertainty analysis. This is merely mentioned to draw attention to the importance of continuing to question the validity of analysis assumptions once changes have been implemented.

In conclusion, the calculated uncertainty levels in the baseline propeller experiments were found to be comparable with those determined by Bose and Luznik (1996) in similar tests. Furthermore, the custom-made podded propeller instrumentation demonstrated the capability of achieving uncertainty levels close to those of the established equipment. Suggested improvements to procedures and techniques for the podded propeller experiments will likely allow for a significant increase in the overall accuracy of the results obtained in future pod tests. The uncertainty analysis results presented provide strong supporting evidence that conclusions based on the experimental data presented in this study provide a very good representation of the true performance characteristics of these model-scale baseline and podded propellers.

Chapter 7 - Conclusions and Recommendations

7.1 Scope

This chapter provides a summarizing discussion of the observations and conclusions presented in previous chapters. This includes a discussion of the primary findings of the baseline and podded propeller experiments, along with a comparison of these two sets of data. This chapter also contains a brief discussion of the two testing approaches used, in addition to an assessment of the influence of the hub taper angle. Based on the results presented in previous chapters, conclusions regarding the effect of the mode of operation and suggestions of ways to reduce uncertainty levels are included.

7.2 Baseline Propeller Tests

For both the 15° and 20° propeller results it was observed that the pull propeller has higher bollard thrust and torque coefficients than the push counterpart, as well as having a higher maximum efficiency. In general, increasing the hub taper angle tends to increase the propeller thrust and torque at the bollard condition and the degree of this influence depends on the specific configuration. Furthermore, increasing the hub taper angle tends to cause a lower propeller efficiency at higher advance coefficients, again with the degree of influence depending on the specific configuration.

7.3 Podded Propeller Tests

For all instances considered the trends observed in the propeller thrust, torque and propeller efficiency appeared to correspond well to those predicted by the baseline tests.

For the 15° push podded propeller, at the bollard condition, the unit thrust was less than the propeller thrust, indicating that the hydrodynamic forces on the pod body and strut reduced the net thrust of the unit.

For the 15° pull podded propeller, at the bollard condition, the unit thrust was greater than the propeller thrust, indicating that the hydrodynamic forces on the pod body and strut increased the net thrust of the unit.

For both the 20° push and pull podded propellers, at the bollard condition, the unit thrust was equal to the propeller thrust, indicating that the hydrodynamic forces on the pod body did not significantly affect the net thrust of these units.

Due to potential uncertainties identified in the results, it is recommended to validate this data through additional future testing.

For all podded propeller units tested, the unit thrust decreases significantly faster as a function of increasing advance coefficient than does the propeller thrust. Correspondingly the unit efficiency is significantly lower than the propeller efficiency for all units and the maximum unit efficiencies typically occur at lower advance coefficients than the maximum propeller efficiencies.

In future investigations, it may be worthwhile to examine the details of the flow around the podded propeller unit using more advanced techniques such as LDV or PIV. These techniques may provide the additional level of detail necessary to provide a greater understanding of the complex flow interactions between the propellers and the pod and strut.

7.4 Comparison of Testing Approaches

The baseline 'propeller only' approach is useful for comparing the relative performance of model scale propellers used on podded propulsion units, as the propeller thrust and efficiency trends were similar to those predicted by the 'podded propeller unit' tests. However, the 'propeller only' approach has limitations.

The magnitudes of the performance characteristics for thrust and torque were observed to be quite different for the baseline 'propeller only' tests than for the 'podded propeller unit' tests. More specifically, the 'propeller only' tests, despite showing similar trends when comparing propeller configurations, did not accurately predict the magnitudes of the performance characteristics and the overall system performance.

Podded propeller unit tests, while more complex and resource-intensive, provide better indication of both how the propeller will operate as a part of the overall propulsion system and how well the overall unit will perform.

From a practical point of view, the overall unit performance is the main parameter of concern, since this is representative of the net thrust and efficiency of the propulsor. Podded propellers are more complex than conventional screw propellers and propellers designed for efficient open water performance will not necessarily guarantee an efficient podded propeller unit, as the influence of the pod and strut greatly reduce the overall unit performance. For this reason, optimization should be focused on the performance of the podded propeller as a system rather than as a sum of parts.

To assess the influence of the fairing adapters on the predicted propeller performance obtained in the baseline 'propeller only' tests it is recommended that any future tests which consider the performance of baseline conical hub propellers include an additional series of 'thrust dummy hub' experiments to test

for the influence of the fairing drag on the measured thrust as described in Chapter 5.

7.5 Influence of Hub Taper Angle

For the baseline pull propellers, increasing the hub taper angle increases the torque and propeller thrust for advance coefficients below the design point. The propeller efficiency is lower for larger hub taper angles and this influence increases for higher advance coefficients.

For the baseline push propellers, increasing the hub taper angle increases the torque, but only slightly increases thrust for high advance coefficients, with negligible effect on the thrust for low advance coefficients. The propeller efficiency is lower for larger hub taper angles, and this effect increases with increasing advance coefficient.

For the pull podded propeller units, increasing the hub taper angle increases the torque, and causes higher propeller thrust at low advance coefficients, but this comes at the cost of lower propeller efficiency in the higher advance coefficient range. The unit thrust does not appear to have a distinct trend as a result of increasing the hub taper angle, although the unit efficiency appears to be consistently lower by a small margin for increasing taper angle.

For the push podded propeller units, increasing the hub taper angle increases the torque and propeller thrust. This effect increases for higher advance coefficients. This increase in taper angle does cause the propeller efficiency to be slightly lower and this effect becomes more dominant for higher advance coefficient. The unit thrust is significantly larger for increased hub taper angle over the entire range of advance coefficient, but the result in terms of unit efficiency is only slightly higher unit efficiency for low advance coefficients, with negligible effect on the overall unit efficiency for high advance coefficients.

For podded propellers, the performance of the pull mode configuration appears to be more sensitive to variations in hub taper angle than the push mode.

The practical implication of these findings are that podded propulsion units for vessels with low speed, high thrust requirements may benefit from larger taper angles, while podded propulsors for more efficient, high speed vessels may benefit from designs with smaller hub taper angles. This work may also guide optimization of future podded propeller designs to help broaden the range of application of this rapidly expanding propulsion alternative.

7.6 Comparison of Push and Pull Configuration

For both 15° and 20° baseline propellers, the push configuration has consistently lower torque and propeller thrust than the pull propeller, causing lower propeller efficiency for the push propeller, particularly for higher advance coefficients.

For the 15° podded propeller units, the push configuration has consistently lower torque and propeller thrust than for a pull mode unit, resulting in slightly lower propeller efficiency for push mode than for pull mode. In addition, the unit thrust coefficient for the push mode was significantly less than that of the pull mode version, which in turn resulted in significantly lower unit efficiency for the push mode when compared to the pull mode.

For the 20° podded propeller units, very similar trends were observed, with consistently lower torque, propeller thrust, unit thrust and efficiencies for the push mode when compared to the pull mode.

In general it may be concluded that pull mode propellers perform slightly better than push mode propellers in terms of all performance characteristics considered: propeller thrust, torque and propeller efficiency for steady, open-water conditions at zero yaw angle to the flow.

Furthermore, for podded propeller unit performance, it may be concluded that a pull mode podded propeller will have consistently higher toque, propeller thrust, unit thrust and correspondingly higher propeller efficiency and unit efficiency than a push mode podded propeller.

In general, baseline push configuration conical-hub propellers have slightly lower propeller thrust and corresponding propeller efficiency than their pull mode counterparts. In addition, push configuration podded propeller units have slightly lower propeller thrust and corresponding propeller efficiency than their pull mode counterparts and significantly lower unit thrust and corresponding unit efficiency than their pull mode counterparts.

While inflow to the propellers will be different for both push mode and pull mode podded propellers, results indicate that differences observed in unit performance as a function of mode of operation are attributed primarily to hydrodynamic forces on the pod and strut body, not due to variation in inflow conditions. This conclusion is based on the observation that the relative differences between push and pull mode operation in terms of propeller thrust, torque and propeller efficiency are in very close agreement for both the baseline tests and the podded propeller unit tests, indicating that the presence of the pod body and strut do not greatly impact the relative propeller performance.

It may therefore be concluded that a key to improving podded propeller unit performance lies in acquiring a better understanding of the hydrodynamic forces acting on the pod body and strut and how they influence the overall system behavior. While propeller optimization will yield some improvements in performance, optimization efforts focused on first optimizing the pod body and strut hydrodynamics offer significant opportunities to improve unit performance.

It may also be concluded that the mode of operation has a more significant effect on the overall unit performance than it does on the propeller performance. The influence of configuration appears to have less effect on the unit performance for larger hub taper angles than for smaller hub taper angles.

7.7 Uncertainty Analysis

The results of the uncertainty analysis for the baseline propeller experiments were found to be comparable with those calculated for similar tests conducted by Bose and Luznik (1996). Comparison of the overall uncertainty levels of data collected using the custom-built podded propeller instrumentation with data collected using the well established Kempf & Remmers propeller boat showed that the new instrumentation is capable of providing levels of accuracy comparable with the established equipment. While the actual uncertainty levels observed in the pod test results presented in this study were found to be higher than the uncertainty for the baseline tests, it is likely that procedural modifications will be effective in greatly reducing these errors.

These uncertainty analysis results provide strong supporting evidence that conclusions based on the experimental data presented in this study provide a very good representation of the true performance characteristics of the model scale baseline and podded propellers considered.

The major factors contributing to the error in the measured variables were identified as curve-fit error, weight error, and the low magnitude of the measurements. Due to time constraints during the testing phase of a project, it is often not practical to try to conduct a complete uncertainty analysis in parallel with the testing. By integrating specific elements of the uncertainty analysis into the calibration procedures, however, it is likely that improvements in accuracy can be achieved. Based on the experience obtained from these experiments, it is recommended that the calibration procedure be modified to include a standard error estimate (SEE) analysis of the calibration data and curve-fit, to reduce the curve-fit error. This approach will help provide the insight needed to refine instrumentation and analysis procedures to obtain the desired levels of accuracy in the calibration data and curve-fits.

To improve the weight error, it has been recommended that the geometric tolerance for the moment arm used in the torque calibration should be reduced. In addition, improving the accuracy of the weights considered would help reduce these uncertainty levels. It is also suggested that in future calibrations, the range of the weights selected should more closely reflect the range of loads expected during testing. Correspondingly, the number of weights used for the calibration procedure should be high enough to provide an adequate resolution of data points over the expected loading range.

To remedy the problem of low magnitude torque readings, one recommended approach to improve accuracy is to run future experiments at higher shaft speeds, which will result in higher loads. This will increase the magnitude of the readings relative to the overall uncertainty in the measurements. Another recommendation is to amplify the torque strain gauge signals prior to digitization. This would help to reduce errors and to increase the signal to noise ratio. One of the identified benefits of using signal amplification is that by adjusting the magnification levels it would allow the signal to noise ratio to be optimized based on the expected loading conditions.

To reduce uncertainty levels in the torque readings obtained from the instrumentation for the baseline propeller tests it has been recommended that the equipment should be examined for a way to redesign it such that no bearings and seals are located between the strain gauges and the propeller. Making such modifications would eliminate the need for the inclusion of a frictional torque component in the analysis. This would significantly help reduce the overall uncertainty levels in the torque coefficient.

7.8 Design Considerations

Based on the results presented above, it may be concluded that the propeller design process should not be conducted completely independent of the

design of the pod and strut. An initial design and comparison of the propellers without the presence of the pod may be useful in indicating which propeller provides the best starting point, but focus should be placed on the overall unit performance. Since the goal should be to maximize the unit thrust and efficiency of the propulsion unit as a system rather than to simply to maximize the propeller thrust and efficiency, an integrated design approach is necessary for all elements of the podded propulsor. Optimizing the propeller design using conventional 'propeller only' techniques will not necessarily result in a more efficient podded propulsion unit. The modes of operation, as well as the hub taper angle both influence the performance of the unit as a system. The interactions between all of these components must be considered to optimize the performance of the entire system.

It would be worthwhile to investigate in further detail the hydrodynamic loading on the pod body and strut in both modes, as there appears to be a combination of both lift and drag forces on the pod that are influencing the overall performance of the unit. While this has limited implications when simply comparing model scale results, this is of much greater importance for extrapolating data for full-scale predictions. Correspondingly, any methods used must appropriately handle the observed differences in the push and pull mode performance.

Only through continued research and development efforts will it be possible to fill in the knowledge gaps that currently exist in the scientific understanding of podded propeller performance. Through greater understanding of the underlying phenomena that influence observed behavior it will be possible to maximize the true potential of this exciting propulsion alternative.

Bibliography

Akinturk, A., Jones, S., Moores, C., Bell, J., (2003), "Measuring Ice Loading on Podded Propellers Systems," *Proceedings of 22nd International Conference on Offshore Mechanics and Arctic Engineering*, vol. 3, Cancun, Mexico, 2003, pp. 795-799.

Akinturk, A., Jones, S., Duffy, D., Rowell, B., (2004), "Ice Loads on Azimuthing Podded Propulsors," *Proceedings of 23rd International Conference on Offshore Mechanics and Arctic Engineering*, vol. 3, Vancouver, BC, 2004, pp. 903-910.

Atlar, M., Prasetyawan, I., Aryawan, W.D., Wang, D., Sasaki, N., (2003), "Cavitation in Ice-Milling with a Podded Propulsor," *Proceedings of 4th ASME/JSME Joint Fluids Engineering Conference*, vol. 2, Honolulu, HI, 2003, pp. 269-278.

Ayaz, Z., Turan, O., Vassalos, D., (2004), "Maneuvering Aspects of Pod-Driven Ships," *Proceedings of T-Pod Conference*, Newcastle, UK, 2004, p. 135.

Backlund, A., Kuuskoski, J., (2000), "The Contra Rotating Propeller (CRP) Concept with a Podded Drive," *Motor Ship Conference*, Amsterdam, The Netherlands, 2000.

Ball, W.E., (2004), "Model Free-Manoeuvring in Calm Water by Partially Azimuthing Podded Drive," *RINA Transactions: International Journal of Maritime Engineering*, vol. 146, part A1, 2004.

Batsford, M., (2002), "Pod Propulsion: A Viable Option for the Canadian Navy," *Maritime Engineering Journal*, Fall 2001/Winter 2002.

Bertaglia, G., Lavini, G., Scarpa, S., (2004), "Hull Design and Optimization with Pod Propellers with 5 and 6 Blades," *Proceedings of T-Pod Conference*, Newcastle, UK, 2004, p. 39.

Bose, N., Luznik, L., (1996), "Uncertainty Analysis in Propeller Open Water Tests," *International Shipbuilding Progress,* 43, no. 435, 1996, pp. 237-246.

Boushkovsky, V.A., Pustoshny, A.V., (2003), "A Crash-Stop Study for an Azipod Propelled Vessel," *Proceedings of FAST 2003 – 7th International Conference on Fast Sea Transportation*, Italy, 2003.

Boushkovsky, V.A., Frolova, I., Kaprantsev, S.V., Pustoshny, A.V., Vasiljev, A.V., Jacolev, A.J., Veikonheimo, T., (2004), "On the Design of a Shafted Propeller Plus Electric Thruster Contra-rotating Propulsion Complex," *Proceedings of T-Pod Conference*, Newcastle, UK, 2004, p. 247.

Brown, G., (2003), "Like Peas in a Pod," *Marine Equipment News*, no. 56, April/May 2003, 2003, p. 45.

Carlton, J.S., (2002), "Podded Propulsors: Some Design and Service Experience," *Proceedings of Marine Propulsion Conference,* Copenhagen, Denmark, 2002.

Cheng, B.H., Dean, J.S., Miller, R.W., and Cave, W.L., (1989), "Hydrodynamic Evaluation of Hull Forms with Podded Propulsors," *Naval Engineers Journal*, vol. 101, no. 3, 1989, p. 197-206.

Chen, B.Y.H., Tseng, C.L., (1995), "A Contrarotating Propeller Design for a High Speed Patrol Boat with Pod Propulsion," *Proceedings of Fast '95 – 3rd International Conference on Fast Sea Transportation*, vol. 2, 1995, pp. 1003-1013.

Coleman, H.W., Steele, W.G., (1999), "Experimentation and Uncertainty Analysis for Engineers," 2nd Edition, *John Wiley & Sons, Inc.,* New York, USA, 1999.

DiFelice, F., Felli, M., Greco, L., Pereira, F., Salvatore, F., Testa, C., (2004), "Numerical and Experimental Investigation Tools for Preliminary Design of Podded Propulsor Components," *Proceedings of T-Pod Conference*, Newcastle, UK, 2004, p. 465.

Facinelli, W.A., Muggeridge, D., (1998), "Integrated System Analysis and Design of Podded Ship Propulsors," *Marine Technology*, vol. 35, no. 3, 1998, p. 151.

Friesh, J., (2001), "Investigations of Podded Drives in a Large Cavitation Tunnel," *Proceedings of PRADS 2001 - 8th International Symposium on Practical Design of Ships and Other Floating Structures,* vol. 2, Shanghai, China, 2001, p. 749.

Friesh, J., (2004), "Cavitation and Vibration Investigations for Podded Drives," *Proceedings of T-Pod Conference*, Newcastle, UK, 2004, p. 387.

Goubault, P., Perree, J., (2004), "Parametric Investigations Designed to Help Focused Pod Technology Developments," *Proceedings of T-Pod Conference*, Newcastle, UK, 2004, p. 27.

Halstensen, S.O., Leivdal, P.A., (1990), "The Development of the SpeedZ Propulsion System," *Proceedings of 7th International High Speed Surface Craft Conference*, 1990.

Hämäläinen, R., and Heerd, J.V., (2003), "Wave Damping Aftbody with Hybrid Podded Propulsors," *SNAME Transactions*, vol. 111, 2003, p. 33.

Heinke, H.J., (2001), "Alternative Propulsion Concepts for Fast Navy Ships, Part II: Podded Drives for Navy Ships," *Unkonventionnelle Rumpfformen für Marineschiffe: STG Sprechtag*, September 2001, Potsdam, Germany, 2001.

Heinke, C., Heinke H.J., (2003), "Investigations About the Use of Podded Drives for Fast Ships," *Proceedings of FAST 2003 - 7th International Conference on Fast Sea Transportation*, Italy, 2003.

Heinke, H.J., (2004), "Investigations about the Forces and Moments at Podded Drives," *Proceedings of T-Pod Conference*, Newcastle, UK, 2004, p. 305

Holtrop, J., (2001), "Extrapolation of Propulsion Tests for Ships with Appendages and Complex Propulsors," *Marine Technology,* vol. 38, no. 3, 2001, pp. 145-157.

Holtrop, J., Valkhof, H., (2003), "Propellers and Propulsion for High-Powered Container Ships," *The Naval-Architect,* September 2003, 2003, pp. 136-144.

Ikeda, J., Ikeda, Y., (2002), "A Feasibility Study on a Podded Propulsion LNG Tanker in Arun, Indonesia - Osaka, Japan Route," *12th International Offshore and Polar Engineering Conference Proceedings*, vol. 4, Kitakyushu, Japan, 2002, p. 525.

IOT Quality System Procedures Manual QP11.2, (1999), "Control of Inspection, Measuring and Test Equipment – Devices and Test Apparatus," *Quality System Procedures Manual*, version 1, Institute for Ocean Technology, Newfoundland, Canada, March 1999.

IOT Standard Test Methods 42-8595-S/TM-2 (2004), "Propeller Open Water Tests," *Institute for Ocean Technology Standard Test Methods*, version 6, Institute for Ocean Technology, Newfoundland, Canada, April 2004.

Islam, M., Taylor, R., Quinton, J., Veitch, B., Bose, N., Colbourne, B., Liu, P., (2004) "Numerical Investigation of Propulsive Characteristics of Podded Propellers," *Proceedings of T-Pod Conference*, Newcastle, UK, 2004, p. 513.

Islam, M., (2004), "Numerical Investigation on Effects of Hub Taper Angle and Pod-strut Geometry on Propulsive Performance of Pusher Propeller Configurations," *Master of Engineering Thesis*, Memorial University of Newfoundland.

ITTC 7.5-02-03-01.3 Revision 00, (2002), "Propulsion, Performance - Podded Propeller Tests and Extrapolation," *ITTC Recommended Procedures,* 23rd International Towing Tank Conference, Venice, Italy, 2002.

ITTC 7.5-02-03-01.2 Revision 00, (2002), "Uncertainty Analysis Example for Propulsion Test," *ITTC Recommended Procedures,* 23rd International Towing Tank Conference, Venice, Italy, 2002.

ITTC 7.5-02-03-02.1 Revision 01, (2002), "Open Water Test," *ITTC Recommended Procedures,* 23rd International Towing Tank Conference, Venice, Italy, 2002.

ITTC 7.5-02-02-02 Revision 01, (2002b), "Uncertainty Analysis, Example for Resistance Tests," *ITTC Recommended Procedures,* 23rd International Towing Tank Conference, Venice, Italy, 2002.

ITTC 7.5-02-01-01, (1999a), "Uncertainty Analysis in EFD, Uncertainty Assessment Methodology," *ITTC Recommended Procedures,* 22nd International Towing Tank Conference, Seoul/Shanghai, 1999.

ITTC 7.5-02-01-02, (1999b), "Uncertainty Analysis in EFD, Guidelines for Towing Tank Tests," *ITTC Recommended Procedures,* 22nd International Towing Tank Conference, Seoul/Shanghai, 1999.

ITTC 7.5-02-01-03, (1999c), "Density and Viscosity of Water," *ITTC Recommended Procedures,* 22nd International Towing Tank Conference, Seoul/Shanghai, 1999.

Jones, S., (2000), "Pod Trouble Makes Waves," *Motor Ship*, vol. 81, no. 963, 2000, p. 5.

Jones, S., (2002a), "Hydrodynamics or Pod Integrity," *Motor Ship*, Vol. 83, no. 985, 2002, p. 18.

Jones, S., (2002b), "Semi-submersible with Redundant DP and Azimuthing Pods," *Motor Ship*, vol. 84, no. 990, 2002, p. 23.

Jones, S., Dyck, P., (2002), "Podded First for Royal Navy," *Motor Ship*, vol. 83, no. 985, 2002, p. 48.

Jones, S., (2003), "Cruise Lines Analyse Pod Stress Waves," *Motor Ship*, vol. 84, no. 995, 2003, p. 80.

Kanerva, M., (1999), "Ferries for the Future," *Cruise & Ferry '99*, Paper No. 3, London, UK, 1999.

Karafiath, G., (1998), "Hydrodynamic Performance with Pod Propulsion – US Navy Experience," *Proceedings of 25th American Towing Tank Conference*, IOWA, USA, 1998, pp. 3-7 to 3-23.

Karafiath, G., Lyons, D., (1999), "Pod Propulsion Hydrodynamics – U.S. Navy Experience," *Proceedings of FAST '99 Conference,* Washington, USA, 1999, pp. 119-135.

Kaul, S., (2004), "New Podded Drives for the Power Range of 1-5 MW," *Proceedings of T-Pod Conference*, Newcastle, UK, 2004, p. 61.

Kavanagh, B., (2004), "Performance Testing of a Podded Propeller in the Cavitation Tunnel," *Laboratory Memorandum*, Institute for Ocean Technology, Newfoundland, Canada, April 2004.

Kim, S.E., Choi, S.H., Veikonheimo, T., (2002), "Model Tests on Propulsion Systems for Ultra-Large Container Vessels (ULCS)," *Proceedings of the 12th International Offshore and Polar Engineering Conference,* Kitakyushu, Japan, 2002.

Kobylinski, L., (2004), "Maneuverability Tests of a Vessel with Pod Propulsion," *Proceedings of T-Pod Conference*, Newcastle, UK, 2004, p. 371.

Kontes, T.C., Kontes, C.Th., (2004), "Experience of Festival Cruises Operating Pod Driven Ships," *Proceedings of T-Pod Conference*, Newcastle, UK, 2004, p. 431.

Kron, P., Holmstrom, L., (1999), "Hydrodynamic Aspects of Mermaid Propulsion System," *Proceedings of 21st Century Cruise Ship Conference,* Vol. 111, No. 3, Part 1.

Kurimo, R., Poustoshny, A.V., Syrkin, E.N., (1997), "Azipod Propulsion for Passenger Cruisers: Details of the Hydrodynamic Development and Experience on the Propeller Design for "Fantasy" Class Cruise Liners," *Proceedings of NAV & HMSV International Conference*, Sorrento, Italy, 1997.

Kurimo, R., (1998), "Sea Trial Experience of the First Passenger Cruiser with Podded Propulsors," *Practical Design of Ships and Mobile Units,* Elsevier Science B.V., 1998 pp. 743-748.

Kurimo, R., Bystm, L., (2003), "Manoeuvring with Pods: Model Tests and Sea Trial of M/S Costa Atlantica," *Proceedings of IMDC `03 - 8th International Marine Design Conference*, vol. 2, Athens, Greece, 2003, p. 163.

Laukia, K., (1996), "The Azipod System – Operational Experience and Designs for the Future," *Proceedings of Motor Ship International Marine Propulsion Conference*, London, UK, 1996, pp. 77-93.

Lavini, G., (2000), "New Hull and Propeller Design for Twin Screw Ships with Electric Pod Drives," *Proceedings of NAV 2000 – International Conference on Ship and Shipping Research,* Italy, 2000, pp. 6.6.1- 6.6.12.

Lepeix, R., (2001), "Hydrodynamic Trends in Hull Lines of Podded Drive Large Cruise Vessels," *Practical Design of Ships and Other Floating Structures,* Elsevier Science Ltd., 2001, pp. 767-775.

MacNeill, A., Taylor, R., Molloy, S., Bose, N., Veitch, B., Randell, T., Liu, P., (2004), "Design of a Model Pod Test Unit," *Proceedings of T-Pod Conference*, Newcastle, UK, 2004, p. 447.

Mewis, F., (2001), "The Efficiency of Pod Propulsion," *Proceedings of HADMAR 2001 Conference*, Bulgaria, 2001.

Molloy, S., Bose, N., Veitch, B., MacNeill, A., Taylor, R., (2004), "Systematic Geometric Variation of Podded Propulsor Models," *Proceedings of T-Pod Conference*, Newcastle, UK, 2004, p. 459.

Mullins, P., (2003), "Japanese Fast Ferries Adopt CRP Propulsion System," *Diesel-and-Gas-Turbine-Worldwide*, vol. 35, no. 8, 2003, p. 60.

Müller, J., (1999), "Podded Drives and Conventional Cargo Tonnage," *Proceedings of 21st Marine Propulsion Conference*, Athens, Greece, 1999, pp. 1-11.

Nakatake, K., Ando, J., Yoshitake, A., Sato, Y., Tamashima, M., (2004), "On Propulsive Performance of a Small Bulk-Carrier Model with Twin Podded Propellers," *Proceedings of T-Pod Conference*, Newcastle, UK, 2004, p. 501.

Niini, M., (1997), "Azipod Propulsion Breakthrough for Large Cruise Ships," *Proceedings of Cruise & Ferry '97,* London, UK, 1997.

Perttu, T., Matti, T., (2001), "Compact Azipod Registered Trademark Quality Power and Thrust for Rigs and Small Ships," *ABB-Review*, no. 4, 2001, pp. 10-13.

Pustoshny, A., Kaprantsev, S., (2001), "Azipod Propeller Blade Cavitation Observations During Ship Maneuvering," *Proceedings of CAV2001 – 4th International Symposium on Cavitation*, CA, USA, 2001.

Rains, D.A., VanLandingham, D. J., and Doyle, T.J., (1979), "Podded Destroyer Propulsion," *Naval Engineers Journal*, Vol. 91, 1979, pp.120-130.

Rains, D.A., VanLandingham, D. J., Schlappi, H. C., Hsiung, C. C., and Kirkman, K. L., (1981), "Hydrodynamics of Podded Ship Propulsion," *Journal of Hydronautics*, Vol. 14, 1981, pp. 18-24.

Raynor, S.J., (2000), "The Benefits of Podded Propulsion in the Offshore Market," *Proceedings of Dynamic Positioning Conference,* Houston, Texas, USA, 2000, pp. 1-11.

Ruponen, P., Matusiak, J., (2004), "Calculation Method for the Steering Forces of a Pod in Hybrid Propulsion," *Proceedings of T-Pod Conference*, Newcastle, UK, 2004, p. 263.

Sarioz, K., Atlar, M., Sarioz, E., Woodward, M.D., Sampson, R., (2004), "Operability of Fast Podded Ropax Ships in Rough Seas," *Proceedings of T-Pod Conference*, Newcastle, UK, 2004, p. 109.

Sasaki, N., Laapio, J., Fagerstrom, B., Juurmaa, K., Wilkman, G., (2004), "Full Scale Performance of Double Acting Tankers 'Tempera & Mastera'," *Proceedings of T-Pod Conference*, Newcastle, UK, 2004, p. 155.

Seokcheon, G., Heungwon, S., Chang, B.J., (2004), "Study on the Powering Performance Evaluation for the CRP-Pod Propulsion Ships," *Proceedings of T-Pod Conference*, Newcastle, UK, 2004, p. 277.

Sigrist, J.F, Gervot, C., Laine, C., LeBert, J.F., Barbarin, R., (2004), "Numerical Model for Naval Pods," *Proceedings of T-Pod Conference*, Newcastle, UK, 2004, p. 419.

Stettler, J.W., Hover, F.S., Triantafyllou, M.S., (2004), "Preliminary Results of an Azimuthing Podded Propulsor Relating to Vehicle Maneuvering," *Proceedings of T-Pod Conference*, Newcastle, UK, 2004, p. 321.

Szantyr, J., (2001), "Experimental Measurements of the Hydrodynamic Characteristics of the Pod Propulsor Models," *Polish Maritime Research,* Poland, 2001, p. 3.

Terwisga, T.V., Quadvlieg, F., Valkhof, H., (2001), "Steerable Propulsion Units: Hydrodynamic Issues and Design Consequences," *Paper for 80th Anniversary of Schottel GmbH & Co.*, August 2001.

Thomsen, J.C.N., (1999), "Steering Control Systems for the Azipod," *World Cruise Industry Review,* London, UK, 1999, p. 19.

Tinsley, D., (2004), "Podolesence," *Propulsion*, April 2004, p. 56.

Toxopeus, S.L., Leoff, G., (2002), "Maneuvering Aspects of Fast Ships with Pods," *Proceedings of 3rd International EuroConference on High-Performance Marine Vehicles,* Bergen, 2002.

Tozer, D., Penfold, A., (2001), "Ultra-Large Container Ships (ULCS)," *Proceedings of Boxship 2001 Conference,* London, UK, 2001.

Trägärdh, P., Lindell, P., Sasaki, N., (2004), "Double Acting Tanker – Experiences from Model Tests and Sea Trials," *Proceedings of T-Pod Conference*, Newcastle, UK, 2004, p. 173.

Trouwborst, W., (1998), "Non-conventional Ship Propulsion; Literature Study on Contra-rotating Propellers and Podded Propulsion," *TNO Report 98-CMC-R133*, Delft, The Netherlands, 1998.

Turan, O., Tuzcu, C., Clelland, Z., Ayaz, Z., (2004), "Effect of Pods on the Roll Behavior of Passenger Vessels," *Proceedings of T-Pod Conference*, Newcastle, UK, 2004, p. 125.

Ukon, Y., Ohashi, K., Fujisawa, J., Hasegawa, J., (2004), "Propulsive Performance of a Contra-rotating Podded Propulsor," *Proceedings of T-Pod Conference*, Newcastle, UK, 2004, p. 289.

Veitch, B., (1995), "Predictions of Ice Contact Forces on a Marine Screw Propeller During the Propeller-Ice Cutting Process," *Acta Polytechnica Scandinavica - Mechanical Engineering Series*, No. 118, Dissertation for Degree of Doctor of Technology, Helsinki, Finland, 1995.

Wang, D., Atlar, M., Glover, E.J., Paterson, I., (2004), "Experimental Investigation of Flow Field Around a Podded Propulsor Using LDA," *Proceedings of T-Pod Conference*, Newcastle, UK, 2004, p. 483.

White, R., (2000), "A Compact Azipod Propulsion System," *Offshore Support Journal*, vol. 3, no. 1, 2000, p. 10.

Woodward, M.D., Atlar, M., Clarke, D., (2004), "A Comparison of the Stopping Modes for Pod Driven Ships," *Proceedings of T-Pod Conference*, Newcastle, UK, 2004, p. 339.

Woodyard, D., (2001), "Popular Pods Still Striving for Perfection," *Marine Propulsion International*, Oct/Nov 2001, p. 26.

Appendix A:
Dimensional Analysis of Podded Propeller Performance

Introduction

This paper will focus on the methodology used to identify and select the experimental parameters used in the planning phase of the study entitled "Experimental Investigation of Hub Taper Angle on the Performance of Push and Pull Configuration Podded Propellers". The findings of this analysis will play an important role in streamlining testing within the proposed research program and will guide the analysis of collected experimental data. It is therefore imperative that great care be taken during these early stages to reduce the likelihood of future problems.

It should be noted that while the propeller geometry will also have a very significant impact on podded propeller performance, this is beyond the scope of this project and in the following analysis it will be assumed that a single standard propeller will be used in all tests. For this reason, the propeller geometry will be defined only in terms of its characteristic dimension: propeller diameter.

Variable Identification

The purpose of this section is to thoroughly consider an operating pod unit to establish which system components will be varied in the above-mentioned study and those which will not be examined. Efforts will be made to avoid eliminating any factors in the identification stages. Prematurely eliminating factors at this stage could have potentially detrimental effects on the results. When it becomes necessary to select specific combinations of factors in later stages, it may be possible to limit the growth of the test series by using experience to eliminate certain combinations of factors from the analysis. At this stage, however, all factors will be identified and considered

For organizational purposes, the variables of interest will be divided into the following three categories to ensure all variables are thoroughly examined: pod geometry variables, performance characteristics, and physical/environmental variables.

Pod Geometry Variables:

Defining this first group of variables entails the clear and complete definition of the geometry of the pod body. Since this project is aimed towards podded units in general, and not one particular design, it is useful to define a general shape that is a generic representation of existing pod designs currently available *(Fig. 1.)*.

By completely defining all major characteristics of this geometry, it will be possible to reduce any ambiguity associated with the size and shape of the pod units tested in this series of tests, which in turn will improve the repeatability of the results. From the above diagram, it can be seen that it is possible to divide the body of the pod shell into three main sections.

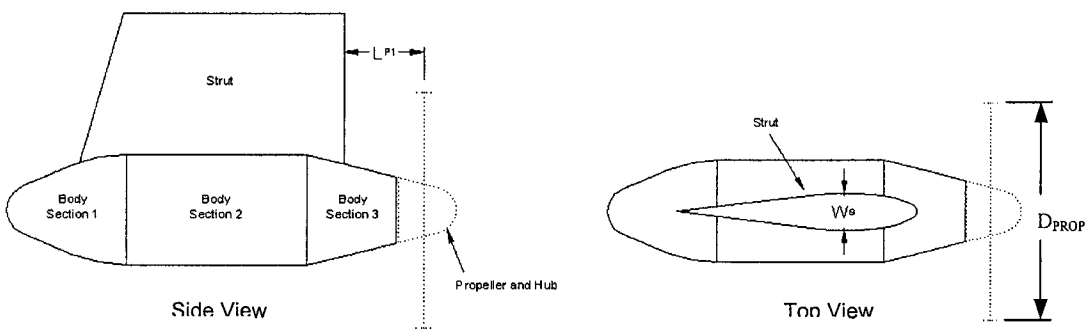

Fig. 1. Generic Pod Geometry

It is also possible to define some general strut dimensions independently of the body dimensions and thereby allow for identification of all the main dimensions *(Fig. 2.)*.

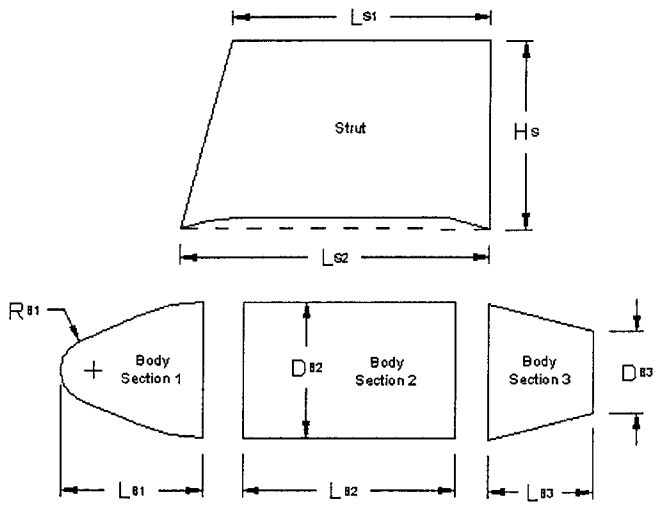

Fig. 2. Main Pod Dimensions

From these diagrams it can be seen that to completely define the geometry of the shell, it is necessary to specify the following geometric variables, all having linear dimensions:

Strut:

L_{P1} = [L] = dist from leading strut edge to prop plane

L_{S1} = [L] = length of top of strut

L_{S2} = [L] = length of bottom of strut

W_S = [L] = width of strut

H_S = [L] = height of strut

Body Section 1:

R_{B1} = [L] = radius of section end fillet

L_{B1} = [L] = overall length of section

Body Section 2:

D_{B2} = [L] = diameter of section

L_{B2} = [L] = length of section

Body Section 3:

D_{B3} = [L] = diameter of forward end of section

L_{B3} = [L] = length of section

Please note that it is assumed that the body sections are joined in a continuous manner and thus the diameters of the mating ends of section 1 and section 3 are equal to D_{B2} and it is therefore unnecessary to separately define these dimensions. It is also assumed that there are no fillets between the strut and the body and that the fillet radii between adjacent body sections remain constant.

All of the above geometric dimensions are linear and therefore require no further manipulation to get linear proportionalities. As previously mentioned, only a single propeller will be used for the entirety of these experiments and so its characteristic dimension can be identified as:

D_{PROP} = [L] = propeller diameter

Given that the propeller diameter will remain constant, it serves as an excellent basis to be used in combination with the aforementioned linear proportionalities to form π terms.

Performance Characteristics:

On a very fundamental level, if we consider the role of the propeller, it becomes evident that its function is to convert the rotary motion of the propeller shaft, which is created by an applied torque, to the translatory motion of vessel through the generation of a reactionary thrust force between the blades and the fluid that the vessel is travelling in. Correspondingly, the performance characteristics most commonly considered for propellers are the torque and thrust. While different actual measurements of thrust and torque may be taken at several locations within the instrumented pod used during the test phase, there is no added benefit in considering more than one torque or thrust value for the purposes of dimensional analysis.

For podded propeller units the performance will also be considered in terms of overall net unit thrust. Since both unit thrust and propeller thrust forces have the same dimensions, we can use a generalized thrust variable for dimensional analysis purposes. Therefore for both propellers and podded propeller units the following response variables which will be studied during experiments are:

$$T = [MLT^{-2}] = \text{Thrust}$$
$$Q = [ML^{2}T^{-2}] = \text{Torque}$$

In this particular testing application, it should be noted that it has been documented [2] that varying the gap width between the propeller hub and the pod body of a podded propeller has a significant effect on the measured values of propeller thrust *(Fig. 3.)*.

This observation may be a result of the limitations of the instrumentation used by researchers to measure the thrust of the propeller, since both intuition and basic force analysis on the pod would lead one to believe that this gap width should not play such a

significant role. Since this phenomena is not completely understood it is difficult to effectively resolve the drag forces present on the pod superstructure.

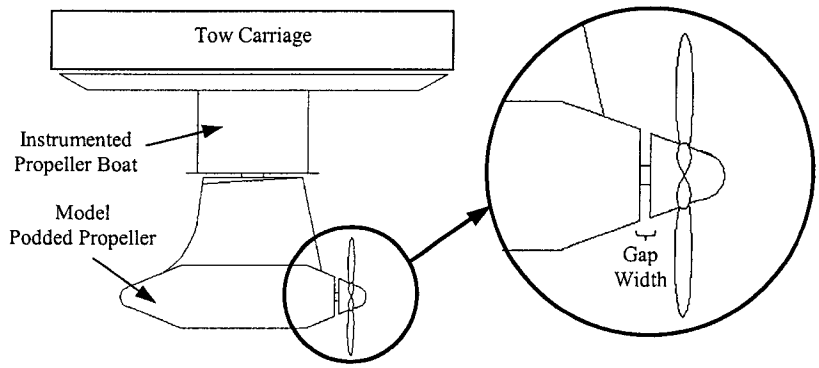

Fig. 3. Model Pod Unit Set-up

Given that this gap width was noted to be of importance, it will be included in the dimensional analysis.

$$w_{GAP} = [L] = \text{gap width between prop hub and pod body}$$

There are also two other factors associated with the propeller that will influence its performance: the rotational speed, n, and the forward velocity, V. Considering these two factors in the analysis will give:

$$n = [T^{-1}] = \text{rotational speed}$$
$$V = [LT^{-1}] = \text{velocity of propeller in direction of travel}$$

To simplify the analysis, it will be assumed that the pod body will always be parallel to the forward velocity and so yaw angle has not been included. Since the above variables are not linear proportionalities, they will require some manipulation to get into the correct form.

Physical/Environmental Variables:

This group of variables includes fluid properties, ambient conditions and other factors that may influence the response variables. In this category the following variables have been identified:

$g = [MLT^{-2}]$ = gravitational acceleration

$\mu = [ML^{-1}T^{-1}]$ = fluid viscosity

$\rho = [ML^{-3}]$ = fluid density

$h = [L]$ =depth of propeller centerline

Dependent and Independent Variables:

From the above categories, we can summarize the dependent and independent variables as follows:

Dependent Variables:

$T = [MLT^{-2}]$; $Q = [ML^{2}T^{-2}]$;

Independent Variables:

$L_{P1} = [L]$;	$L_{S1} = [L]$;	$L_{S2} = [L]$;
$W_S = [L]$;	$H_S = [L]$;	$R_{B1} = [L]$;
$L_{B1} = [L]$;	$D_{B2} = [L]$;	$L_{B2} = [L]$;
$D_{B3} = [L]$;	$L_{B3} = [L]$;	$w_{GAP} = [L]$;
$h = [L]$;	$D_{PROP} = [L]$;	$n = [T^{-1}]$;
$V = [LT^{-1}]$;	$g = [MLT^{-2}]$;	$\mu = [ML^{-1}T^{-1}]$;
$\rho = [ML^{-3}]$;		

Dimensional Analysis

Dimensional analysis is instrumental both in guiding the initial planning of the experimentation and in planning how to analyze and arrange dimensionless groups once the data has been collected. By thoroughly considering the entire experimental life cycle of the project, it is possible to increase the efficiency of the program and reduce the likelihood of collecting useless data or omitting variables that are crucial to the analysis.

The starting point for this stage of the analysis will be to write a functional equation that describes the physical phenomena that is to be studied. For the following analysis, Barr's Method of Synthesis will be applied in an attempt to provide the opportunity to find more convenient solutions and additional insight into the alternative solutions that are available. Where appropriate, practical consideration of the usefulness of certain combinations will be taken into account since this may allow for the selection of the most convenient and physically relevant arrangements of terms.

Linear Terms:

From these variables we see that the majority already have linear dimensions. Given that there are fourteen (n=14) existing linear terms to combine in groups of two terms (r=2), we can find ninety-one possible combinations (nCr=91) of these factors. It is therefore necessary to use logical justification for the selection of the thirteen π terms that are selected from these possibilities *(Table 1)*. To monitor the effects of varying the pod shell geometry, it would be logical to ensure that the propeller geometry remains constant throughout the tests. Thus the propeller diameter will serve as the reference dimension to create π terms from the existing linear term, since it would allow for the entire pod shell to be easily scaled relative to the propeller. Some of these linear dimensions however, may be more conveniently non-dimensionalized using other linear

terms and therefore other forms may be considered to ensure the most appropriate form is selected.

Parameters	π Term #	π Terms	Variable/Fixed	Justification	
L_{P1}	π_1	L_{P1}/D_{PROP}	Variable Ratio	Parameter of Interest	
L_{S1}	π_2	L_{S1}/D_{PROP}	Fixed for this series	Future work	
L_{S2}	π_3	L_{S2}/L_{S1}	Fixed for this series	Future work	Strut
W_S	π_4	W_S/L_{S1}	Fixed for this series	Future work	Strut
H_S	π_5	H_S/L_{S1}	Fixed for this series	Future work	Strut
R_{B1}	π_6	R_{B1}/D_{B2}	Fixed Ratio	Scale with Diameter	Strut
L_{B1}	π_7	L_{B1}/D_{PROP}	Variable Ratio	Parameter of Interest	Shell
D_{B2}	π_8	D_{B2}/D_{PROP}	Variable Ratio	Parameter of Interest	Shell
L_{B2}	π_9	L_{B2}/D_{PROP}	Variable Ratio	Parameter of Interest	Shell
D_{B3}	π_{10}	D_{B3}/D_{PROP}	Variable Ratio	Parameter of Interest	Shell
L_{B3}	π_{11}	L_{B3}/D_{PROP}	Variable Ratio	Parameter of Interest	Shell
w_{GAP}	π_{12}	w_{GAP}/D_{PROP}	Fixed at 0.02	Test Results – Mewis[1]	Shell
H	π_{13}	h/D_{PROP}	Fixed at 2	ITTC Procedures[2]	Shell

[1] Mewis, F. *The Efficiency of Pod Propulsion*, HADMAR 2001 Conference Proceedings, 2001

[2] International Towing Tank Conference 2002, *Testing Procedures*

Table 1 – Justification for Selection of π Terms for Linear Parameters

Since the focus of the proposed series examines the geometry of the pod shell only, it is possible to reduce the size of the test matrix by specifying a single strut geometry for the entire series. When one considers the role of the strut in the operation of the pod unit, it becomes evident that in oblique flows, such as that which would occur in a turning maneuver, the strut surface acts as a lifting surface and serves to assist in these operations. Studying the effects of strut geometry on pod unit performance in oblique flows would be a much more involved process than this analysis since this would necessitate inclusion of yaw angle, which as previously stated is not considered.

By defining generic strut geometry for this test series it will be possible to develop sequential test series' to build on the finding of these tests if further investigation of the strut geometry is desired in the future.

For the purposes of this analysis, the strut geometry has been included simply for completeness and the strut dimensions specified will remain constant throughout the test series to minimize the number of experimental runs required. It should be noted that the location of the strut relative to the propeller will still be included. If the leading edge of the strut were placed close to the propeller, it is reasonable to expect that it would interfere more with the wake of the propeller than it would if it were placed far away. For this reason, the location of the leading edge of the strut relative to the plane of the propeller is believed to be an important factor in the performance of the unit. Since this variable can be adequately tested with a generic strut, this factor will still be included.

Functional Equation - Thrust:

The thrust forces have dimensions $[MLT^{-2}]$. Using Barr's Method of Synthesis we need to get four linear proportionalities out of five (n=5) variables offering nCr = 10 possible linear combinations of two variables (r=2) *(Table 2)*. While any of the linear terms identified in the above section can be used to obtain π terms from the linear proportionalities, for reasons previously discussed, only D_{PROP} has been included.

$$T = \Phi(V, n, g, \mu, D_{PROP}, \underbrace{\pi_1, \pi_2, \pi_3, \ldots, \pi_{13}}_{\pi \text{ terms created from above linear parameters}}) \qquad (1)$$

Thrust: Using $(T, V, n, g, \mu) + (D_{PROP}, \pi_1, \pi_2, \pi_3, \ldots, \pi_{13})$

To get the four linear proportionalities out of five (n=5) variables using Barr's Method of Synthesis we can select from the ten (nCr=10) possible linear combinations of two

variables (r=2) *(Table 3).* It should be noted that for the following equations T is a general thrust variable that can be interchanged with either the propeller thrust or the net pod unit thrust.

Variables	Linear Proportionalities
T, V	$(T/\rho V^2)^{1/2}$
T, n	$(T/\rho n^2)^{1/4}$
T, g	$(T/\rho g)^{1/3}$
T, μ	$(T/\mu n)^{1/2}$
V, n	(V/n)
V, g	(V^2/g)
V, μ	$(\mu/\rho V)$
n, g	(g/n^2)
n, μ	$(\mu/n\rho)^{1/2}$
g, μ	$(\mu^{2/3}/\rho^{2/3}g^{1/3})$

4 from these

Table 3: Possible Linear Combinations for Thrust

While efforts are made not to be dogmatic to standard numbers, it is useful to identify those present in the above list and consider their relevance to this series. If we consider the above linear combinations, we can see that the following standard numbers are present:

Froude Number (Fn): *(V^2/g) and a linear term* (2)

Reynolds Number (Re): *$(\mu/\rho V)$ and a linear term* (3)

Form of K_T from Standard Propeller Tests: *$(T/\rho n^2)^{1/4}$ and a linear term* (4)

Advance Coefficient, J, from
Standard Propeller Tests: *(V/n) and a linear term* *(5)*

If these four standard numbers are selected, they can be combined with any one of the fourteen linear terms previously identified to give the remaining four π terms. Given that the propeller diameter is to be held constant for this series and that this diameter is frequently the standard dimension used for non-dimensionalizing these equations, it is possible to write the following standard forms:

$$\overbrace{\Phi\{(T/\rho n^2 D_{PROP}{}^4)}^{K_T}, \overbrace{(V^2/gD_{PROP})}^{Fn}, \overbrace{(\mu/\rho V D_{PROP})}^{Re}, \overbrace{(V/nD_{PROP})}^{J}, \overbrace{\pi_1, \pi_2, \pi_3, \ldots, \pi_{13,}\}}^{\pi\ Terms} \quad (6)$$

In addition to being a convenient solution, these standard numbers also present some opportunities for direct comparison with data collected from conventional screw propellers since most existing propeller performance data is presented in this manner. This fact will certainly play a very large role in the selection of non-dimensionalized arrangements for the thrust and torque relationships.

Since other useful forms may be available, it is worthwhile to consider other non-dimensional forms. The combination given below would be particularly useful if it were determined that it would be more worthwhile to relate the thrust on the pod unit to the free-stream velocity, since the unit thrust will also be influenced by drag on the pod body. However from a practical stand point, meaningful comparisons of propeller thrust and unit thrust would only be possible if the same forms are used. It is therefore most likely that the standard forms would be used for both thrust measurements.

$$\Phi\{(T/\rho V^2 D_{PROP}{}^2), (g/n^2 D_{PROP}), (\mu/\rho n D_{PROP}{}^2), (V/nD_{PROP}), \pi_1, \pi_2, \pi_3, \ldots, \pi_{13,}\} \quad (7)$$

Another possible option may be:

$$\Phi\{(T/\rho g D_{PROP}^3), (\mu^{2/3}/\rho^{2/3} g^{1/3} D_{PROP}), \overbrace{(\mu/\rho V D_{PROP})}^{Re}, \overbrace{(V/nD_{PROP})}^{J}, \overbrace{\pi_1, \pi_2, \pi_3, \ldots \pi_{13},}^{\pi\ Terms}\} \quad (8)$$

Despite the other possible forms considered, in the case of thrust it is more likely that standard terms would be used given past experience with these forms. Not only do the standard numbers provide a convenient solution, but also these numbers allow the measured thrust of the propeller and unit to be benchmarked against existing data. This will allow for a better understanding of the observed trends and provide more insight into the behavior of the system.

Functional Equation - Torque:

The functional equation for torque is closely related to the thrust, since its dimension only varies by a single linear term. The functional relationship can be written as given below.

$$Q = \Phi(V, n, g, \mu, D_{PROP}, \underbrace{\pi_1, \pi_2, \pi_3, \ldots, \pi_{13}}_{\pi \text{ terms created from above linear parameters}}) \quad (9)$$

Torque: Using (Q, V, n, g, μ) + $(D_{PROP}, \pi_1, \pi_2, \pi_3, \ldots, \pi_{13})$

Again, applying Barr's Method of Synthesis to the above variables it is possible to get ten (nCr=10) combinations of two variables (r=2) from a total of five (n=5) variables. From these possible linear proportionalities, four groups must selected *(Table 4)*.

Considering the traditional choice of numbers we can get:

$$\overbrace{K_Q}^{} \quad \overbrace{Fn}^{} \quad \overbrace{Re}^{} \quad \overbrace{J}^{} \quad \overbrace{\pi\ Terms}^{}$$

$$\Phi\{(Q/\rho n^2 D_{PROP}{}^5), (V^2/gD_{PROP}), (\mu/\rho V D_{PROP}), (V/nD_{PROP}), \pi_1, \pi_2, \pi_3, \ldots, \pi_{13,}\} \quad (10)$$

Variables	Linear Proportionalities
Q, V	$(Q/\rho V^2)^{1/3}$
Q, n	$(Q/\rho n^2)^{1/5}$
Q, g	$(Q/\rho g)^{1/4}$
Q, μ	$(Q/\mu n)^{1/3}$
V, n	(V/n)
V, g	(V^2/g)
V, μ	$(\mu/\rho V)$
n, g	(g/n^2)
n, μ	$(\mu/n\rho)^{1/2}$
g, μ	$(\mu^{2/3}/\rho^{2/3}g^{1/3})$

4 from these

Table 4: Possible Linear Combinations for Torque

As with thrust, using standard numbers to present the torque data also offers opportunities for comparison with data collected from conventional screw propellers. It is likely that in the actual test series the standard numbers will be used, however, for completeness other arrangements are considered below:

$$\Phi\{(Q/\rho V^2 D_{PROP}{}^3), (g/n^2 D_{PROP}), (\mu/\rho n D_{PROP}{}^2), \overbrace{(V/nD_{PROP})}^{J}, \overbrace{\pi_1, \pi_2, \pi_3, \ldots, \pi_{13,}}^{\pi\ Terms}\} \quad (11)$$

While this arrangement still uses the advance coefficient, J, the torque is related to the forward speed instead of the rotational speed. While this arrangement may be useful in some instances, from a practical point of view the rotational speed of a full-scale propeller, which is adjusted by varying the motor RPM, is more easily adjusted than the forward speed, which depends on the ship speed. In this capacity we can see the usefulness of the standard K_Q arrangement. Another option may be:

$$\Phi\{(Q/\rho g D_{PROP}^4), (\mu^{2/3}/\rho^{2/3} g^{1/3} D_{PROP}), \overbrace{(\mu/\rho V D_{PROP})}^{Re}, \overbrace{(V/n D_{PROP})}^{J}, \overbrace{\pi_1, \pi_2, \pi_3, \ldots \pi_{13,}}^{\pi\ Terms}\} \quad (12)$$

Again in this arrangement, the torque coefficient may not be the best choice since it is related to the density, gravitational acceleration and the propeller diameter, which as previously mentioned would be held constant throughout the test series.

Final Selection of Variables:

Based on the above discussions, it has been determined that the standard numbers in combination with the π terms specified in *Table 1* will be selected for use in the experiments that are to follow this report. Eliminating repeated variables and summarizing these terms gives the following:

$(Q/\rho n^2 D_{PROP}^5)$;	$(T/\rho n^2 D_{PROP}^4)$;	$(V^2/g D_{PROP})$;	(L_{B3}/D_{PROP});
$(\mu/\rho V D_{PROP})$;	$(V/n D_{PROP})$;	(L_{P1}/D_{PROP});	(L_{S1}/D_{PROP});
(L_{S2}/L_{S1});	(W_S/L_{S1});	(H_S/L_{S1});	(R_{B1}/D_{B2});
(L_{B1}/D_{PROP});	(D_{B2}/D_{PROP});	(L_{B2}/D_{PROP});	(D_{B3}/D_{PROP});
(w_{GAP}/D_{PROP});	(h/D_{PROP});		

Discussions and Conclusions

Using the above analysis as a guide it will be possible to make better decisions about the appropriateness of the selected non-dimensional forms to use when analyzing experimental results. While the details of these experiments are beyond the scope of this paper, it is clear to see how the above dimensional analysis is useful in helping with experimental planning.

This may be illustrated by considering the parameters below, which have been identified as variables which should be held constant throughout all experiments in order to minimize the number of experimental runs required, while allowing focus to be placed on the primary parameters of interest.

(L_{S1}/D_{PROP}); (L_{S2}/L_{S1}); (W_S/L_{S1}); (H_S/L_{S1});
(R_{B1}/D_{B2}); (h/D_{PROP}); (w_{GAP}/D_{PROP});

Two of the non-dimensional arrangements identified in this analysis that are commonly of interest in experimental hydrodynamics are Froude number and Reynolds number. As discussed, these parameters will be monitored, but are not directly important to the podded propeller performance study. Froude number is generally included in resistance tests and other tests involving surface waves, however for this case, the propeller unit will be deeply submerged and so it is not of great relevance. For Reynolds number it is important to ensure that this parameter it is greater than 10^6 at all times during testing. This ensures that the propeller is operating in a turbulent flow regime so as to minimize the effects of laminar flow on the obtained results.

(V^2/gD_{PROP}); $(\mu/\rho VD_{PROP})$;

The advance coefficient, J, will be varied throughout the experiments, primarily by changing V, while n remains constant.

$$J = (V/nD_{PROP});$$

Experimental measurements will be taken for the propeller thrust, unit thrust and shaft torque response variables. Based on the above analysis, their corresponding dimensionless parameters will most likely be of the form:

$(T_{PROP}/\rho n^2 D_{PROP}^4)$; $(T_{UNIT}/\rho n^2 D_{PROP}^4)$; $(Q/\rho n^2 D_{PROP}^5)$; } **Response Variables**

The remaining terms serve as dimensional ratios that may be used to help reduce the number of required experiments, since ratios of dimensions may be used to provide similitude between models if it is not possible to have all identical dimensions on each model podded propeller tested. The remaining terms listed below will serve as the basis for the factorial experiments to be developed in the future to look at the influence of pod geometry on podded propeller performance.

(L_{P1}/D_{PROP}); (L_{B1}/D_{PROP}); (D_{B2}/D_{PROP});
(L_{B2}/D_{PROP}); (D_{B3}/D_{PROP}); (L_{B3}/D_{PROP}); } **Main Factors – use in factorial design of experiments**

As illustrated in the preceding paragraphs, many possible options for analyzing and displaying experimental data arise from dimensional analysis. While certain arrangements of terms may appear to be the best choice for many applications, it does not necessarily mean that they are the best for all applications. Though a large number of potential terms were identified in this paper, for practical purposes discussed it is most likely that standard forms will be used.

References

1. *Hydrodynamic Performance with Pod Propulsion – U.S. Navy Experience*, Karafiath G., Lyons, D., ATTC, Iowa City, 1998
2. *The Efficiency of Pod Propulsion*, Mewis, F., HADMAR 2001 Conference Proceedings, 2001

Bibliography

1. *Class Notes – EN9516*, Sharp, J.J., 2002
2. *Pod Propulsion: A Viable Option for the Canadian Navy*, Batsford, M., Maritime Engineering Journal, Fall 2001/Winter 2002
3. *Propulsion, Podded Propulsor Tests and Extrapolation,* International Towing Tank Committee, 2002
4. *Principals of Naval Architecture,* Vol. II – Resistance and Propulsion, Lewis, E., Society of Naval Architects and Marine Engineers, USA, 1988

Appendix B:
Laboratory Procedures

Laboratory Procedures

Podded Propeller Instrumentation Installation

Given the sensitivity of the equipment, it was very important to be careful during installation to prevent damage to the instrumentation. Because of the large sizes of the various subassemblies of the instrumentation package, it was necessary to install each subassembly separately.

The main subassembly of the equipment, shown in Figure 1, consists of the main frame, live frame, six-component balance, main drive motor and the main structural struts. While being transported it was necessary to ensure that the six-component balance was isolated in a way that prevented damage to the load cells during installation. This was accomplished by installing four threaded studs into the holes tapped into the four machined pads on the main frame.

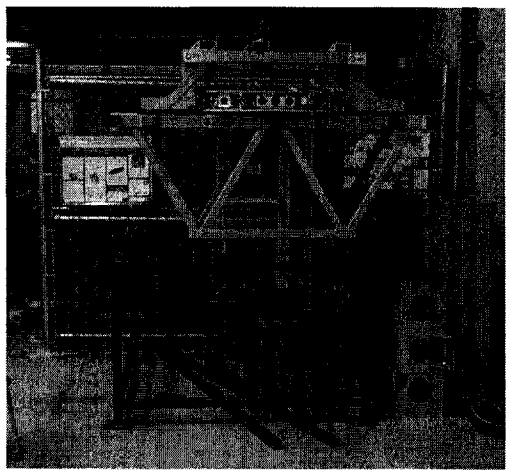

Figure 1: Main Sub-assembly of Podded Propeller Instrumentation

As shown in Figure 2 these studs were installed by placing the end of the stud through the hole in the live plate and threading two nuts onto the end of stud that is under the live plate. The end of the stud protruding underneath these two nuts was then screwed into the tapped hole on the machined pad of the main frame until about ½" of the stud was threaded into the frame. The bottom nut was then tightened down onto the face of the machined pad using a wrench and

the stud was then manually checked to ensure it was solidly locked into the frame.

Figure 2: Installed Lock Studs Secure Live Plates during Transportation

A third nut was threaded onto the top of the stud and hand-tightened until it came to rest on the top of the live plate. The middle nut was then hand-tightened until it came to rest on the bottom face of the live plate. At this point the top two nuts were touching opposite sides of the live plate and were snugged in place by hand such that they jammed together on the live plate. Wrenches were not used for this, since the purpose of these two jamming nuts was to prevent load from being transferred from the live plate through the flex links to the load cells. If the nuts had been tightened using a wrench, it may have been possible to unevenly tighten them such that the load cells may have been preloaded enough to damage them. This process was repeated for all four studs.

Once all of the locking studs had been put in place, the fork lift was used to move the main frame subassembly to the side of the tank. Once at the side of the tank, nylon slings were run through the ends of the structural tubes and connected to a steel spreader beam. This beam was connected to the electric overhead hoist located over the tow tank, which was used to lift this subassembly over the side of the tank as illustrated in Figure 3. Using the electric hoist, the main frame subassembly was lowered into the desired position onto two sliding

platforms which span the width of the tank. The electric hoist was then disconnected and the beam was laid on top of the sub assembly.

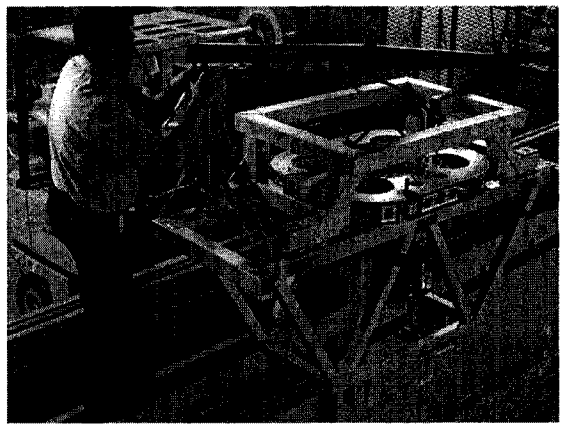

Figure 3: Main Frame Sub-assembly Being Lowered into the Tank

The next step was to remove the ladders and utility platform from the towing carriage. This provided the space necessary to allow the towing carriage to be driven over the two sliding platforms and the main frame subassembly. Once the tow carriage had been driven over the main frame sub assembly, the electric hoist was again connected to the spreader beam. The subassembly was then slowly raised up so that the lowest point of the equipment was well above the height of the rails of the carriage.

Since the electric hoist runs on a rail which is not on center with the centerline of the tow carriage, it was necessary to also use a manual chain hoist which runs on a rail centered over the tow carriage to install the equipment in the proper position. This was accomplished by connecting the clasp of the manual chain hoist to the spreader beam while the equipment was still suspended from the electric hoist. The manual hoist was tightened until the chain of the electric hoist went slack. The electric hoist was then slowly released and the equipment moved into position directly under the rail of the manual hoist and directly above the rails of the tow carriage. The clasp of the electric hoist was removed and the equipment was slowly and carefully lowered until the precision machined mounting pads on the corners of the main frame came to rest on the rails of the carriage, as shown in Figure 4. A pry bar was carefully used to align the

equipment such that precision machined reference surfaces on the frames were parallel with the precisely aligned rails of the tow carriage.

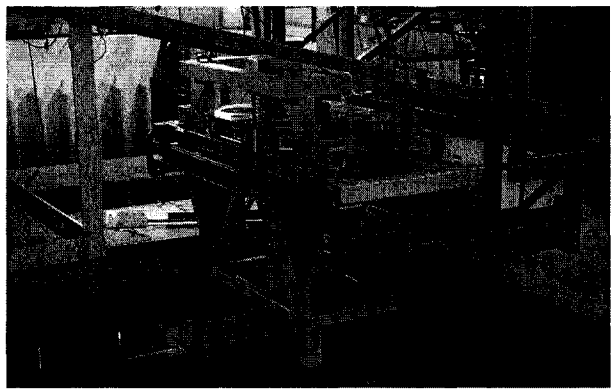

Figure 4: Main Frame Subassembly Installed in the Tow Carriage

Once in the final desired position, the main frame sub-assembly was clamped in place and the installation of the remaining components commenced.

The next components to be installed were the legs of the lift system frames. These two legs were positioned on the ends of the main frame and the bolts were threaded about one inch into the frame, but not tightened completely. The top lifting frame subassembly was then carried onto the towing carriage, where it was wrapped with nylon straps and connected to the manual chain hoist. This top lifting frame was then raised and moved along the rail of the hoist until it was positioned over the two legs. The top lifting frame was then lowered into position and bolted to the mounting surfaces on the top part of the legs and the hoist was disconnected and moved away from the area. Once these top bolts were tightened, the bottom bolts connecting the legs to the main frame were tightened.

After cleaning the dirt out of the threads and applying a thin film of grease, the four lead screws were fed in through the holes in the top lifting frame and the ends were inserted into the bronze nuts connected to the four corners of the live frame. The four thrust bearing units were then attached to the top of the lead screws and the lead screws were threaded through the bronze nuts until the bottom end of the lead screws came to rest in the radial bearing supports in the main frame subassembly.

Once all of the lead screws were completely tightened, the cups of the top thrust bearings were put in place, followed by washers and the outer nut for the bearing mounts. This outer nut was tightened using a large adjustable wrench and the pre-loading nuts were then threaded into the outer nuts. The pre-load nuts were tightened until the thrust bearings were slightly compressed. The large adjustable wrench was used to snug the pre-load nuts in place. The set-screws in the top of the pre-load nuts were then tightly screwed against the faces of the outer nuts to prevent the pre-load nuts from backing off. Next the pulley spacers were slid over the exposed ends of the top of the lead screws. The four lift system pulleys were then slid down over the ends of the shafts, the keys were inserted and the set screws were tightened to fix the pulleys into position.

The next step was to install the lift system driving motor subassembly. This subassembly was carried onto the carriage and positioned on the top mounting bracket located on the top lifting frame, as shown in Figure 4-8 below. The four mounting bolts for the lift system motor were threaded through the mounting holes, but not tightened completely to allow for adjustment. The long drive belt was then wrapped around the four pulleys on the lead screws and around the small driving pulley on the lift system motor subassembly. The lift system motor subassembly was then pulled into position by looping the cable from the manual hoist around the frame of the driving motor subassembly, through a rigid frame on the tow carriage and connecting to the clasp to the bottom of the hoist, then tightening the hoist until the main drive belt was tight. Once the belt was tight, the mounting bolts were tightened into position to maintain the tension on the belt. The lift system driving motor was then plugged into the motor controller.

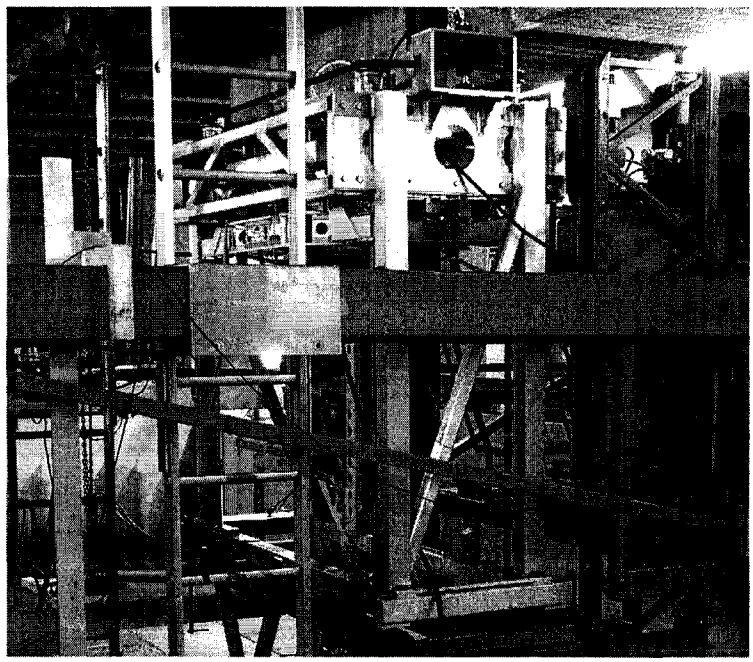

Figure 5: Completely Assembled Lift System

Next the safety bolts connecting the live frame to the main frame, which were put in place to keep these components secure during transportation, were removed. Also, all four lock studs, connecting the live plate to the main frame were removed – this was very important as attempting to use the lift system while these lock studs are in place could damage the instrumentation.

Once all safety connectors used during transportation mode had been removed, four safety rods were installed to allow for safe lifting of the six-component balance to install the instrumented pod unit. These four safety rods consisted of lengths of threaded rod with nuts and washers on each end. The top ends of the rods were fed through a piece of aluminum C-channel resting across the top surface of the lift frame and the bottom end of the rods passed through holes in the bottom live plate. In the event that the flex links were to break during installation and assembly, this safety mechanism would help support the suspended components.

<u>NOTE:</u> Serious injury or death could result if these safety rods are not properly installed and flex links break while working on equipment!

Once the safety rods were installed, the controller for the lift system motor was turned on and the live frame was raised to the maximum height. All of the screws connecting the structural struts were loosened to accommodate the installation of the instrumented pod unit. The pod unit was then carried onto the carriage and suspended between the rails of the carriage on a piece of 2"x2" oak. The pod unit was then carefully aligned with the struts and the live frame was lowered using the lift mechanism controls until the mating surfaces of the struts and the pod unit were aligned. The mounting bolts were securely fastened and all remaining screws on the struts were tightened.

The next step was to install the gear box on the top of the pod unit subassembly. This was accomplished by laying the gearbox on the machined surface of the pod unit strut and loosely bolting the two mounting plates to both the gearbox and the mounting surfaces of the pod strut. The set screw for the pulley which drives the belt of the pod unit was loosened and the drive belt was placed over the pulley. Next the coupling between the gear box and the main drive motor was connected and aligned using feeler gauges. Once the gearbox and coupling had been aligned, the height of the gearbox was adjusted to properly tension the belt. The bolts on the mounting plate were tightened to ensure the gearbox stayed in the correct position. The set screws on the motor coupling were tightened and the drive gear was manually rotated through several cycles to allow the pulley and the drive belt to self-align. Once this pulley had been aligned, the set screw on the drive pulley was tightened.

Next the gap spacing was verified to be at 2.7 mm using feeler gauges. The pod shell was then installed by placing the two halves of the shell on the mounting surfaces of the pod unit. These two halves were connected using socket head cap screws and all screw holes were plugged to ensure consistent exterior geometry. Removal of this shell geometry simply required the pod unit to be raised out of the water to allow for the removal of the connecting screws which secured the shell to the instrumentation. Different external pod geometries

were accommodated by simply removing the current shell and screwing the new shell form factor onto the instrumented model.

Once the appropriate shell geometry was installed, the propeller was installed. This was accomplished by first attaching the appropriate adapter ring to the face of the hub of the propeller shaft and then sliding the propeller onto this instrumented hub. Prior to installing the propeller, a thick film of grease was applied to the front and aft faces of the propeller. The base of the propeller was seated on the adapter ring and the screws were carefully installed and tightened through the front face of the propeller. A thin film of grease was placed around the nose cone and it was installed on the instrumentation. Any excess grease that worked through the seams was wiped away. To change the propeller, the unit was raised out of the water, the nose cone was removed, the propeller screws were removed and jacking screws were used in the propeller hub to push the propeller off the instrumentation. These jacking screw prevent users from having to pull on the blades of the propeller, which can damage both instrumentation and the propeller. Once the propeller had been removed, excess grease was wiped off and the process was repeated with the new propeller.

The final step of the installation was to install and adjust the height of the wave shroud. This was accomplished by first placing the two wave shroud halves on the sliding platforms in the tank, as shown in Figure 6 below. Next the manual cable hoist was suspended from a nylon strap attached to midway along one side of the lift frame. The cable was extended to the maximum length and connected to a nylon strap wrapped around the frame of the wave shroud.

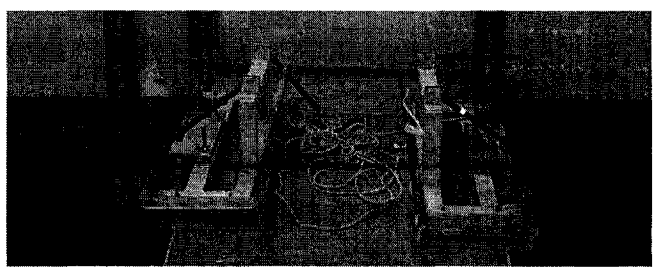

Figure 6: Wave Shroud

Next the wave shroud component was lowered into the water and allowed to swing out underneath the middle of the tow carriage. Using the manual cable hoist, the wave shroud was then raised into position underneath the main frame. A nut and washer was placed on each of the threaded rods on the top of the wave shroud. The threaded rods were then fed up through the holes in the bottom member of the main frame while a washer and nut were placed on the tops of the threaded rods to support the weight of the shroud. This process was then repeated for the second half of the wave shroud. The bottom surfaces of the two halves of the wave shroud were aligned and the height was set by adjusting the nuts on the threaded rods. Once in the desired position, the bottom nuts were tightened until each of the threaded rods was secured in position. The alignment was confirmed by clamping both halves together, as shown in Figure 7 below.

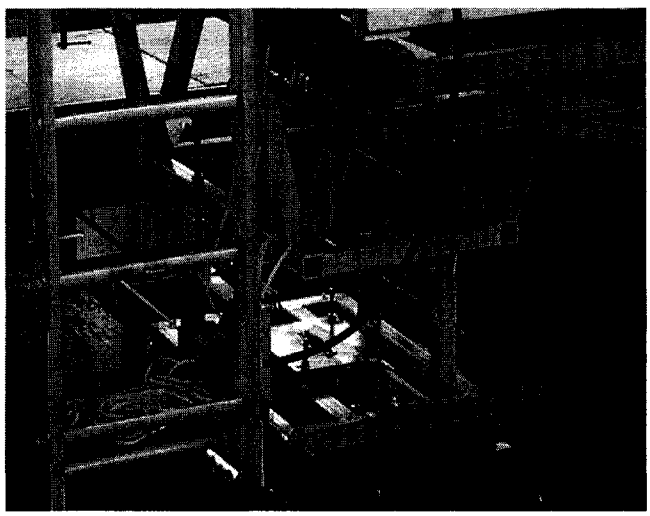

Figure 7: Installed Wave Shroud

Once both sides of the wave shroud were properly installed, the clamps were removed and the ropes connected to each side of the wave shroud were used to retract each half. This provided the room necessary to lower the pod instrumentation into the tank. Using the lift system controls the pod unit was lowered into the water, as shown in Figure 8, until the live frame came to rest on the machined pads of the main frame. The wave shroud ropes were released

and the shroud was closed and clamped into position. The spacing beneath the bottom of the strut and the top of the shell was the adjusted to the desired value.

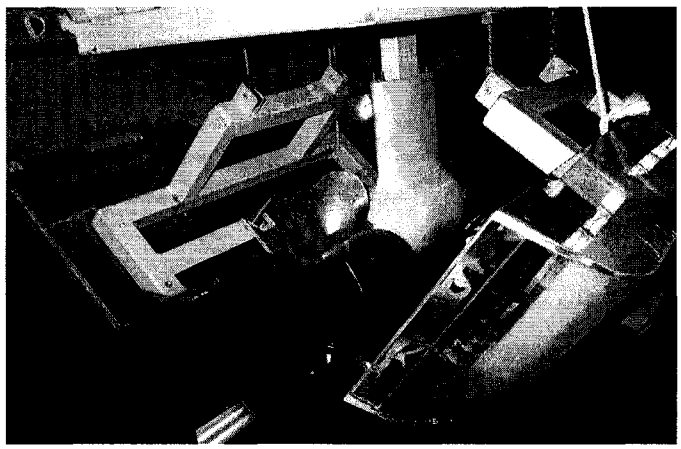

Figure 8: Adjusting the Strut Fairing

The safety rods were then removed and the bolts which connect the live frame to the main frame were securely fastened. A set of safety studs, which have four machined flats on the sides were installed on the live plate in the same manner as the lock studs, except only a single nut was used to lock the safety studs into the main frame. These safety studs were aligned so that the edges of the machined flats were parallel with the slots in the live plates. The purpose of these studs was to hold the instrumentation in place in the event of flex link failure during testing.

The controller for the lift system was then turned off and disconnected from the power supply and the main drive motor was connected. All of the labeled connectors for the various sensors on the instrumentation were plugged into the junction box of the data acquisition system. The data acquisition computer was powered up, all appropriate channels were activated and correct equipment operation was verified.

SAFETY NOTES:

- **Always ensure the safety rods are properly installed when the lift mechanism is in place. Failure to install these safety rods could result in serious injury or death should the flex links break causing the equipment to fall on the operator.**
- **Never try to put the safety rods in place while the lift mechanism is moving or has power supplied to it – only install the safety rods when the controller POWER is OFF. There is sufficient power in this system to severely injure or kill someone should they get caught in the mechanisms.**
- **Do not operate the lift mechanism at high speeds, as the resulting vibration may cause unsafe behavior in the system.**

Operational Notes

Each day of testing, prior to running any experiments, the instrumentation was visually inspected for signs of fatigue and wear to ensure safe operation of the equipment and this process was repeated periodically throughout the day. Once the safety checks was done, the pod unit was 'run in' to ensure the instrumentation was operating at steady conditions before testing began. Typically this was accomplished by setting the propeller controller to 3Hz and allowing the propeller to run for about 10 minutes prior to starting testing.

If testing stopped for any more than thirty minutes, the instrumented pod was raised completely out of the water using the lift system, since leaving the unit submerged for any substantial amount of time could lead to potential corrosion problems and/or flooding of the instrumentation. This precaution was of extreme importance since either of these problems could have led to timely and expensive repair work, as well as lost testing time.

Appendix C:

Tabular Data for Baseline Propeller Tests

15 Degree Puller Propeller

Baseline Propeller Open Water Test Results			
J	$10K_Q$	K_T	η
0.0000	0.6793	0.4753	0.0%
0.0618	0.6593	0.4607	6.9%
0.1235	0.6359	0.4428	13.7%
0.1846	0.6046	0.4157	20.2%
0.2463	0.5755	0.3915	26.7%
0.3086	0.5454	0.3662	33.0%
0.3701	0.5127	0.3369	38.7%
0.4321	0.4802	0.3096	44.3%
0.4944	0.4463	0.2819	49.7%
0.5552	0.4109	0.2519	54.2%
0.6167	0.3756	0.2244	58.6%
0.6797	0.3353	0.1941	62.6%
0.7403	0.2964	0.1630	64.8%
0.8017	0.2571	0.1324	65.7%
0.8655	0.2115	0.0996	64.8%
0.9254	0.1671	0.0668	58.9%
0.9874	0.1211	0.0331	43.0%
1.0506	0.0689	-0.0040	-1.8%

15 Degree Pusher Propeller

Baseline Propeller Open Water Test Results			
J	$10K_Q$	K_T	η
0.0000	0.6596	0.4489	0.0%
0.0619	0.6386	0.4344	6.7%
0.1232	0.6098	0.4125	13.3%
0.1857	0.5813	0.3897	19.8%
0.2470	0.5507	0.3653	26.1%
0.3089	0.5193	0.3396	32.1%
0.3711	0.4881	0.3141	38.0%
0.4322	0.4557	0.2876	43.4%
0.4938	0.4231	0.2615	48.6%
0.5563	0.3915	0.2361	53.4%
0.6168	0.3577	0.2097	57.6%
0.6787	0.3236	0.1825	60.9%
0.7416	0.2903	0.1554	63.2%
0.8021	0.2537	0.1285	64.7%
0.8642	0.2118	0.0990	64.3%
0.9256	0.1705	0.0698	60.3%
0.9869	0.1266	0.0391	48.6%
1.0489	0.0812	0.0071	14.6%
1.1105	0.0294	-0.0283	-51.3%

20 Degree Puller Propeller

Baseline Propeller Open Water Test Results			
J	$10K_Q$	K_T	η
0.5800	0.4172	0.2506	55.4%
0.6200	0.3919	0.2300	57.9%
0.6600	0.3655	0.2086	59.9%
0.7000	0.3385	0.1867	61.5%
0.7400	0.3109	0.1646	62.4%
0.7800	0.2828	0.1424	62.5%
0.8200	0.2544	0.1203	61.7%
0.8600	0.2254	0.0981	59.6%
0.9000	0.1958	0.0760	55.6%
0.9400	0.1654	0.0539	48.8%
0.9800	0.1337	0.0316	36.9%
1.0200	0.1005	0.0090	14.6%
1.0400	0.0831	-0.0025	-4.9%

20 Degree Pusher Propeller

Baseline Propeller Open Water Test Results			
J	$10K_Q$	K_T	η
0.0000	0.6648	0.4492	0.0%
0.0620	0.6424	0.4329	6.6%
0.1235	0.6158	0.4120	13.1%
0.1851	0.5874	0.3888	19.5%
0.2471	0.5574	0.3635	25.7%
0.3095	0.5269	0.3380	31.6%
0.3712	0.4972	0.3127	37.2%
0.4329	0.4674	0.2874	42.4%
0.4947	0.4359	0.2614	47.2%
0.5563	0.4056	0.2369	51.7%
0.6179	0.3735	0.2118	55.8%
0.6799	0.3406	0.1841	58.5%
0.7415	0.3083	0.1572	60.2%
0.8037	0.2710	0.1307	61.7%
0.8658	0.2321	0.1027	61.0%
0.9275	0.1925	0.0747	57.3%
0.9891	0.1510	0.0441	46.0%
1.0508	0.1053	0.0111	17.6%
1.1123	0.0584	-0.0206	-20.6%

Appendix D:

Tabular Data for Podded Propeller Tests

15 Degree Puller Propeller

Podded Propeller Open Water Test Results					
J	$10K_Q$	K_{T_PROP}	η_{PROP}	K_{T_UNIT}	η_{UNIT}
0.000	0.679	0.4866	0.0%	0.4972	0.0%
0.099	0.638	0.4517	11.2%	0.4555	11.3%
0.595	0.410	0.2554	59.0%	0.2416	55.8%
0.695	0.351	0.2100	66.1%	0.1928	60.7%
0.793	0.293	0.1660	71.5%	0.1417	61.0%
0.990	0.165	0.0744	71.0%	0.0350	33.5%
0.199	0.599	0.4181	22.1%	0.4228	22.3%
0.397	0.513	0.3403	42.0%	0.3371	41.6%
0.298	0.555	0.3794	32.5%	0.3807	32.6%
0.496	0.461	0.2974	51.0%	0.2868	49.2%
0.891	0.233	0.1196	72.9%	0.0900	54.9%
1.088	0.094	0.0248	45.8%	-0.0196	-34.0%

15 Degree Pusher Propeller

Podded Propeller Open Water Test Results					
J	$10K_Q$	K_{T_PROP}	η_{PROP}	K_{T_UNIT}	η_{UNIT}
0.0000	0.6517	0.4596	0.0%	0.4375	0.0%
0.0994	0.6183	0.4295	11.0%	0.4103	10.5%
0.1987	0.5723	0.3898	21.5%	0.3647	20.2%
0.2981	0.5185	0.3481	31.9%	0.3216	29.4%
0.3542	0.4976	0.3285	37.2%	0.3002	34.0%
0.4963	0.4278	0.2732	50.5%	0.2378	43.9%
0.5956	0.3768	0.2325	58.5%	0.1970	49.6%
0.6942	0.3242	0.1923	65.5%	0.1511	51.5%
0.7934	0.2798	0.1556	70.2%	0.1136	51.3%
0.8922	0.2231	0.1138	72.4%	0.0674	42.9%
0.9899	0.1704	0.0717	66.3%	0.0248	22.9%
1.0899	0.0986	0.0184	32.3%	-0.0306	-24.2%

20 Degree Puller Propeller

Podded Propeller Open Water Test Results					
J	$10K_Q$	K_{T_PROP}	η_{PROP}	K_{T_UNIT}	η_{UNIT}
0.0000	0.7070	0.5016	0.0%	0.5002	0.0%
0.0999	0.6701	0.4613	10.9%	0.4641	11.0%
0.1996	0.6204	0.4240	21.7%	0.4157	21.3%
0.2993	0.5752	0.3839	31.8%	0.3782	31.3%
0.3987	0.5266	0.3427	41.3%	0.3371	40.6%
0.4968	0.4768	0.2983	49.5%	0.2899	48.1%
0.5972	0.4167	0.2542	58.0%	0.2402	54.8%
0.6958	0.3652	0.2063	62.6%	0.1910	57.9%
0.7948	0.2989	0.1624	68.7%	0.1402	59.3%
0.8901	0.2377	0.1160	69.1%	0.0942	56.2%
0.9917	0.1622	0.0704	68.5%	0.0339	33.0%
1.0869	0.0953	0.0218	39.6%	-0.0196	-35.6%

20 Degree Pusher Propeller

Podded Propeller Open Water Test Results					
J	$10K_Q$	K_{T_PROP}	η_{PROP}	K_{T_UNIT}	η_{UNIT}
0.0000	0.6696	0.4681	0.0%	0.4670	0.0%
0.0994	0.6313	0.4389	11.0%	0.4338	10.9%
0.1988	0.5840	0.3976	21.5%	0.3872	21.0%
0.2981	0.5427	0.3623	31.7%	0.3472	30.3%
0.3974	0.4938	0.3211	41.1%	0.2994	38.3%
0.4963	0.4445	0.2804	49.8%	0.2512	44.6%
0.5953	0.3919	0.2384	57.6%	0.2040	49.3%
0.6942	0.3440	0.2042	65.6%	0.1651	52.6%
0.7948	0.2987	0.1650	69.9%	0.1206	51.1%
0.8917	0.2591	0.1277	70.0%	0.0807	45.8%
0.9904	0.1917	0.0834	68.6%	0.0322	26.4%
1.0889	0.1323	0.0420	55.0%	-0.0181	-24.6%

Appendix E:

Uncertainty Analysis for Baseline Propeller Tests

Model Particulars

Definition	Symbol	Value	Unit
Propeller Diameter	D_{PROP}	270	mm
Input Test Data Set For Analysis			
Temperature	Temp	17.2	C
Density	ρ	998.975	kg/m^3
For J = 0.1			
Carriage Speed	V	0.40	m/s
Shaft Speed	n	14.97	rps
Advance Coefficient	J	0.10	
Average Propeller Thrust	T	510.89	N
Average Torque	Q	20.31	Nm
For J = 0.4			
Carriage Speed	V	1.617	m/s
Shaft Speed	n	14.97	rps
Advance Coefficient	J	0.40	
Average Propeller Thrust	T	365.451	N
Average Torque	Q	15.458	Nm
For J = 0.7			
Carriage Speed	V	2.830	m/s
Shaft Speed	n	14.97	rps
Advance Coefficient	J	0.70	
Average Propeller Thrust	T	209.064	N
Average Torque	Q	10.259	Nm

Bias Limits

Temperature/Density/Viscosity

Temperature Error:

The thermometer used has been calibrated by the manufacturer and has a guaranteed accuracy of +/- 0.5 degrees C and therefore an assumed bias limit as follows:

$B_{Temp\text{-}Cal}$	**0.5**	°C

The thermometer has a scale accurate to 1 °C. A reading error of half this is assumed:

$B_{Temp\text{-}Scale}$	**0.5**	°C

The range of test temperatures observed during testing was 0.2 deg. C. As suggested by Bose and Luznik (1996), this precision error is treated as follows:

$B_{Temp\text{-}Range}$	**0.1**	°C

These error estimates are fossilized into a single temperature reading estimate using the methods of Coleman and Steele (1999):

$B_{Temp\text{-}Range}$	**0.714**	°C

Density Error:

The density-temperature expression given in ITTC 7.5-02-02-02 for the curve fit to the table of density-temperature data in ITTC 7.5-02-01-03 gives the following:

$$\rho = 1000.1 + 0.00552(t^{o}) - 0.0077(t^{o})^{2} + 0.00004(t^{o})^{3}$$

nominal density	1000.1
coefficient 1	0.0552
coefficient 2	-0.0077
coefficient 3	0.00004

The derivative of the above expression gives the following:

$$|\delta\rho/\delta t^{o}| = |\, 0.0552 - 0.0154t^{o} + 0.000120(t^{o})^{2} \,|$$

Based on the above expressions we can combine them to give:

$B_{\rho 1}$	-0.0870896	kg/m^3

Based on the ITTC Procedures, the errors due to data reducation are estimate as:

$B_{\rho 2}$	0.070	kg/m^3

Since the density value calculated in this analysis is based on the test temperature, there are no conceptual errors as indicated in the ITTC method 7.5-02-02-02. These components of the density expression error may be combined to give:

$B_{\rho\text{-Eqn}}$	**0.112**	**kg/m^3**

Temperature related density errors may be calculated by considering the density at the lower and upper limits of difference between the average temperature and the fossilized temperature error:

At T = 17.3	998.958 kg/m^3
At T = 17.1	998.992 kg/m^3
Density Difference	0.035 kg/m^3

The bias limit for this is taken as half of the difference of the density over this temperature range.

$B_{\rho\text{-Temp}}$	**0.017**	**kg/m^3**

The two contributing elements of error may be combined to give the overall limit using RSS:

B_ρ	**0.113**	**kg/m^3**

Viscosity Error:

For the viscosity, the assumed viscosity-temperature relationship adopted by ITTC Procedure 7.5-02-01-03 has been used. This is given as:

$$\nu = (1.72256 - 0.0476t^\circ + 0.000585t^{\circ 2})10^{-6}$$

nominal viscosity	1.72256
coefficient 1	-0.0476
coefficient 2	0.000585

Taking the partial derivative of this expression with respect to the temperature give:

$$\delta\nu/\delta t^\circ = (0.00117t^\circ - 0.0476)10^{-6}$$

Based on the test temperature, the bias in viscosity due to error in temperature calibration is:

$B_{\nu 1} = \lvert\delta\nu/\delta t^\circ\rvert\, B_{Temp}$	-2.7476E-08 m^2/s

Since the above expression is representative of a curve fit to a table of data, there is an inherent error that may be estimated by taking the difference of the viscosity value calculated using this expression and the viscosity value given in the tables in the ITTC Procedure 7.5-02-01-03. This bias error may be estimated as follows:

$B_{\nu 2}$	-4.15E-10 m^2/s

Combining these two limits gives the following total viscosity bias limit:

B_ν	**2.748E-08**	**m^2/s**

Propeller Diameter

The errors in the propeller geometry due to errors in the CNC machining process are estimated as:

D_{CNC} (+/-)	0.1 mm

The propeller blades were hand finished to get the desired surface finish. This error is estimated as:

D_{Polish} (+/-)	0.2 mm

Based on the above findings we can estimate the bias limit for propeller diameter as:

B_D	**0.224 mm**

Shaft Speed

The tachometer was assumed to have an accuracy of +/- 1 rpm and therefore an assumed bias limit as follows:

$n_{Calibration}$ (+/-)	0.0167 rps

B_n	**0.0167 rps**

Advance Speed

Recent upgrades to the towing carriage control system and speed measuring equipment at IOT-NRC has made it difficult to quanitfy the uncertainty in this parameter. An estimate was compiled based on ITTC recommendations and the best available information to provide an estimate of this bias limit.

Resolution	10000 pulse/m
Diameter of Wheel	0.5 m
Max. Pulse Duration	2.00E-07 s
Min. Pulse Duration	1.20E-07 s
Max. Output Signal	5 Volts
Circuit Speed	100 ms
AD/DA Card	16 bits

Using methods based on an adaptation of ITTC recommended procedure 7.5-02-02-02 the following carriage speed error estimate has been found by dividing the measurement system into components and estimating the elemental errors associated with each.

For an AD/DA Card with this resolution the number of pulses corresponding to the max. output signal is:

Max. # of Pulses	65536 pulses

Based on this information we can calculate the number of encoders windows as follows:

# of windows	6366 pulses/revolution

The carriage speed is measured via an optical encoder wheel. It is calculated by counting the number of pulses emitted per time segment as a precision machined wheel of known diameter and having a set number of pulses per revolution rotates on the rails. The carriage speed is calculated as follows:

$$V = n\pi D/6366\delta t$$

The bias associated with the pulse count (n) may be broken down into calibration error, data acquition error and data reduction error as follows:

Calibration Error	3.75844E-05 Volts

Bn_1	1 pulse

Since there is a AD conversion and a DA conversion, each one has an assumed error as outlined below:

AD Conversion Error	0.000114441 Volts
Bn_2	1.5 pulses

DA Conversion Error	0.000114441 Volts
Bn_3	1.5 pulses

A data reduction error is introduced when the voltage signal is converted back to a frequency that can be used to calculate speed. This bias limit is introduced by the linear curve fit obtained from a set of calibration data that is applied to the measured data to allow this conversion. This is estimated using the standard error estimate and based on the ITTC guidelines we get the following:

Curve Fit Error	0.000019 Volts
Bn_4	0.25 pulses

Now combining these values using RSS we can get a total estimate of the error due to the pulse count:

Bn	2.3585 pulses

The bias associated with the diameter of the wheel is specified by the manufacturer as follows:

B_D	0.0001 m

The time base, δt, of the oscillator module of the circuit will also influence the overall error . Based on the ITTC guidelines, it is assumed that the time base of the ocillator module is:

$B_{\delta t}$	1.025E-05 s

Based on the speed given, an estimate of the bias limit for the carriage speed is given as:

$\delta U/\delta n$	0.00247
$\delta U/\delta D$	6.38900
$\delta U/\delta t$	-31.94500

The error associated with the speed measurement process is given as:

$B_{U\text{-}Equip}$	0.00586 m/s

During testing, the propeller boat stirs up the tank and a small amount of remaining circulation is estimated based on the experience of Bose and Luznik (1996) to produce an error of:

$B_{U\text{-}Circ}$	0.00100 m/s

These contributing factors may be combined using RSS to give the following overall bias limit:

B_U	**0.00595 m/s**

Thrust

The errors associated with the thust measuements have been divided into three main categories,

calibration errors, curve fit errors, and testing errors. Since data aquistion errors will influence the uncertainty levels of both the calibration data, which is used to generate the curves to convert the test data voltage signals into loading values, the data aquisiton error actually influences the overall uncertainty in two ways, in that it first introduces uncertainty into the calibration data used to get the curve-fits, in addition to the actual test data collected, which is also subject to these uncertainties. Therfore errors associated with the data acquistion would be best treated as contributors to the error of both the calibration and test data sets, rather than simply treating it as an independent source of error. From a practical point of view, this analysis approach more accurately traces the error propogation in the results and typically would provide a slightly larger error estimate than would be obtained if data acquisition were treated as an independent source of error. Based on this observation, one has to be careful that they are not underestimating the total error by simply treating data acquisition independently of the number of data sets which are involved in the attainment of the final result. Data sets which are used in separate steps in the overall data analysis process should each factor in the error associated with their acquisition.

Calibration Errors:

When considering the data associated with the calibration of the equipment, the first step is to map out the process and identify potential sources of error in that process. Loading during calibration is accomplished by adding weights to a calibration fixture suspended from the pod unit. These weights were weighed on a scale accurate to +/- 1g. This error in these weights may be estimated as follows:

Calibration Weights	0.0000 kg	0.0001 kg
	5.0000 kg	0.0001 kg
	20.0000 kg	0.0001 kg
	39.9999 kg	0.0001 kg
	59.9999 kg	0.0001 kg
	49.9999 kg	0.0001 kg
	30.0000 kg	0.0001 kg
	10.0000 kg	0.0001 kg
Total Weight	214.9997 kg	
Error in Weight	0.000282843 kg	
B_{T-C1}	0.002774687 N	

The fixture used for calibrating the propeller thrust is a vertical fixture. There may be slight alignment errors due to misalignment of this fixture. This error has been estimated as follows:

Error in Loading Angle (+/-)	0.5 degrees
B_{T-C2} = Tprop*(1-cos(0.5))	0.013776329 N

For this instrumentation, it may assumed that a small error may be attributed to the misalignment of the load cell inside the pod. This would have a slight influence on the thrust voltage signal generated and based on an adaptation of ITTC recommended procedure 7.5-02-02-02 the error is estimated as:

Error in Load Cell Align (+/-)	0.25 degrees
B_{T-C3} = Tprop*(1-cos(0.25))	0.003444099 N

Based on the results of Bose and Luznik (1996) an estimate of the error in the static zero due to the influence of the bearings and seals is estimated as follows:

B_{T-C4}	0.089 N

Since the calibration data is also acquired using an AD card, an error due to this conversion also occurs and is calculated as follows:

AD Card Resolution	16 bits

AD Card Voltage Range	10 volts
AD Card Error	1 bit
B_{T-C5}	0.040627 N

Curve-Fit Errors:

The calibration data is used to establish the force-voltage relationship from a curve fit of the data which introduces an additional error, estimated using the standard error estimate as follows:

Weight (kg)	Actual (N)	Predicted (N)	$(Y_i - (ax_i - b))^2$
0.0000	0	0.58	0.3364
5.0000	49.04	48.78	0.0676
20.0000	196.16	195.72	0.1936
39.9999	392.32	392.16	0.0256
59.9999	588.48	588.61	0.0169
49.9999	490.4	490.56	0.0256
30.0000	294.24	294.28	0.0016
10.0000	98.08	98.03	0.0025
m	-133.12800		
b	-84.85530		
SEE [N]	0.33412		
2SEE [N]	0.66823		

B_{T-CF}	0.66823 N

Test Condition Errors:

The errors in the thrust during testing may also be broken down into elemental components. Once such error is in the alignment of the equipment to the towing direction of the carriage. In this facility alignment was more accurate due to the installation method and is estimated as:

Error in Equip Angle (+/-)	0.1 degrees
B_{T-T1} = Tprop*(1-cos(1))	0.000666778 N

Again, as with the calibrations, a small error may be attributed to the misalignment of the load cell. This would have an influence on the voltage signal that was produced as a result of the loading. Based on an adaptation of ITTC recommended procedure 7.5-02-02-02 the error is estimated as:

Error in Load Cell Align (+/-)	0.25 degrees
B_{T-T2} = Tprop*(1-cos(0.25))	0.003444099 N

Again the static zero estimate will affect the test condition data and must be included to factor in the influence of the bearings and seals. This is again estimated as follows:

B_{T-T3}	0.089 N

Since the test data is also acquired using an AD card, an error due to this conversion also occurs and is calculated as follows:

AD Card Resolution	16 bits
AD Card Voltage Range	10 volts
AD Card Error	1 bit
B_{T-T4}	0.040627 N

Total Propeller Thrust Error:

The total propeller thrust error may be calculated by combining the above estimates using RSS:

B_{Tprop}	**0.682567 N**

Torque and Frictional Torque

Calibration Errors:

As indicated in ITTC 7.5-02-03-02.2, the error in torque calibration should consider both moment arm errors and weight errors as follows:

$$B_{Q\text{-}C1} = [(Ma*B_W)^2 + (F*B_{Ma})^2]^{1/2}$$

To reduce the error associated with the calibration weights, each individual weight was measured on a high quality digital scale, accurate to +/- 0.1 g. This error may be estimated as follows:

Calibration Weights	10.0000 kg	0.0001 kg
	20.0000 kg	0.0001 kg
	30.0000 kg	0.0001 kg
Total Weight	59.9999 kg	
Error in Weight	0.000173205 kg	
B_W	0.001698553 N	

The moment arm used to calibrate the torque was assumed accurate to 0.2 mm and had the length as specified below. The bias contribution due to the error in this length is estimated as follows:

Ma	0.25 m
B_{Ma}	0.0002 m

$B_{Q\text{-}C1}$	0.1177 Nm

The error due the change in the angle of the lever arm over the calibration range introduced an error estimated as below:

$B_{Q\text{-}C2}$	0.0120 Nm

Since the calibration data is also acquired using an AD card, an error due to this conversion also occurs and is calculated as follows:

AD Card Resolution	16 bits
AD Card Voltage Range	10 volts
AD Card Error	1 bit
$B_{Q\text{-}C3}$	0.0473 Nm

As with thrust, errors in the static zero of the torque reading was included based on the work of Bose and Luznik (1996) as follows:

$B_{Q\text{-}C4}$	0.0120 Nm

Curve-Fit Errors:

The calibration data is used to establish the kgm-voltage relationship from a curve fit of the data which introduces an additional error, estimated using the standard error estimate as follows:

Applied Weight (kg)	Applied Torque (Nm)	Predicted (Nm)	$(Y_i - (ax_i - b))^2$
-10.0000	-24.52	-24.444	0.0058
-20.0000	-49.04	-48.947	0.0086
-30.0000	-73.56	-73.664	0.0108
10.0000	24.52	24.477	0.0018
20.0000	49.04	48.981	0.0035
30.0000	73.56	73.596	0.0013
m	15.8152		
b	-0.5340		
SEE [Nm]	0.08926		
2SEE [Nm]	0.17851		

$B_{Q\text{-}CF1}$	0.17851 Nm

Test Condition Errors:

Since the torque test data is also acquired using an AD card, an error due to this conversion also occurs and is calculated as follows:

AD Card Resolution	16 bits
AD Card Voltage Range	10 volts
AD Card Error	1 bit
$B_{Q\text{-}T1}$	0.0473 Nm

Again the static zero errors introduce error into the test data and is estimated based on Bose and Luznik (1996) as follows:

$B_{Q\text{-}T2}$	0.0120 Nm

Total Torque Error:

Combining the above error contributions, we can calculate the total toque bias limit as follows:

B_Q	**0.225007 Nm**

Precision Limits

The precision limits were estimated for three advances speeds, using five repeat runs for a given test. The standard deviation of each data set was calculated according to the expressions given in ITTC QM 7.5-02-01-01. As outlined in this method, the precision limit is then estimated using:

$$P_i = K*S_i$$

The variable K is the coverage factor, which for a 95-percent confidence interval equals 2 and the S_i term is the calculated standard deviation of the data. This gave the following precision limit values:

	J = 0.1	J = 0.4	J = 0.7
Advance Speed (+/-)	**0.00014**	**0.00043**	**0.00106**
Thrust (+/-)	**0.21688**	**0.19794**	**0.40813**
Torque (+/-)	**0.00931**	**0.00592**	**0.00269**

The zero torque and shaft speed precision estimates were calcualted using the same method. These precision limits were estimated as:

Zero Torque (+/-)	**0.0034**
Shaft Speed (+/-)	**0.0167**

Bias and Precision Limits

Variable	Bias Errors		Bias Limit		Precision Errors		Precision Limit	
Temperature	Calibration:	+/- 0.5 °C.	Fossilized into +/- 0.714 °C for Temperature		Scale: Range:	+/- 0.5 °C. +/- 0.10 °C.		
Density	Temp Related Errors: Density Eqn Errors:	+/- 0.017 kg/m^3 +/- 0.112 kg/m^3	Overall Limit:	+/- 0.113 kg/m^3				
Propeller Diameter	CNC Machining Errors: Hand Polishing Errors:	+/- 0.0001 m +/- 0.0002 m	Overall Limit:	+/- 0.000224 m				
Shaft Speed	Calibration:	+/- 0.0167 rps	Overall Limit:	+/- 0.0167 rps	Scale:	+/- 0.0167 rps	Overall Limit:	+/- 0.0167 rps
Advance Speed	Measurement Errors: Tide Effects:	+/- 0.00586 m/s +/- 0.001 m/s	Overall Limit:	+/- 0.00595 m/s			J = 0.1 J = 0.4 J = 0.7	+/- 0.00014 m/s +/- 0.00043 m/s +/- 0.00106 m/s
PropellerThrust	Weights: Loading Angle: Load Cell Align: Static Zero: A/D Error: Curve Fit: Equipment Angle: Load Cell Align: Static Zero: A/D Error:	+/- 0.00277 N +/- 0.01378 N +/- 0.00344 N +/- 0.08900 N +/- 0.04063 N +/- 0.66823 N +/- 0.00067 N +/- 0.00344 N +/- 0.08900 N +/- 0.04063 N	*Calibration Data Errors* Overall Limit: *Testing Data Errors*	+/- 0.68257 N			J = 0.1 J = 0.4 J = 0.7	+/- 0.21688 N +/- 0.19794 N +/- 0.40813 N
Torque	Weights: Lever Angle: A/D Error: Static Zero: Curve Fit: Static Zero: A/D Error:	+/- 0.11768 Nm +/- 0.01200 Nm +/- 0.04733 Nm +/- 0.01200 Nm +/- 0.17851 Nm +/- 0.01200 Nm +/- 0.04733 Nm	*Calibration Data Errors* Overall Limit: *Testing Data Errors*	+/- 0.22501 Nm			J = 0.1 J = 0.4 J = 0.7	+/- 0.00931 Nm +/- 0.00592 Nm +/- 0.00269 Nm
Frictional Torque	Weights: Lever Angle: A/D Error: Static Zero: Curve Fit: Static Zero: A/D Error:	+/- 0.11768 Nm +/- 0.01200 Nm +/- 0.04733 Nm +/- 0.01200 Nm +/- 0.17851 Nm +/- 0.01200 Nm +/- 0.04733 Nm	*Calibration Data Errors* Overall Limit: *Testing Data Errors*	+/- 0.22501 Nm			+/- 0.0033752 Nm	

Overall Uncertainty

The bias and precision limits may be summarized as follows:

	J = 0.1	J = 0.4	J = 0.7
ρ	998.98	998.98	998.98
B_ρ	0.11308	0.11308	0.11308
P_ρ	-	-	-
$(U_\rho/\rho)^2$	1.281E-08	1.281E-08	1.281E-08
D	0.27	0.27	0.27
B_D	0.00022	0.00022	0.00022
P_D	-	-	-
$(U_D/D)^2$	6.859E-07	6.859E-07	6.859E-07
n	14.97	14.97	14.97
B_n	0.01667	0.01667	0.01667
P_n	0.01667	0.01667	0.01667
$(U_n/n)^2$	2.480E-06	2.480E-06	2.480E-06
V	0.40	1.62	2.83
B_V	0.00595	0.00595	0.00595
P_V	0.00014	0.00043	0.00106
$(U_V/V)^2$	2.166E-04	1.361E-05	4.558E-06
T	510.89	365.45	209.06
B_T	0.68257	0.68257	0.68257
P_T	0.21688	0.19794	0.40813
$(U_T/T)^2$	1.965E-06	3.782E-06	1.447E-05
$Q - Q_o$	20.31	15.46	10.26
B_Q	0.22501	0.22501	0.22501
P_Q	0.00931	0.00592	0.00269
$(U_Q/(Q - Q_o))^2$	1.230E-04	2.120E-04	4.811E-04
$Q - Q_o$	20.31	15.46	10.26
B_{Qo}	0.22501	0.22501	0.22501
P_{Qo}	0.00338	0.00338	0.00338
$(U_{Qo}/(Q - Q_o))^2$	1.228E-04	2.119E-04	4.812E-04

Combining the precision limit and bias limit estimates we can get the following estimates of overall uncertainty for the measured parameters:

$$(U_x) = ((B_x)^2 + (P_x)^2)^{1/2}$$

	J = 0.1	J = 0.4	J = 0.7
U_ρ	0.11308	0.11308	0.11308
U_D	0.00022	0.00022	0.00022
U_n	0.02357	0.02357	0.02357
U_V	0.00595	0.00596	0.00604
U_T	0.71619	0.71069	0.79528
U_Q	0.22520	0.22508	0.22502
U_{Qo}	0.22503	0.22503	0.22503

Using the uncertainty expressions for each of the data reduction equations we get the following estimates for the data reduction equations:

	J = 0.1	J = 0.4	J = 0.7
(U_{K_T}/K_T)	0.5%	0.5%	0.6%
(U_{K_T})	0.00205	0.00153	0.00105
(U_{K_Q}/K_Q)	1.7%	2.1%	3.1%
(U_{K_Q})	0.00104	0.00102	0.00101
(U_J/J)	1.5%	0.4%	0.3%
(U_J)	0.00148	0.00164	0.00195

Overall Uncertainty

	Advance Coefficient Value	Thrust Coefficient K_T (+/-)	Percentage Error in K_T (+/-)	Torque Coefficient K_Q (+/-)	Percentage Error in K_Q (+/-)	Advance Coefficient Error (+/-)
9 rps	0.1	0.00205	0.5%	0.00104	1.7%	0.00148
	0.4	0.00153	0.5%	0.00102	2.1%	0.00164
	0.7	0.00105	0.6%	0.00101	3.1%	0.00195

Appendix F:

Uncertainty Analysis for Podded Propeller Tests

Model Pod Particulars

Definition	Symbol	Value	Unit
Propeller Diameter	D_{PROP}	270	mm
Pod Diameter	L_{POD}	139	mm
Pod Overall Length	L_{WL}	410	mm
Pod Fore Taper Length	L_{FORE}	85	mm
Pod Fore Taper Angle	θ_{FORE}	15	degrees
Pod Aft Taper Length	L_{AFT}	125	mm
Pod Aft Taper Angle	θ_{AFT}	25	degrees
Pod Fillets	R	50	mm
Strut Height	H_{STRUT}	300	mm
Strut Width	W_{STRUT}	60	mm
Strut Chord Length	L_{STRUT}	225	mm
Strut Perimeter	P_{STRUT}	484	mm
Strut Distance	D_{STRUT}	44	mm

Input Test Data Set For Analysis			
Temperature	Temp	16.25	C
Density	ρ	999.135	kg/m^3
For J = 0.1			
Carriage Speed	V	0.243	m/s
Shaft Speed	n	9.05	rps
Advance Coefficient	J	0.10	
Average Propeller Thrust	T	186.758	N
Average Unit Thrust	Tunit	178.413	N
Average Torque	Q	7.259	Nm
For J = 0.4			
Carriage Speed	V	0.972	m/s
Shaft Speed	n	9.06	rps
Advance Coefficient	J	0.40	
Average Propeller Thrust	T	143.098	N
Average Unit Thrust	Tunit	130.773	N
Average Torque	Q	5.853	Nm
For J = 0.7			
Carriage Speed	V	1.701	m/s
Shaft Speed	n	9.08	rps
Advance Coefficient	J	0.69	
Average Propeller Thrust	T	84.093	N
Average Unit Thrust	Tunit	66.060	N
Average Torque	Q	3.828	Nm

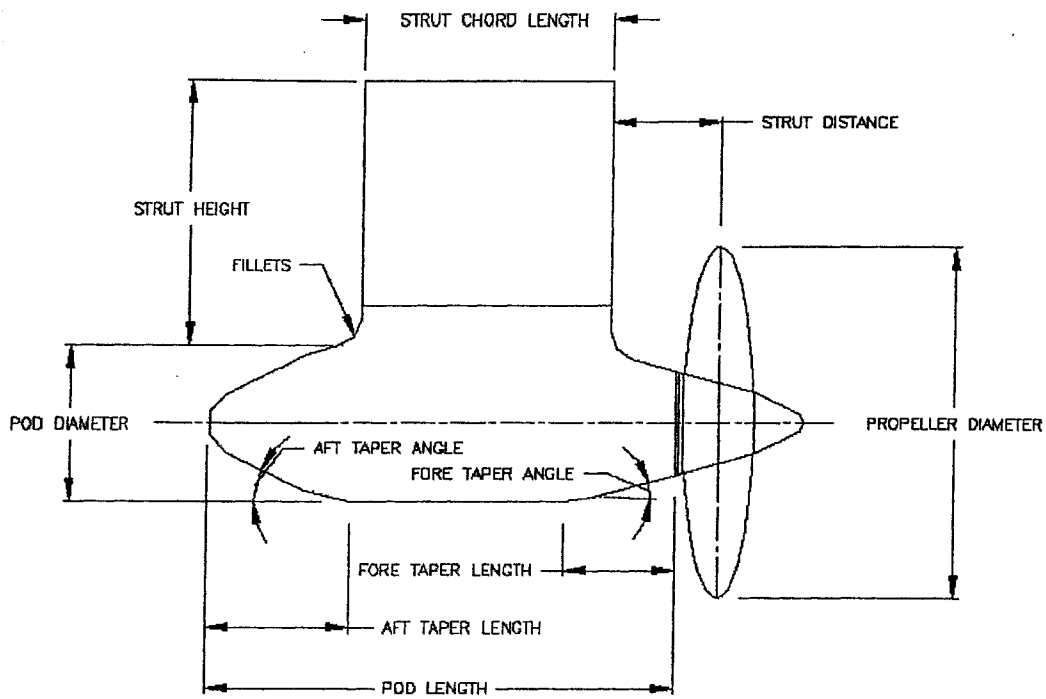
STRUT CHORD LENGTH
STRUT DISTANCE
STRUT HEIGHT
FILLETS
POD DIAMETER
PROPELLER DIAMETER
AFT TAPER ANGLE
FORE TAPER ANGLE
FORE TAPER LENGTH
AFT TAPER LENGTH
POD LENGTH

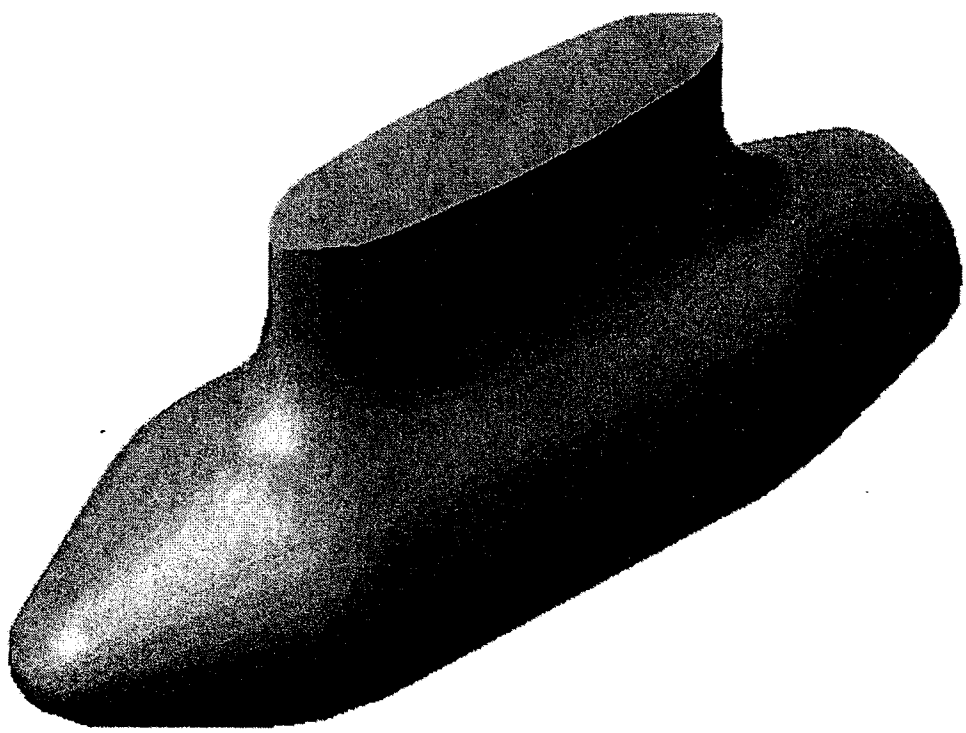

Bias Limits

Temperature/Density/Viscosity

Temperature Error:

The thermometer used has been calibrated by the manufacturer and has a guaranteed accuracy of +/- 0.5 degrees C and therefore an assumed bias limit as follows:

$B_{Temp\text{-}Cal}$	0.5	°C

The thermometer has a scale accurate to 0.10 °C. A reading error of half this is assumed:

$B_{Temp\text{-}Scale}$	0.05	°C

The range of test temperatures observed during testing was 1.1 deg. C. As suggested by Bose and Luznik (1996), this precision error is treated as follows:

$B_{Temp\text{-}Range}$	0.55	°C

These error estimates are fossilized into a single temperature reading estimate using the methods of Coleman and Steele (1999):

$B_{Temp\text{-}Range}$	0.745	°C

Density Error:

The density-temperature expression given in ITTC 7.5-02-02-02 for the curve fit to the table of density-temperature data in ITTC 7.5-02-01-03 gives the following:

$$\rho = 1000.1 + 0.00552(t^{o}) - 0.0077(t^{o})^{2} + 0.00004(t^{o})^{3}$$

nominal density	1000.1
coefficient 1	0.0552
coefficient 2	-0.0077
coefficient 3	0.00004

The derivative of the above expression gives the following:

$$|\delta\rho/\delta t^{o}| = | 0.0552 - 0.0154t^{o} + 0.000120(t^{o})^{2} |$$

Based on the above expressions we can combine them to give:

$B_{\rho 1}$	-0.08168125	kg/m^3

Based on the ITTC Procedures, the errors due to data reducation are estimate as:

$B_{\rho 2}$	0.070	kg/m^3

Since the density value calculated in this analysis is based on the test temperature, there are no conceptual errors as indicated in the ITTC method 7.5-02-02-02. These components of the density expression error may be combined to give:

$B_{\rho\text{-}Eqn}$	0.108	kg/m^3

Temperature related density errors may be calculated by considering the density at the lower and upper limits of difference between the average temperature and the fossilized temperature error:

At T = (16.25 - 0.745) = 15.5	999.2538565	kg/m^3
At T = (16.25 + 0.745) = 16.9	999.0104795	kg/m^3

Density Difference	0.243377046	kg/m^3

The bias limit for this is taken as half of the difference of the density over this temperature range.

$B_{\rho\text{-Temp}}$	**0.122**	**kg/m^3**

The two contributing elements of error may be combined to give the overall limit using RSS:

B_ρ	**0.162**	**kg/m^3**

Viscosity Error:

For the viscosity, the assumed viscosity-temperature relationship adopted by ITTC Procedure 7.5-02-01-03 has been used. This is given as:

$$\nu = (1.72256 - 0.0476t^{\circ} + 0.000585t^{\circ 2})10^{-6}$$

nominal viscosity	1.72256
coefficient 1	-0.0476
coefficient 2	0.000585

Taking the partial derivative of this expression with respect to the temperature give:

$$\delta\nu/\delta t^{\circ} = (0.00117t^{\circ} - 0.0476)10^{-6}$$

Based on the test temperature, the bias in viscosity due to error in temperature calibration is:

$B_{v1} = \lvert\delta\nu/\delta t^{\circ}\rvert B_{Temp}$	-2.85875E-08 m^2/s

Since the above expression is representative of a curve fit to a table of data, there is an inherent error that may be estimated by taking the difference of the viscosity value calculated using this expression and the viscosity value given in the tables in the ITTC Procedure 7.5-02-01-03. This bias error may be estimated as follows:

B_{v2}	-4.15E-10 m^2/s

Combining these two limits gives the following total viscosity bias limit:

B_ν	**2.859E-08**	**m^2/s**

Propeller Diameter

The errors in the propeller geometry due to errors in the CNC machining process are estimated as:

D_{CNC} (+/-)	0.1 mm

The propeller blades were hand finished to get the desired surface finish. This error is estimated as:

D_{Polish} (+/-)	0.2 mm

Based on the above findings we can estimate the bias limit for propeller diameter as:

B_D	**0.224 mm**

Shaft Speed

The tachometer used has been calibrated by the manufacturer and has a guaranteed accuracy of +/- 1 rpm and therefore an assumed bias limit as follows:

$n_{Calibration}$ (+/-)	0.0167 rps

B_n	0.0167 rps

Advance Speed

The specifications of the carriage speed measuring equipment, as taken from the carraige user manuals and from the work of Bose and Luznik (1996) at the MUN towing tank facilities are:

Resolution	10000 pulse/m
Diameter of Wheel	0.5 m
Max. Pulse Duration	2.00E-07 s
Min. Pulse Duration	1.20E-07 s
Max. Output Signal	5 Volts
Circuit Speed	100 ms
AD/DA Card	12 bits

Using methods based on an adaptation of ITTC recommended procedure 7.5-02-02-02 the following carriage speed error estimate has been found by dividing the measurement system into components and estimating the elemental errors associated with each.

For an AD/DA Card with this resolution the number of pulses corresponding to the max. output signal is:

Max. # of Pulses	4096 pulses

Based on this information we can calculate the number of encoders windows as follows:

# of windows	6366 pulses/revolution

The carriage speed is measured via an optical encoder wheel. It is calculated by counting the number of pulses emitted per time segment as a precision machined wheel of known diameter and having a set number of pulses per revolution rotates on the rails. The carriage speed is calculated as follows:

$$V = n\pi D/6366\delta t$$

The bias associated with the pulse count (n) may be broken down into calibration error, data acquition error and data reduction error as follows:

Calibration Error	0.001220703 Volts
Bn_1	1 pulse

Since there is a AD conversion and a DA conversion, each one has an assumed error as outlined below:

AD Conversion Error	0.001831055 Volts
Bn_2	1.5 pulses

DA Conversion Error	0.001831055 Volts
Bn_3	1.5 pulses

A data reduction error is introduced when the voltage signal is converted back to a frequency that can be used to calculate speed. This bias limit is introduced by the linear curve fit obtained from a set of calibration data that is applied to the measured data to allow this conversion. This is estimated using the standard error estimate and based on the ITTC guidelines we get the following:

Curve Fit Error	0.000305 Volts
Bn_4	0.25 pulses

Now combining these values using RSS we can get a total estimate of the error due to the pulse count:

Bn	2.3585 pulses

The bias associated with the diameter of the wheel is specified by the manufacturer as follows:

B_D	0.0001 m

The time base, δt, of the oscillator module of the circuit will also influence the overall error .. Based on the ITTC guidelines, it is assumed that the time base of the ocillator module is:

$B_{\delta t}$	1.025E-05 s

Based on the speed given, an estimate of the bias limit for the carriage speed is given as:

δU/δn	0.00247
δU/δD	6.38900
δU/δt	-31.94500

The error associated with the speed measurement process is given as:

$B_{U\text{-}Equip}$	0.00586 m/s

During testing, the pod unit stirs up the tank and a small amount of remaining circulation is estimated based on the experience of Bose and Luznik (1996) to produce an error of:

$B_{U\text{-}Circ}$	0.00100 m/s

These contributing factors may be combined using RSS to give the following overall bias limit:

B_U	**0.00595 m/s**

Propeller Thrust

The errors associated with the thust measuements have been divided into three main categories, calibration errors, curve fit errors, and testing errors. Since data aquistion errors will influence the uncertainty levels of both the calibration data, which is used to generate the curves to convert the test data voltage signals into loading values, the data aquisiton error actually influences the overall uncertainty in two ways, in that it first introduces uncertainty into the calibration data used to get the curve-fits, and secondly the actual test data collected is subject to these uncertainties. Therefore, the errors associated with the data acquistion would be best treated as contributors to the error of both the calibration and test data sets, rather than simply treating it as an independent source of error. From a practical point of view, this analysis approach more accurately traces the error propogation in the results and typically would provide a slightly larger error estimate than would be obtained if data acquisition were treated as an independent source of error. Based on this observation, one has to be careful that they are not underestimating the total error by simply treating data acquisition independently of the number of data sets which are involved in the attainment of the final result. Data sets which are used in separate steps in the overall data analysis process should each factor in the error associated with their acquisition.

Calibration Errors:

When considering the data associated with the calibration of the equipment, the first step is to map out the process and identify potential sources of error in that process. Loading during calibration is accomplished by adding weights to a calibration fixture suspended from the pod unit. These weights were weighed on a scale accurate to +/- 1g. This error in these weights may be estimated as follows:

Calibration Weights	0.0000 kg	0.0001 kg
	2.5246 kg	0.0001 kg
	10.0036 kg	0.0001 kg
	9.9936 kg	0.0001 kg
	10.00120 kg	0.0001 kg
	10.00460 kg	0.0001 kg
	10.01980 kg	0.0001 kg
	10.00560 kg	0.0001 kg
Total Weight	62.5530 kg	
Error in Weight	0.000282843 kg	
$B_{T\text{-}C1}$	0.00277 N	

The fixture used for calibrating the propeller thrust is a vertical fixture. There may be slight alignment errors due to misalignment of this fixture. This error has been estimated as follows:

Error in Loading Angle (+/-)	0.5 degrees
B_{T-C2} = Tprop*(1-cos(0.5))	0.00525 N

For this instrumentation, it may assumed that a small error may be attributed to the misalignment of the load cell inside the pod. This would have a slight influence on the thrust voltage signal generated and based on an adaptation of ITTC recommended procedure 7.5-02-02-02 the error is estimated as:

Error in Load Cell Align (+/-)	0.25 degrees
B_{T-C3} = Tprop*(1-cos(0.25))	0.00131 N

Slight variation in the static zero value was observed and estimated as:

B_{T-C4}	0.14110 N

Since the calibration data is also acquired using an AD card, an error due to this conversion also occurs and is calculated as follows:

AD Card Resolution	12 bits
AD Card Voltage Range	10 volts
AD Card Error	1 bit
B_{T-C5}	0.23904 N

Curve-Fit Errors:

The calibration data is used to establish the force-voltage relationship from a curve fit of the data which introduces an additional error, estimated using the standard error estimate as follows:

Weight (kg)	Voltage	Predicted (kg)	$(Y_i - (ax_i - b))^2$
0.00	0.00000	0.07	0.004564218
10.00	-0.20124	9.92	0.007114935
20.00	-0.40305	19.80	0.039265129
30.00	-0.61768	30.31	0.094657431
40.00	-0.81530	39.98	0.000498814
50.02	-1.01932	49.97	0.002979712
60.03	-1.22449	60.01	0.000249677
m	-48.95496		
b	0.06756		
SEE [kg]	0.17282		
SEE [N]	1.69475		

B_{T-CF}	3.38951 N

Test Condition Errors:

The errors in the thrust during testing may also be broken down into elemental components. Once such error is in the alignment of the equipment to the towing direction of the carriage. This may be estimated as follows:

Error in Equip Angle (+/-)	1 degrees
B_{T-T1} = Tprop*(1-cos(1))	0.02102 N

Again, as with the calibrations, a small error may be attributed to the misalignment of the load cell. This would have an influence on the voltage signal that was produced as a result of the loading. Based on an adaptation of ITTC recommended procedure 7.5-02-02-02 the error is estimated as:

Error in Load Cell Align (+/-)	0.25 degrees
B_{T-T2} = Tprop*(1-cos(0.25))	0.00131 N

Since the static zero estimate will also affect the test condition data and must be included.

B_{T-T3}	0.14110 N

Since the test data is also acquired using an AD card, an error due to this conversion also occurs and is calculated as follows:

AD Card Resolution	12 bits
AD Card Voltage Range	10 volts
AD Card Error	1 bit
B_{T-T4}	0.23904 N

Total Propeller Thrust Error:

The total propeller thrust error may be calculated by combining the above estimates using RSS:

B_{Tprop}	**3.41224 N**

Unit Thrust

As with propeller thrust, the unit thrust errors have been divided into three main categories, calibration errors, curve fit errors, and test condition errors based on the same reasoning.

Calibration Condition Errors:

Loading during calibration is accomplished by adding weights to a calibration jig at a specified angle. The same set of calibration weights were used for the unit thrust calibration as for the propeller thrust Using the same method as above, the error associated with the calibration weights is estimated as follows:

Calibration Weights	0.0000 kg	0.0001 kg
	2.5246 kg	0.0001 kg
	10.0036 kg	0.0001 kg
	9.9936 kg	0.0001 kg
	10.00120 kg	0.0001 kg
	10.00460 kg	0.0001 kg
	10.01980 kg	0.0001 kg
	10.00560 kg	0.0001 kg
Total Weight	62.5530 kg	
Error in Weight	0.000282843 kg	
B_{UT-C1}	0.00277 N	

Since the unit thrust loads are horizontal loads there are potential alignment errors that may occur due to misalignment of the calibration equipment. This error has been estimated as follows:

Error in Loading Angle (+/-)	1 degrees
B_{UT-C2} = Tunit*(1-cos(1))	0.01905 N

For this instrumentation, it may assumed that a small error may be attributed to the misalignment of the load cell. This would have an influence on the voltage signal that was produced as a result of the loading. Based on an adaptation of ITTC recommended procedure 7.5-02-02-02 the error is estimated as:

Error in Load Cell Align (+/-)	0.25 degrees
B_{UT-C3} = Tunit*(1-cos(0.25))	0.00119 N

Slight variation in the static zero value was observed and estimated as:

B_{UT-C4}	0.10643 N

Since the calibration data is also acquired using an AD card, an error due to this conversion

also occurs and is calculated as follows:

AD Card Resolution	12 bits
AD Card Voltage Range	10 volts
AD Card Error	1 bit
B_{UT-C5}	0.22567 N

Curve-Fit Errors:

The calibration data is used to establish the force-voltage relationship from a curve fit of the data which introduces an additional error, estimated using the standard error estimate as follows:

Weight (kg)	Voltage	Predicted (kg)	$(Y_i - (ax_i - b))^2$
0	0.0000	-0.03	0.000803666
10	0.2143	9.88	0.015460883
20	0.4309	19.89	0.012778421
30	0.6475	29.90	0.010807469
40	0.8635	39.88	0.014527129
50	1.0810	49.93	0.004615467
60	1.2966	59.90	0.010387814
50	1.0849	50.11	0.012604457
40	0.8700	40.18	0.033293398
30	0.6534	30.17	0.029050196
20	0.4355	20.10	0.010233677
10	0.2186	10.07	0.005581781
0	0.0010	0.02	0.000361956
m	46.21727		
b	-0.02835		
SEE [kg]	0.12080		
SEE [N]	1.18459		

B_{UT-CF}	2.36918 N

Test Condition Errors:

The errors that occur during the testing phase may also be broken down into elemental errors. Once such error is in the alignment of the equipment to the towing direction of the carriage. This may be estimated as follows:

Error in Equip Angle (+/-)	1 degrees
B_{UT-T1} = Tunit*(1-cos(1))	0.01905 N

Again, as with the calibrations, a small error may be attributed to the misalignment of the load cell. This would have an influence on the voltage signal that was produced as a result of the loading. Based on an adaptation of ITTC recommended procedure 7.5-02-02-02 the error is estimated as:

Error in Load Cell Align (+/-)	0.25 degrees
B_{UT-T2} = Tunit*(1-cos(0.25))	0.00119 N

Since the static zero estimate will also affect the test condition data and must be included.

B_{UT-T3}	0.10643 N

Since the test data is also acquired using an AD card, an error due to this conversion also occurs and is calculated as follows:

AD Card Resolution	12 bits
AD Card Voltage Range	10 volts
AD Card Error	1 bit
B_{UT-T4}	0.22567 N

Total Unit Thrust Error:

The total error associated with the unit thrust may be calculated by using RSS:

B_{Tunit}	2.415236 N

Torque

Calibration Errors:

As indicated in ITTC 7.5-02-03-02.2, the error in torque calibration should consider both moment arm errors and weight errors as follows:

$$B_{Q\text{-}C1} = [(Ma*B_W)^2 + (F*B_{Ma})^2]^{1/2}$$

To reduce the error associated with the calibration weights, each individual weight was measured cn a high quality digital scale, accurate to +/- 0.1 g. This error may be estimated as follows:

Calibration Weights	1.1058	kg	0.0001 kg
	1.0001	kg	0.0001 kg
	1.1710	kg	0.0001 kg
	0.4572	kg	0.0001 kg
	1.0009	kg	0.0001 kg
Total Weight	4.7350	kg	
Error in Weight	0.000223607	kg	
B_W	0.002192822	N	

It should be noted that lever arm angle error was neglected, since the moment arm used was designed such that it had a radius equal to the moment arm length, and therefore, regardless of the angle, the effective moment arm distance was constant over the range of angles considered.

In addition, the static zero estimate and frictional effects are not present in this design as with other equipment, since the strain gauge was located such that the there were no seals, bearings or other mechanical components between the guages and the propeller.

The moment arm used to calibrate the torque was assumed accurate to 0.2 mm and had the length as specified below. The bias contribution due to the error in this length is estimated as follows:

Ma	0.5 m
B_{Ma}	0.0002 m

$B_{Q\text{-}C1}$	0.009351348 Nm

Since the calibration data is also acquired using an AD card, an error due to this conversion also occurs and is calculated as follows:

AD Card Resolution	12 bits
AD Card Voltage Range	10 volts
AD Card Error	1 bit
$B_{Q\text{-}C2}$	0.067124 Nm

As with thrust, errors in the static zero of the torque reading was included based on the observed differences in the zero torque value.

$B_{Q\text{-}C3}$	0.0352 Nm

Curve-Fit Errors:

The calibration data is used to establish the kgm-voltage relationship from a curve fit of the data which introduces an additional error, estimated using the standard error estimate as follows:

Applied Weight (kg)	Applied Torque (kgm)	Voltage	Predicted (kgm)	$(Y_i - (ax_i - b))^2$
0.0000	0.0000	0.6574	-0.0028	7.59098E-06
1.1058	0.5529	0.2601	0.5543	1.86717E-06
2.1059	1.0530	-0.0952	1.0523	4.79533E-07
3.2769	1.6385	-0.5122	1.6369	2.55218E-06
3.7341	1.8671	-0.6752	1.8653	2.96839E-06
4.7350	2.3675	-1.0333	2.3673	3.58327E-08
3.7341	1.8671	-0.6774	1.8684	1.90368E-06
3.2769	1.6385	-0.5148	1.6405	4.28983E-06
2.1059	1.0530	-0.0984	1.0568	1.48237E-05
1.1058	0.5529	0.2568	0.5589	3.58825E-05
0.0000	0.0000	0.6579	-0.0034	1.12933E-05
m	-1.4018			
b	0.9188			
SEE [kgm]	0.00305			
SEE [Nm]	0.02990			

$B_{Q\text{-}CF1}$	0.059807626 Nm

Test Condition Errors:

Since the torque test data is also acquired using an AD card, an error due to this conversion also occurs and is calculated as follows:

AD Card Resolution	12 bits
AD Card Voltage Range	10 volts
AD Card Error	1 bit
$B_{Q\text{-}T1}$	0.067124 Nm

Again errors in the static zero of the torque affect the test condition reading and must be included to account for differences in the zero torque value.

$B_{Q\text{-}T2}$	0.0352 Nm

Total Torque Error:

Combining the above error contributions, we can calucate the total toque bias limit as follows:

B_Q	**0.123113 Nm**

Propeller Thrust Coefficient - Total Bias Limit

Based on ITTC 7.5-02-03-02.2, the total bias limit for the thrust coefficient is calculated as follows:

For J = 0.1

$K_{Tprop} = T/(\rho n^2 D^4)$	
K_{Tprop}	0.4294

$(B_{KT})^2 = ((\delta K_T/\delta T)B_T)^2 + ((\delta K_T/\delta n)B_n)^2 + ((\delta K_T/\delta \rho)B_\rho)^2 + ((\delta K_T/\delta D)B_D)^2$	
$(\delta K_T/\delta T) = 1/(\rho n^2 D^4)$	0.002299447
$(\delta K_T/\delta n) = -2T/(\rho n^3 D^4)$	-0.094903704
$(\delta K_T/\delta \rho) = -T/(\rho^2 n^2 D^4)$	-0.000429811
$(\delta K_T/\delta D) = -4T/(\rho n^2 D^5)$	-6.362063104

Combining these values with the previously calculated bias limits gives the following:

$B_{KT\_J0.1}$	**0.0081 -**
$B_{KT\_J0.1}$	**1.8931 %**

For J = 0.4

$K_{Tprop} = T/(\rho n^2 D^4)$	
K_{Tprop}	0.3290

$(B_{KT})^2 = ((\delta K_T/\delta T)B_T)^2 + ((\delta K_T/\delta n)B_n)^2 + ((\delta K_T/\delta \rho)B_\rho)^2 + ((\delta K_T/\delta D)B_D)^2$	
$(\delta K_T/\delta T) = 1/(\rho n^2 D^4)$	0.002299447
$(\delta K_T/\delta n) = -2T/(\rho n^3 D^4)$	-0.072717249
$(\delta K_T/\delta \rho) = -T/(\rho^2 n^2 D^4)$	-0.00032933
$(\delta K_T/\delta D) = -4T/(\rho n^2 D^5)$	-4.874748932

Combining these values with the previously calculated bias limits gives the following:

$B_{KT\_J0.4}$	**0.0080 -**
$B_{KT\_J0.4}$	**2.4355 %**

For J = 0.7

$K_{Tprop} = T/(\rho n^2 D^4)$	
K_{Tprop}	0.1934

$(B_{KT})^2 = ((\delta K_T/\delta T)B_T)^2 + ((\delta K_T/\delta n)B_n)^2 + ((\delta K_T/\delta \rho)B_\rho)^2 + ((\delta K_T/\delta D)B_D)^2$	
$(\delta K_T/\delta T) = 1/(\rho n^2 D^4)$	0.002299447
$(\delta K_T/\delta n) = -2T/(\rho n^3 D^4)$	-0.042733006
$(\delta K_T/\delta \rho) = -T/(\rho^2 n^2 D^4)$	-0.000193534
$(\delta K_T/\delta D) = -4T/(\rho n^2 D^5)$	-2.864694098

Combining these values with the previously calculated bias limits gives the following:

B_{KT}	**0.0079 -**
$B_{KT\_J0.4}$	**4.0879 %**

Unit Thrust Coefficient - Total Bias Limit

Based on ITTC 7.5-02-03-02.2, the total bias limit for the thrust coefficient is calculated as follows:

For J = 0.1

$K_{Tunit} = T/(\rho n^2 D^4)$	
K_{Tunit}	0.4103

$(B_{KT})^2 = ((\delta K_T/\delta T)B_T)^2 + ((\delta K_T/\delta n)B_n)^2 + ((\delta K_T/\delta \rho)B_\rho)^2 + ((\delta K_T/\delta D)B_D)^2$	
$(\delta K_T/\delta T) = 1/(\rho n^2 D^4)$	0.002299447
$(\delta K_T/\delta n) = -2T/(\rho n^3 D^4)$	-0.090663241
$(\delta K_T/\delta \rho) = -T/(\rho^2 n^2 D^4)$	-0.000410606
$(\delta K_T/\delta D) = -4T/(\rho n^2 D^5)$	-6.077795023

Combining these values with the previously calculated bias limits gives the following:

$B_{KTunit\ J0.1}$	**0.0059 -**
$B_{KTunit\ J0.1}$	**1.4416 %**

For J = 0.4

$K_{Tunit} = T/(\rho n^2 D^4)$	
K_{Tunit}	0.3007

$(B_{KT})^2 = ((\delta K_T/\delta T)B_T)^2 + ((\delta K_T/\delta n)B_n)^2 + ((\delta K_T/\delta \rho)B_\rho)^2 + ((\delta K_T/\delta D)B_D)^2$	
$(\delta K_T/\delta T) = 1/(\rho n^2 D^4)$	0.002299447
$(\delta K_T/\delta n) = -2T/(\rho n^3 D^4)$	-0.066454392
$(\delta K_T/\delta \rho) = -T/(\rho^2 n^2 D^4)$	-0.000300966
$(\delta K_T/\delta D) = -4T/(\rho n^2 D^5)$	-4.454905523

Combining these values with the previously calculated bias limits gives the following:

$B_{KTunit\ J0.4}$	**0.0058 -**
$B_{KTunit\ J0.4}$	**1.9122 %**

For J = 0.7

$K_{Tunit} = T/(\rho n^2 D^4)$	
K_{Tunit}	0.1519

$(B_{KT})^2 = ((\delta K_T/\delta T)B_T)^2 + ((\delta K_T/\delta n)B_n)^2 + ((\delta K_T/\delta \rho)B_\rho)^2 + ((\delta K_T/\delta D)B_D)^2$	
$(\delta K_T/\delta T) = 1/(\rho n^2 D^4)$	0.002299447
$(\delta K_T/\delta n) = -2T/(\rho n^3 D^4)$	-0.033569139
$(\delta K_T/\delta \rho) = -T/(\rho^2 n^2 D^4)$	-0.000152032
$(\delta K_T/\delta D) = -4T/(\rho n^2 D^5)$	-2.250375593

Combining these values with the previously calculated bias limits gives the following:

$B_{KTunit\ J0.7}$	**0.0056 -**
$B_{KTunit\ J0.7}$	**3.6896 %**

Torque Coefficent - Total Bias Limit

Based on ITTC 7.5-02-03-02.2, the total bias limit for the torque coefficient is calculated as follows:

For J = 0.1

$K_Q = Q/(\rho n^2 D^5)$	
K_Q	0.061821426

$(B_{KQ})^2 = ((\delta K_Q/\delta Q)B_Q)^2 + ((\delta K_Q/\delta n)B_n)^2 + ((\delta K_Q/\delta \rho)B_\rho)^2 + ((\delta K_Q/\delta D)B_D)^2$	
$(\delta K_Q/\delta Q) = 1/(\rho n^2 D^5)$	0.008516471
$(\delta K_Q/\delta n) = -2Q/(\rho n^3 D^5)$	-0.013662194
$(\delta K_Q/\delta \rho) = -Q/(\rho^2 n^2 D^5)$	-6.18749E-05
$(\delta K_Q/\delta D) = -5Q/(\rho n^2 D^6)$	-1.144841223

Combining these values with the previously calculated bias limits gives the following:

$B_{KQ\ J0.1}$	**0.00110309 -**
$B_{KQ\ J0.1}$	**1.784315998 %**

For J = 0.4

$K_Q = Q/(\rho n^2 D^5)$

K_Q	0.049851053

$(B_{KQ})^2 = ((\delta K_Q/\delta Q)B_Q)^2 + ((\delta K_Q/\delta n)B_n)^2 + ((\delta K_Q/\delta \rho)B_\rho)^2 + ((\delta K_Q/\delta D)B_D)^2$	
$(\delta K_Q/\delta Q) = 1/(\rho n^2 D^5)$	0.008516471
$(\delta K_Q/\delta n) = -2Q/(\rho n^3 D^5)$	-0.011016807
$(\delta K_Q/\delta \rho) = -Q/(\rho^2 n^2 D^5)$	-4.98942E-05
$(\delta K_Q/\delta D) = -5Q/(\rho n^2 D^6)$	-0.923167656

Combining these values with the previously calculated bias limits gives the following:

$B_{KQ\ J0.4}$	**0.001084304 -**
$B_{KQ\ J0.4}$	**2.175087587 %**

For J = 0.7

$K_Q = Q/(\rho n^2 D^5)$	
K_Q	0.032601228

$(B_{KQ})^2 = ((\delta K_Q/\delta Q)B_Q)^2 + ((\delta K_Q/\delta n)B_n)^2 + ((\delta K_Q/\delta \rho)B_\rho)^2 + ((\delta K_Q/\delta D)B_D)^2$	
$(\delta K_Q/\delta Q) = 1/(\rho n^2 D^5)$	0.008516471
$(\delta K_Q/\delta n) = -2Q/(\rho n^3 D^5)$	-0.007204691
$(\delta K_Q/\delta \rho) = -Q/(\rho^2 n^2 D^5)$	-3.26294E-05
$(\delta K_Q/\delta D) = -5Q/(\rho n^2 D^6)$	-0.60372645

Combining these values with the previously calculated bias limits gives the following:

$B_{KQ\ J0.7}$	**0.001063953 -**
$B_{KQ\ J0.7}$	**3.263535077 %**

Advance Coefficent - Total Bias Limit

Based on ITTC 7.5-02-03-02.2, the total bias limit for the advance coefficient is calculated as follows:

For J = 0.1

$J = V_A/nD$	
J	0.099

$(B_J)^2 = ((\delta J/\delta V_A)B_{VA})^2 + ((\delta J/\delta n)B_n)^2 + ((\delta J/\delta D)B_D)^2$	
$(\delta J/\delta V_A) = 1/(nD)$	0.409249028
$(\delta J/\delta n) = -V_A/(n^2 D)$	-0.010988676
$(\delta J/\delta D) = -V_A/(nD^2)$	-0.368324125

Combining these values with the previously calculated bias limits gives the following:

$B_{J\ J0.1}$	**0.002442536 -**
$B_{J\ J0.1}$	**2.456106078 %**

For J = 0.4

$J = V_A/nD$	
J	0.398

$(B_J)^2 = ((\delta J/\delta V_A)B_{VA})^2 + ((\delta J/\delta n)B_n)^2 + ((\delta J/\delta D)B_D)^2$	
$(\delta J/\delta V_A) = 1/(nD)$	0.409249028

$(\delta J/\delta n) = -V_A/(n^2D)$	-0.043954702
$(\delta J/\delta D) = -V_A/(nD^2)$	-1.473296501

Combining these values with the previously calculated bias limits gives the following:

$B_{J\_J0.4}$	**0.002563369 -**
$B_{J\_J0.4}$	**0.64440247 %**

For J = 0.7

$J = V_A/nD$	
J	0.696

$(B_J)^2 = ((\delta J/\delta V_A)B_{VA})^2 + ((\delta J/\delta n)B_n)^2 + ((\delta J/\delta D)B_D)^2$	
$(\delta J/\delta V_A) = 1/(nD)$	0.409249028
$(\delta J/\delta n) = -V_A/(n^2D)$	-0.076920729
$(\delta J/\delta D) = -V_A/(nD^2)$	-2.578268877

Combining these values with the previously calculated bias limits gives the following:

$B_{J\_J0.7}$	**0.002810976 -**
$B_{J\_J0.7}$	**0.403798978 %**

Precision Limits

The precision limits were estimated for three advances speeds, using five repeat runs for a given test. The standard deviation of each data set was calculated according to the expressions given in ITTC QM 7.5-02-01-01. As outlined in this method, the precision limit is then estimated using:

$$P_i = K*S_i$$

The variable K is the coverage factor, which for a 95-percent confidence interval equals 2 and the S_i term is the calculated standard deviation of the data. This gave the following precision limit values:

	J = 0.1	J = 0.4	J = 0.7
V (+/-)	0.00014	0.00043	0.00106
T_{PROP} (+/-)	0.17977	0.39589	0.50176
T_{UNIT} (+/-)	0.59463	0.68789	0.56562
Q (+/-)	0.00344	0.01884	0.06406

The shaft speed precision estimates is based on the a display reading precision error asssumed to be equal to as +/- the smallest scale division, which was one rpm.

Shaft Speed (+/-)	0.0167

Bias and Precision Limits

Variable	Bias Errors		Bias Limit		Precision Errors		Precision Limit	
Temperature	Calibration:	+/- 0.5 °C.	Fossilized into +/- 0.745 °C for Temperature		Scale: Range:	+/- 0.05 °C. +/- 0.55 °C.		
Density	Temp Related Errors: Density Eqn Errors:	+/- 0.122 kg/m^3 +/- 0.108 kg/m^3	Overall Limit:	+/- 0.162 kg/m^3				
Propeller Diameter	CNC Machining Errors: Hand Polishing Errors:	+/- 0.0001 m +/- 0.0002 m	Overall Limit:	+/- 0.000224 m				
Shaft Speed	Calibration:	+/- 0.0167 rps	Overall Limit:	+/- 0.0167 rps	Scale:	+/- 0.0167 rps	Overall Limit:	+/- 0.0167 rps
Advance Speed	Measurement Errors: Tide Effects:	+/- 0.00586 m/s +/- 0.001 m/s	Overall Limit:	+/- 0.00595 m/s			J = 0.1 J = 0.4 J = 0.7	+/- 0.00014 m/s +/- 0.00043 m/s +/- 0.00106 m/s
PropellerThrust	Weights: Loading Angle: Load Cell Align: Static Zero: A/D Error: Curve Fit: Equipment Angle: Load Cell Align: Static Zero: A/D Error:	+/- 0.00276 N +/- 0.00525 N +/- 0.00131 N +/- 0.14110 N +/- 0.23904 N +/- 3.38951 N +/- 0.00525 N +/- 0.00131 N +/- 0.14110 N +/- 0.23904 N	*Calibration Data Errors* Overall Limit: *Testing Data Errors*	+/- 3.40696 N			J = 0.1 J = 0.4 J = 0.7	+/- 0.1798 N +/- 0.3959 N +/- 0.5018 N
Unit Thrust	Weights: Loading Angle: Load Cell Align: Static Zero: A/D Error: Curve Fit: Equipment Angle: Load Cell Align: Static Zero: A/D Error:	+/- 0.00276 N +/- 0.01905 N +/- 0.00119 N +/- 0.10643 N +/- 0.22567 N +/- 2.36918 N +/- 0.01905 N +/- 0.00119 N +/- 0.10643 N +/- 0.22567 N	*Calibration Data Errors* Overall Limit: *Testing Data Errors*	+/- 2.41523 N			J = 0.1 J = 0.4 J = 0.7	+/- 0.59463 N +/- 0.6879 N +/- 0.5656 N
Torque	Weights: Static Zero: A/D Error: Curve Fit: Static Zero: A/D Error:	+/- 0.00935 Nm +/- 0.03522 Nm +/- 0.0671 Nm +/- 0.0598 Nm +/- 0.03522 Nm +/- 0.0671 Nm	Overall Limit:	+/- 0.12311 Nm			J = 0.1 J = 0.4 J = 0.7	+/- 0.0034 Nm +/- 0.0188 Nm +/- 0.0641 Nm

Overall Uncertainty

The bias and precision limits may be summarized as follows:

	J = 0.1	J = 0.4	J = 0.7
ρ	999.14	999.14	999.14
B_ρ	0.16242	0.16242	0.16242
P_ρ	-	-	-
$(U_\rho/\rho)^2$	2.643E-08	2.643E-08	2.643E-08
D	0.27	0.27	0.27
B_D	0.00022	0.00022	0.00022
P_D	-	-	-
$(U_D/D)^2$	6.859E-07	6.859E-07	6.859E-07
n	9.1	9.1	9.1
B_n	0.0167	0.0167	0.0167
P_n	0.01667	0.01667	0.01667
$(U_n/n)^2$	6.783E-06	6.771E-06	6.746E-06
V	0.24	0.97	1.70
B_V	0.00595	0.00595	0.00595
P_V	0.00014	0.00043	0.00106
$(U_V/V)^2$	5.995E-04	3.764E-05	1.262E-05
T_{PROP}	186.76	143.10	84.09
B_{TPROP}	3.41224	3.41224	3.41224
P_{TPROP}	0.17977	0.39589	0.50176
$(U_{TPROP}/T_{PROP})^2$	3.348E-04	5.763E-04	1.682E-03
T_{UNIT}	178.41	130.77	66.06
B_{TUNIT}	2.41524	2.41524	2.41524
P_{TUNIT}	0.59463	0.68789	0.56562
$(U_{TUNIT}/T_{UNIT})^2$	1.015E-06	9.164E-06	5.769E-05
Q	7.26	5.85	3.83
B_Q	0.12311	0.12311	0.12311
P_Q	0.00344	0.01884	0.06406
$(U_Q/(Q))^2$	2.879E-04	4.527E-04	1.314E-03

Combining the precision limit and bias limit estimates we can get the following estimates of overall uncertainty for the measured parameters:

$$(U_x) = ((B_x)^2 + (P_x)^2)^{1/2}$$

	J = 0.1	J = 0.4	J = 0.7
U_ρ	0.16242	0.16242	0.16242
U_D	0.00022	0.00022	0.00022
U_n	0.02357	0.02357	0.02357
U_V	0.00595	0.00596	0.00604
U_{TPROP}	3.41697	3.43512	3.44893
U_{TUNIT}	0.17977	0.39589	0.50176
U_Q	2.48736	2.51129	2.48058
U_{Qo}	0.12316	0.12455	0.13878

Using the uncertainty expressions for each of the data reduction equations we get the following estimates for the data reduction equations:

	J = 0.1	J = 0.4	J = 0.7
(U_{KTPROP}/K_{TPROP})	1.9%	2.5%	4.1%
(U_{KTPROP})	0.00829	0.00816	0.00802
(U_{KTUNIT}/K_{TUNIT})	0.6%	0.7%	1.0%
(U_{KTUNIT})	0.00257	0.00207	0.00149
(U_{Ko}/K_Q)	1.8%	2.2%	3.7%
(U_{Ko})	0.00113	0.00111	0.00120
(U_J/J)	2.5%	0.7%	0.4%
(U_J)	0.00246	0.00269	0.00313

Overall Uncertainty

	Advance Coefficient Value	Prop Thrust Coefficient K_{Tprop} (+/-)	Percentage Error in K_{Tprop} (+/-)	Unit Thrust Coefficient K_{Tunit} (+/-)	Percentage Error in K_{Tunit} (+/-)	Torque Coefficient K_Q (+/-)	Percentage Error in K_Q (+/-)	Advance Coefficient Error (+/-)
9 rps	0.1	0.00829	1.9%	0.00257	0.6%	0.00113	1.8%	0.00246
	0.4	0.00816	2.5%	0.00207	0.7%	0.00111	2.2%	0.00269
	0.7	0.00802	4.1%	0.00149	1.0%	0.00120	3.7%	0.00313